THÈSE DE DOCTORAT

de l'Université de recherche Paris Sciences et Lettres
PSL Research University

Préparée à École Normale Supérieure Paris

Dissolution Dynamic Nuclear Polarization of Deuterated Molecules

Polarisation Dynamique Nucléaire par Dissolution de Molécules Deutériées

Ecole doctorale n°388

Chimie physique et chimie analytique de Paris Centre

Spécialité : Resonance Magnetique Nucleaire

**Soutenue par Aditya JHAJHARIA
le 20 Octobre 2017**

Dirigée par **Prof.
Geoffrey BODENHAUSEN**

COMPOSITION DU JURY :

Dr LESAGE Anne
ISA Lyon, Rapporteur

Dr BERTHAULT Patrick
CEA Saclay, Rapporteur

Prof. BODENHAUSEN Geoffrey
ENS Paris, Directeur de thèse

Dr KURZBACH Dennis
ENS Paris, Co-directeur de thèse

Prof. IVANOV Konstantin L.
ITC Russia, président du jury

Abstract

Nowadays, Nuclear Magnetic Resonance (NMR) has become an inevitable spectroscopic technique that can be applied in many fields of science and medicine. However it is limited by low sensitivity due to the low nuclear polarization, defined by the difference of populations between the energy levels involved, thus leading to long experimental times. This drawback can be overcome by using the huge polarization of unpaired electrons compared to nuclear spins and its transfer to nuclear spins at low temperatures (using microwave irradiation) to achieve a large nuclear magnetization - a method know as dynamic nuclear polarization (DNP).

Sami Jannin and co-workers have recently combined the cross-polarization (CP) method with DNP at very low temperatures to polarize low γ nuclei faster by transferring the electron polarization to protons and then to low γ nuclei like ^{13}C. This thesis demonstrates that the efficiency of the CP method can be improved by switching the microwave irradiation off for a few hundred milliseconds prior to CP. By performing these microwave gating experiments, ^{13}C polarizations for sodium [1-^{13}C]acetate as high as 64% could be achieved with a polarization build-up time constant as short as 160 s.

The hyperpolarized sample can subsequently be rapidly dissolved to achieve NMR signal enhancement in the liquid state at ambient temperature. This method has been developed by Ardenkjaer-Larsen and co-workers in 2003 and became known as dissolution-dynamic nuclear polarization (D-DNP). It can provide signal enhancements by a factor of up to four orders of magnitude in liquid state at room temperature.

Combining D-DNP with CP techniques from ^{1}H to ^{13}C can be used to create to create long-lived states (LLS) in deuterated molecules like ethanol-d$_6$ and DMSO-d$_6$, which can have much longer life times than conventional Zeeman magnetization. These LLS can be detected indirectly via the asymmetric multiplets in ^{13}C NMR spectra in solution state at room temperature after

dissolution due to scalar couplings between ^{13}C and ^{2}H. These LLS result from population imbalances between spin manifolds of distinct irreducible representations of the relevant symmetry groups of the investigated deuterated moities. In this thesis we have investigated LLS in CD_2 and CD_3 groups. Lifetimes of these LLS can exceed the spin-lattice relaxation times $T_1(^2H)$ of deuterium nuclei by a factor up to 20 (depending on the underlying molecular dynamics) and can be obtained by monitoring the decay of the asymmetry of the ^{13}C multiplet. These observations can expend the scope of DNP by adding ^{2}H nucleus to the list of possible observables.

Acknowledgement

First, I would like to express my sincere gratitude to my thesis supervisor, Prof. Geoffrey Bodenhausen, who gave me the opportunity to work in a great scientific environment. Thanks to his unconditional support he gave me the opportunity to explore the fascinating world of magnetic resonance during the last three years. His immense knowledge, motivation and enthusiasm drove me towards the right direction in science. His guidance helped me throughout my research and writing of this thesis.

A huge thanks goes to Dr Dennis Kurzbach, co-supervisor of my thesis. He arrived at ENS during the summer of 2015, and ever since he has been a driving force. He is really an inspiring and encouraging person to work with. Through his knowledge and experience he can easily interconnect different domains of science, which brings an interdisciplinary tangent to our research. For me, he reflects the qualities of a good scientist. Thank you, Dennis for everything, this thesis would not have been possible without you.

I would like to thank the jury members of this thesis: Prof. Ivanov Konstantin, with whom I had helpful discussions during his visit to Paris. He has given me an immense support in sharing his immense knowledge. Sincere thanks also to the reporters of my thesis, Dr. Anne Lesage and Dr. Patrick Berthault, for accepting my invitation.

When I came to ENS, the DNP polarizer was not yet in operation, and Dr Daniel Abergel used to sit behind the polarizer, showing how concerned he was by taking care of it, even though it was not functional. Many thanks to Dr James Kempf and Dr Matthias Weller for providing their continuous support during and after the installation of the polarizer. They were always extremely helpful in providing all possible assistance to make our DNP system work. I am thankful to Dr Dmitry Eshchenko and Dr Roberto Melzi for sharing their knowledge and showing us how the DNP system works experimentally. A special thanks to

Daniel, a great scientist, DNP could have not been possible to run without his efforts. He has a vast knowledge of the subject. It usually takes me longer to understand his deep thinking. Those long and fruitful discussions are really appreciated.

My sincere thanks to Dr Aurélien Bornet and Prof. Sami Jannin for providing me the opportunity to learn about dissolution DNP when I was in Lausanne, which was my first experience with DNP experiments. Thanks to Dr Aurélien Bornet and Dr Daniele Mammoli for being my NMR mentors and for helping me during my stay in Lausanne.

I would like to thank my lab mates, and especially the dissolution-DNP team members for creating a friendly environment at the workplace. Dennis has been a key member of the team and his unique creativity, called *D-DNP dance* motivates PhD's to work enthusiastically during the experiments (only our group members know how to do the DNP dance!). Dennis, Daniel, Estel Canet, Emmanuelle Weber, Sina Marhabaie, Aude Sadet, thanks to all of you. A special thanks goes to Emmanuelle for helping with the French translation of the thesis summary.

I would like to specially thank Nicolas Birlirakis for sharing his knowledge and experience with me. He was my first NMR mentor in Paris and has always been helpful in professional and personal life. Thank you, Nicolas. Thanks to a great knowledgeable scientist, Philippe Pelupessy, even though we did not share any scientific projects together, he has always been readily available for help. I must mention my dear friend, Dr Rudra Purusottam for giving me the confidence to work better and for always being supportive.

I share my office with Dr Philippe Pelupessy, Sina Marhabaie, Xiao Ji (who just left for China after his PhD defense). Sina, whom I usually say *Jahanpanah*, who can explain the subject in simple words, a big *thank you* for encouraging and fruitful discussions. Thanks to Xiao for interesting Indo-China political conversations.

Table of Contents

Résumé

En 1938, Isidor Isaac Rabi[1-2] découvre le principe de la Résonance Magnétique Nucléaire (RMN). Ses travaux ont par la suite été prolongés par Bloch[3] et Purcell[4] qui, en 1946, ont observé ce phénomène sur les liquides et les solides, respectivement. En 1964, Richard Ernst introduit la transformée de Fourier (TF) et facilite l'étude spectrale des signaux RMN. La RMN sera par la suite sujette à de grands développements jusqu'à constituer aujourd'hui un outil indispensable de la science moderne. Permettant de déterminer la structure et la cinétique des molécules, cette technique est notamment très utilisée en chimie. Dans le domaine de la biologie, elle figure parmi les méthodes les plus puissantes pour obtenir des informations sur les propriétés dynamiques des protéines. Son importance en médecine est également cruciale. De fait, elle intervient sous la forme d'Imagerie par Résonance Magnétique (IRM) et de Spectroscopie par Résonance Magnétique (SRM) pour des applications *in vivo* quotidiennes.

Le spin est généralement associé à un nombre quantique : le nombre quantique de spin. Les noyaux doivent posséder un nombre quantique de spin non-nul pour permettre l'observation d'un signal en RMN. Le moment magnétique nucléaire (μ) est relié à l'opérateur de spin (I) par l'équation :

$$\mu = \gamma I$$

où γ correspond à une constante caractéristique du noyau appelée rapport gyromagnétique.

En présence d'un champ magnétique, le moment magnétique nucléaire (μ) interagit avec le champ magnétique statique B_0. Cette interaction correspond à l'effet Zeeman et son énergie s'exprime comme :

$$E = -\mu \cdot B_0 = -\gamma I \cdot B_0$$

B_0 est conventionnellement orienté selon l'axe z du repère orthonormé (O, x, y, z). Ainsi, la relation précédente devient :

$$E = -\mu_Z B_0 = -\gamma m \hbar B_0$$

où m représente le nombre quantique magnétique qui peut prendre des valeurs entières entre $-I$ et $+I$ tandis que $\hbar$ correspond à la constante de Planck réduite. Dans le cas d'un spin ½, la levée de la dégénérescence des niveaux d'énergie engendrée par l'effet Zeeman mène à la création de deux niveaux d'énergie distincts communément appelés α et β. En présence d'un champ magnétique externe B_0, la différence d'énergie (ΔE) entre ces deux états s'exprime de la manière suivante :

$$\Delta E = \gamma \hbar B_0$$

Lorsqu'un spin non-nul est placé dans un champ magnétique B_0, il tend à s'aligner avec celui-ci. Dès lors qu'une impulsion radiofréquence (RF) est appliquée au système, les spins sont excités et l'aimantation n'est plus alignée avec le champ magnétique externe. Après l'arrêt de l'impulsion, le système retourne à l'équilibre. Ce phénomène appelé relaxation peut être décomposé en deux contributions distinctes, chacune engendrée par des processus différents: la relaxation longitudinale (spin-réseau) et la relaxation transversale (spin-spin). La première correspond à une perte d'énergie, soit une dissipation de l'énergie du système dans le réseau. Elle est caractérisée par un taux de relaxation R_1. La deuxième, quant à elle, est associée à un taux de relaxation R_2 et engendrée par une perte de cohérence des spins dans le plan.

Le processus de relaxation est généralement lent en RMN comparé à d'autres méthodes spectroscopiques. Les expériences s'en retrouvent donc allongées. De plus, cette technique est limitée par sa faible sensibilité. Certains spins non-nuls très importants en chimie comme ^{13}C et ^{15}N sont particulièrement difficiles à observer avec une sensibilité suffisante, à cause à la fois de leurs faibles rapports gyromagnétiques (γ) et de leurs faibles abondances naturelles. Pour éviter les expériences trop longues et améliorer la sensibilité du signal, plusieurs approches ont été développées comme par exemple l'augmentation du champ magnétique externe des spectromètres ou encore l'utilisation de cryo-sondes. D'autre part, des méthodes de corrélation hétéronucléaire ont également permis

d'améliorer la sensibilité des signaux. Cependant, la polarisation nucléaire reste limitée par les propriétés intrinsèques des noyaux.

L'ensemble de cette étude repose sur l'utilisation d'une technique permettant de s'affranchir des limites apportées par la nature même des noyaux en exploitant les propriétés magnétiques des électrons : la Polarisation Dynamique Nucléaire (PDN, ou DNP en anglais).   La théorie derrière la PDN, c'est-à-dire le transfert de la polarisation des électrons aux noyaux, a tout d'abord été développée par Overhauser en 1953.[5] Elle a par la suite été confirmée par l'expérience de Carver et Slichter,[6] qui a révélé une forte amélioration de l'intensité des signaux associés aux noyaux ^{6}Li dans un métal. Le mécanisme responsable de ce transfert de polarisation porte désormais le nom d'effet Overhauser.

Il existe également d'autres mécanismes de transfert de polarisation du spin électronique au spin nucléaire : l'effet solide (SE pour *'solid effect'*), l'effet croisé (CE pour *'cross effect'*) et le mélange thermique (TM pour *'thermal mixing'*). En effet, à la fin des années 50', Abragam et Proctor proposent d'exciter le système en utilisant les transitions interdites électron-noyau c'est-à-dire, les fréquences $\omega_S \pm \omega_I$ où ω_S et ω_I correspondent respectivement aux fréquences de Larmor de l'électron et du noyau. Ils nomment ce processus *'l'effet solide'* (*'solid effect'* ou SE). L'effet solide est particulièrement efficace dans le cas où la largeur de raie (δ) de la résonance du spin électronique (ESR) est plus petite que la fréquence de Larmor du noyau. Par contre, *l'effet croisé* (*'cross effect'* ou CE) est dominant lorsque la relation $\Delta > \omega_n > \delta$, où δ et Δ correspondent respectivement aux largeurs de raies homogène et inhomogène du spectre des spins électroniques, est vérifiée. Les mécanismes du SE et du CE sont fondés sur la mécanique quantique de systèmes composés d'un petit nombre de deux à trois spins. Cependant, pour être à même de décrire des systèmes réels, il est nécessaire de prendre en compte toutes les interactions spin-spin dans le cas de systèmes composés d'un grand nombre de particules. Il faut donc avoir recours à une autre théorie reposant sur la description thermodynamique du système de spins : le mélange thermique (*'thermal mixing'* ou TM).

L'objectif de la PDN étant de pallier à la faible sensibilité de la RMN, cette technique a tout d'abord été appliquée à la RMN du solide. Elle a été combinée avec la méthode de la rotation à l'angle magique ('Magic Angle Spinning' ou MAS). La PDN s'est surtout fait connaître dès 1993 grâce aux travaux de Griffin qui s'est appuyé sur le développement des gyrotrons (sources stables et puissantes de microonde). Cette association entre la PDN et la RMN du solide porte aujourd'hui le nom de MAS-DNP.[7-8] Les expériences de MAS-DNP sont généralement réalisées à des températures avoisinant les 100 K.

La méthode DNP, cette fois-ci sans recours au MAS, est devenue célèbre à la suite de l'idée révolutionnaire d'Ardenkjaer-Larsen en 2003. De fait, celui-ci a introduit le concept de la PDN par dissolution : le système soumis à un fort champ magnétique est tout d'abord polarisé par PDN à très basse température, puis rapidement transporté jusqu'à un spectromètre (RMN ou IRM) dans lequel la détection a lieu. Ce procédé permet d'obtenir des signaux dont l'intensité est multipliée par un facteur pouvant atteindre 10^5 dans le cas du ^{13}C à température ambiante.

L'idée derrière la PDN consiste à tirer parti du très grand moment magnétique d'un électron non-apparié en le transférant aux spins nucléaires qui, eux, possèdent un moment magnétique beaucoup moins important. Il devient alors possible d'atteindre une très grande polarisation nucléaire. La PDN par dissolution est particulièrement efficace lorsque le système est polarisé à des températures avoisinant les 1.2 K : la polarisation des électrons étant alors proche de 100%. Le transfert de polarisation électronique aux spins nucléaires couplés peut s'effectuer par les quatre mécanismes mentionnés précédemment (OE, SE, CE, ou TM) dont l'efficacité dépend de nombreux facteurs tels que la température ou la source microonde.

Au sein du laboratoire des biomolécules de l'ENS à Paris, nous utilisons deux aimants pour la PDN par dissolution : un pour la polarisation de l'échantillon à basse température appelé 'polariseur', l'autre pour la détection du signal à température ambiante. Dans le polariseur, un échantillon vitrifié contenant des

radicaux est irradié par une irradiation microonde de 188.2 GHz. Lorsque le système est hyperpolarisé, l'échantillon est dissous à l'aide de 5 mL de D$_2$O chauffé à 180°C sous une pression de 10.5 bar, puis directement éjecté dans le polariseur. Une fois dissous, le liquide hyperpolarisé est transféré jusqu'à un spectromètre ayant un champ de 9.4 T ou de 18.8 T, à travers un tunnel magnétique qui maintient un champ constant de 0.9 T durant tout le trajet. Le processus prend généralement entre 4 et 10 secondes et est schématisé sur la Fig. 1.
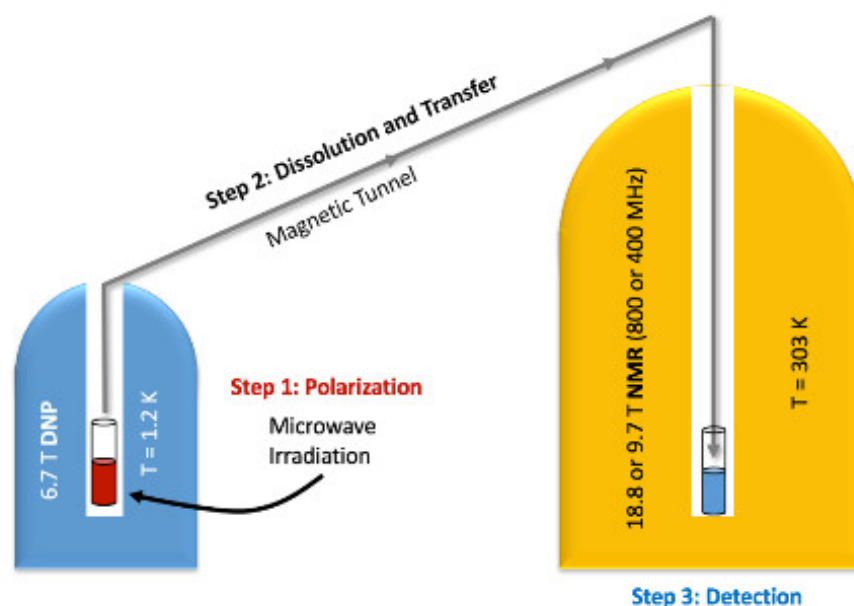
Figure 1. Principe de la PDN par dissolution. Un échantillon vitrifié à 1.2 K contenant des radicaux est plongé dans un champ magnétique de 6.7 T et irradié par une microonde de 188.2 GHz (gauche). Une fois hyperpolarisé, l'échantillon est dissous puis transféré dans un spectromètre RMN de 400 ou de 800 MHz (droite). Ce procédé permet d'obtenir des spectres dont l'intensité peut être augmentée de 4 à 5 ordres de grandeur.

Les radicaux possédant une raie de résonance paramagnétique électronique (RPE) fine comme le trityl sont particulièrement efficaces pour polariser directement le ^{13}C. Cependant, le transfert de polarisation de l'électron à l'isotope du carbone est très lent à 1.2 K.[9] Par conséquent, les expériences de PDN du ^{13}C s'avèrent très chronophages. Pour remédier à ce problème, le radical que nous avons utilisé au cours de cette étude est le TEMPOL (4-hydroxy-2,2,6,6

-tetramethylpiperidin-1-oxyl) pour lequel la polarisation des ^{1}H est particulièrement efficace. La PDN a par la suite été combinée à la technique de la polarisation croisée (*cross-polarisation* ou CP). Le principe de la CP repose sur l'augmentation de la polarisation des noyaux comportant un faible γ en leur transférant la polarisation des noyaux ayant un γ plus élevé. Ce procédé fonctionne dans les cas où une forte interaction dipolaire couple les noyaux en question. Afin que ce processus puisse avoir lieu entre des spins hétéronucléaires, la différence entre leurs niveaux d'énergie respectifs doit être équivalente. La transition d'énergie d'un spin à l'autre devient alors permise. La condition nécessaire à ce transfert de polarisation internucléaire porte le nom de '*condition de Hartmann-Hahn*' qui a été formulée en 1962.[10] Sami Jannin et al. ont utilisé cette méthode à très basse température et l'ont combinée à la PDN par dissolution dans le but de transférer la magnétisation des protons hyperpolarisés à des noyaux à faible rapport gyromagnétique tels que ^{13}C, ^{15}N, etc. Ainsi, le TEMPOL permet une polarisation rapide des protons par PDN et peut être combiné à une CP entre le ^{1}H et le ^{13}C, ce qui permet d'obtenir rapidement une forte polarisation du [13]C.[11-12]

La PDN à basse température nécessite la saturation par irradiation microonde des spins électroniques de l'agent paramagnétique. Cependant, la saturation des spins électroniques écourte le temps de relaxation des protons dans le repère tournant $T_{1\rho}$ (^{1}H). La présence d'électrons dans des états excités contribue au taux de relaxation des protons dans le repère tournant et, ainsi, leur temps de relaxation est raccourci. Durant ma thèse, je me suis penché sur le problème de l'optimisation de l'efficacité de la CP dans la PDN à basse température. Si on éteint l'irradiation microonde juste avant la CP, la polarisation des électrons a la possibilité de retourner à l'état fondamental favorisé par l'équilibre de Boltzmann. Cela n'est valable qu'à basse température. L'augmentation du temps de relaxation des protons dans le repère tournant ($T_{1\rho}$) permet d'augmenter la durée de l'intervalle pendant laquelle la condition de Hartmann-Hahn est vérifiée et, donc, d'augmenter la polarisation transférée au [13]C. Dans cette thèse, nous démontrons que la polarisation du [13]C à 1.2 K peut être considérablement

augmentée par cette méthode, donnant lieu dans le cas du [1-^{13}C]acetate à une polarisation du carbone $P(^{13}C) = 64\%$.

Les noyaux associés à un nombre quantique de spin de ½ ont généralement une relaxation assez lente. Par conséquent, la plupart des applications de la PDN par dissolution s'appliquent à ceux-ci. Ils disposent d'une distribution de charge sphérique tandis que les spins avec un nombre quantique supérieur à ½ possèdent un moment quadripolaire de par leur distribution de charge non-sphérique. Ce moment interagit avec le gradient de champ électrique (*electric field gradient* ou EFG) qui est issu de l'asymétrie de la distribution de la densité électronique autour du noyau. Des fluctuations du gradient de champ électrique génèrent une source de relaxation supplémentaire pour les noyaux quadripolaires. Dans cette thèse, je cherche à démontrer comment partiellement neutraliser cette source de relaxation additionnelle. Cette approche s'inspire des travaux de Levitt et de ses collaborateurs sur les états de spin de longue durée de vie (*long-lived states* ou LLS).[13-14] Les LLS ont la particularité de réduire l'influence des contributions de l'interaction dipolaire sur la relaxation en exploitant le principe d'exclusion de Pauli qui mène à la séparation dynamique des états de spin appartenant à des sous-ensembles de symétrie différentes. La réduction des contributions quadripolaires par l'exploitation des propriétés de symétrie d'un système sera discutée dans cette thèse.

Cette thèse est principalement axée sur les spins sujets à l'interaction quadripolaire et plus particulièrement sur le deutérium. Au premier abord, le noyau de deutérium ne semble pas présenter des caractéristiques intéressantes pour la PDN par dissolution puisque son aimantation longitudinale (D_z), qui est proportionnelle à sa polarisation, a un temps de relaxation $T_1(D_z)$ typiquement de l'ordre de la seconde. Etant donné que, dans notre laboratoire, le transfert de substances hyperpolarisées vers un spectromètre (RMN ou IRM) requiert entre 4 et 10 secondes (sans utiliser un système d'injection haute pression [15]), l'essentiel de la polarisation est perdu par relaxation quadripolaire avant même que l'échantillon n'atteigne l'appareil de détection. Afin de remédier à ce problème, nous proposons ici un moyen pour hyperpolariser des états de longue durée de

vie d'un système contenant une paire de noyaux de deutérium ayant un couplage scalaire à un noyau ^{13}C. Cette approche est fondée sur l'utilisation de la polarisation croisée (CP) pour polariser les noyaux qui nous intéressent, ainsi que l'exploitation des propriétés des états de longue durée de vie.

Ainsi nous proposons d'inclure le deutérium aux noyaux observables par PDN par dissolution, ouvrant par la même occasion de nouvelles pistes telles que l'étude de la dynamique de molécules deutériées ou encore l'amélioration de la sensibilité de la RMN du deutérium. Ce travail a été récemment publié.[16-17]

Lors de cette étude, les spectres ^{13}C de l'ethanol-d_6, du DMSO-d_6 et de l'acétone-d_6 (dans un mélange composé d'un agent vitrifiant (glycérol-d_8), d'un réservoir de protons (H_2O) permettant d'effectuer la CP entre le solvant et le ^{13}C des molécules deutériées et du TEMPOL) ont été observés en abondance naturelle (1.1 %). Nous nous focaliserons sur la dynamique des spins des groupements $^{13}CD_2$ de l'ethanol-d_6 et $^{13}CD_3$ du DMSO-d_6 et de l'acétone-d_6.

Dans nos expériences effectuées à 1.2K, la séquence de la CP utilise des impulsions radiofréquence adiabatiques à balayage fréquentiel pour transférer une partie de l'aimantation des ^1H à celle des ^{13}C par le biais de l'interaction dipolaire longue portée entre des spins de molécules différentes. Ce processus n'est possible seulement lorsque la condition de Hartmann-Hahn est vérifiée.[18] L'objectif d'une CP est le transfert de la polarisation d'un noyau doté d'un spin I vers le spin S d'un autre noyau en utilisant le couplage dipolaire qui existe entre ces noyaux. Plus exactement, il s'agit de la composante x de l'aimantation Ix d'un premier ensemble de spins qui est convertie en composante x de l'aimantation S_X d'un ensemble de spins différent. Dans notre cas, I = ^1H et S = ^{13}C. Nous utiliserons par conséquent la notation I_x = H_x et S_x = C_x. Lorsque le système est refroidi à très basse température (1.2 K), les raies spectrales des noyaux s'élargissent considérablement et la puissance des impulsions radiofréquence utilisées lors de la polarisation croisée n'est plus suffisante pour exciter l'ensemble des spins. Ainsi, la conversion de H_x à C_x n'est pas idéalement effectuée au cours de la CP et cette imperfection donne lieu à la création de

cohérences antiphases telles que $3^{-1/2}C_xD_z$, $3^{-1/2}C_xD'_z$ et doublement antiphases telles que $2^{-1/2}C_xD_zD'_z$ dans un système de spin CD_2 dans lequel il y a trois spins isolés : ^{13}C, D et D'. Après l'impulsion finale de la CP qui vise à induire une nutation de l'aimantation du plan transverse vers l'axe aligné au champ magnétique (soit un angle de $-\pi/2$), des cohérences de spin d'ordre deux et trois ayant un temps de relaxation longitudinale plus long que celle de l'aimantation de Zeeman du spin du deutérium sont créées. Ces cohérences crées lors de la CP correspondent à des termes tels que : $3^{-1/2}C_zD_z$, $3^{-1/2}C_zD'_z$ and $2^{-1/2}C_zD_zD'_z$.[19]

Une fois que le système de spin polarisé avec la CP a atteint sa polarisation maximale, l'échantillon est dissout avec 5 ml de D_2O chauffé à 180°C sous une pression de 10.5 bar. Le transfert ultérieur du mélange hyperpolarisé en 10 s en passant par un tunnel magnétique de 0.9 T[20] jusqu'à un spectromètre RMN de 400 ou 800 MHz est suivi par la détection des noyaux ^{13}C à température ambiante.

Lors de la détection de l'échantillon hyperpolarisé, nous pouvons observer une asymétrie dans le spectre du ^{13}C. En effet, les transitions à bas champ (L_1, L_2) du quintuplet du groupement $^{13}CD_2$ dans le spectre en solution à haute température ont des intensités plus importantes que celles attendues (1 :2 :3 :2 :1), tandis que les transitions à champ fort (L_5, L_6) voient leur intensité atténuée. Ce phénomène est illustré par la figure 2 sur laquelle est représenté le spectre expérimental du quintuplet du ^{13}C hyperpolarisé de l'éthanol-d_6 à différents intervalles de temps après dissolution.

Pendant et après la dissolution, plusieurs processus interviennent. Nous avons interprété l'asymétrie observée dans le spectre du ^{13}C comme provenant de la projection des cohérences $2^{-1/2}C_zD_zD'_z$, $3^{-1/2}C_zD_z$ et $3^{-1/2}C_zD'_z$ sur des états ayant des durées de vie bien plus longues que les deux termes $3^{-1/2}/2D_z$ et $3^{-1/2}/2D_z'$ qui correspondent à l'aimantation longitudinale de Zeeman. Ceux-ci ont un temps de relaxation $T_1(D_z) = T_1(D_z') = 0.7$ s dans le groupe CD_2 de l'éthanol-d_6 dans nos conditions expérimentales. Un déséquilibre des populations entre les états symétriques et antisymétriques donne lieu à des états dits de « longue durée de

vie » dans le système CD_2. Ces états impliquent une différence de population au sein du sous-système D_2 entre le sextet qui est symétrique et le triplet qui, lui, est antisymétrique. Nous ferons référence à ces états en tant que STI (*sextet-triplet imbalance*). Ces STI peuvent affecter les intensités des cinq transitions du quintuplet du ^{13}C après dissolution. Etant donné que leur relaxation est bien plus lente que celle des termes $3^{-1/2}/2D_z$ et $3^{-1/2}/2D'_z$, l'effet des STI est observable longtemps après la dissolution.[19, 21-22]
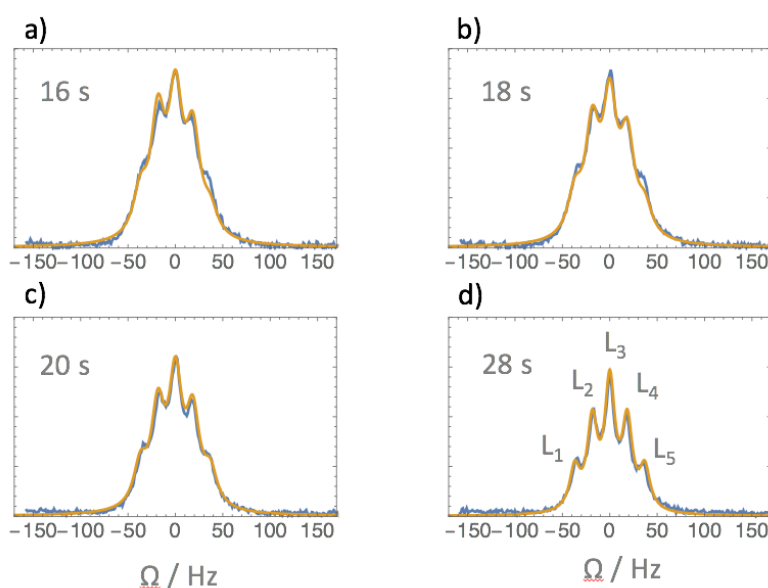
Figure 1.2. Bleu : Spectres expérimentaux montrant les quintuplets du ^{13}C du groupe $^{13}CD_2$ de l'éthanol-d_6 hyperpolarisé, détectés à des intervalles de 16, 18, 20 et 28 s après dissolution. Jaune : spectres simulés par SpinDynamica de Mathematica ™. Les transitions individuelles sont étiquetées de L_1 à L_5, des champs faibles au champs forts (c'est-à-dire des hautes aux basses fréquences, ou de gauche à droite, voir figure d). Dans l'approximation des hautes températures qui prédomine normalement à température ambiante, le groupement CD_2 engendre un quintuplet symétrique respectant les rapports 1:2:3:2:1.

Après avoir traité l'hyperpolarisation du groupement $^{13}CD_2$, nous nous intéresserons au groupement $^{13}CD_3$ pour lequel les mêmes principes peuvent être appliqués. Pendant la polarisation du ^{13}C générée par la CP, la faible impulsion RF est insuffisante pour découpler l'interaction dipolaire entre le carbone et les noyaux de deutérium voisins. Par conséquent, la CP ^1H-^{13}C génère des cohérences hétéronucléaires entre le carbone et le deutérium de la

forme : $\frac{1}{3}C_zD_z$, $6^{-1/2}C_zD_zD_z'$, et encore $\frac{1}{2}C_zD_zD_z'D_z''$, et toutes les permutations qui s'y rapportent. Ces opérateurs projettent des STI sur des états de longue durée de vie. De fait, ils peuvent survivre plus longtemps que l'aimantation de Zeeman du spin des noyaux de deuterium présents dans le groupement CD_3.[23] Lors de nos expériences, une fois la dissolution effectuée, un septuplet asymétrique du ^{13}C a été observé à la place du septuplet symétrique attendu (1:3:6:7:6:3:1). Le phénomène est tout à fait similaire aux observations faites précédemment pour le groupement CD_2. Le multiplet provenant du spin du ^{13}C des groupes $^{13}CD_3$ du DMSO-d_6 après dissolution et transféré dans un spectromètre conventionnel de 400 MHz est illustré sur la figure 3. Il est constitué de sept raies numérotées de L_1 à L_7 de gauche à droite, en utilisant la même convention que pour le CD_2.
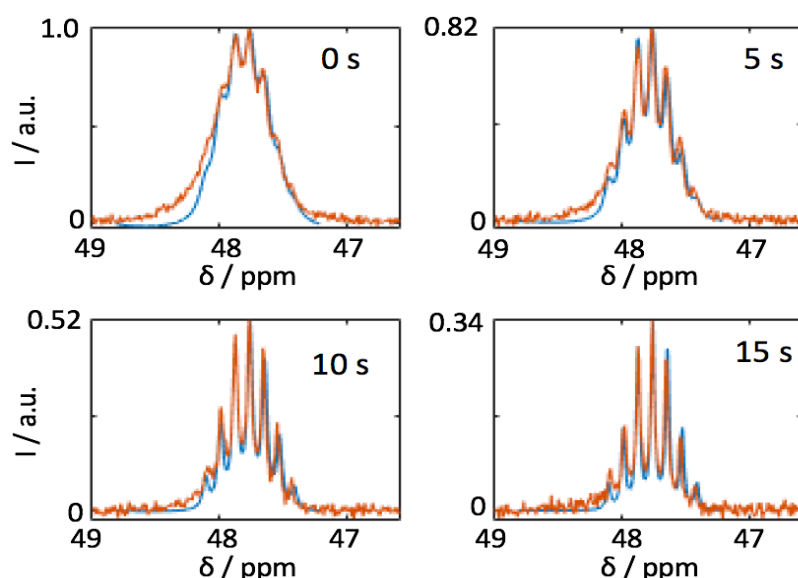
Figure 3. (orange) Signaux correspondant aux groupements $^{13}CD_3$ du DMSO-d_6 hyperpolarisé observés expérimentalement et détectés à des intervalles de 0, 5, 10 et 15 s après dissolution. (bleu) simulations réalisées avec SpinDynamica de Mathematica ™. Immédiatement après la dissolution (t = 0 s), le septuplet présente une importante asymétrie. 15 s plus tard, l'équilibre thermique est rétabli, les raies du septuplet du spectre recouvrent la répartition des amplitudes 1:3:6:7:6:3:1. Notez que l'échelle verticale est progressivement réduite de 100%, à 82, 52 et 34%.

Le groupe $^{13}CD_3$ correspond à un système de type SI_3 avec des spins nucléaires S = 1/2 et I = 1. Il appartient au groupe de symétrie C_{3v}. L'asymétrie observée dans

le spectre du ^{13}C du groupement $^{13}CD_3$ provient de la différence des populations de quatre sous-ensembles distincts A, E1, E2 et B qui correspondent aux représentations irréductibles des sous-ensembles du groupe de symétrie C_{3v}. Un tel déséquilibre dans les populations a été généré au sein des groupements CD_3 du DMSO-d_6 et de l'acétone-d_6. Ce déséquilibre entre les sous-ensembles des méthyles deutériés correspond à un SSI (*spin-state imbalance*) c'est-à-dire à un déséquilibre des états de spin. Sa durée de vie peut être jusqu'à 20 fois supérieure au temps de relaxation spin-réseau (T_1) des noyaux de deutérium.

Pour les groupes CD_2 et CD_3, le déséquilibre des populations peut être déterminé indirectement par l'asymétrie des spectres du ^{13}C et la durée de vie d'un tel état transitoire peut être obtenue en suivant la décroissance de cette asymétrie.[24-27]

La durée de vie $T_{SSI}(D_3)$ permet d'accéder à l'énergie d'activation de la rotation du groupement méthyle. En effet, plus la rotation du groupe CD_3 est rapide, plus la séparation des quatre sous-ensembles de symétrie du groupe C_{3v} est assurée. Ainsi, une longue durée de vie $T_{SSI}(D_3)$ constitue une mesure indirecte de la rotation rapide des méthyles.

Après un certain temps, tous les termes comprenant un opérateur de spin du deutérium relaxent vers leur valeur d'équilibre et seule la magnétisation C_z, initialement peuplée par la CP, demeure. Les proportions des amplitudes correspondant aux hautes températures sont donc rétablies (Fig. 2 et 3).

Lorsque le système est polarisé directement, c'est-à-dire que l'on n'a pas recours à la CP mais que les ^{13}C sont polarisés spontanément par l'effet du pompage des microondes sur les différents réservoirs de spin, nous n'observons pas d'asymétrie. Cela s'explique par le fait que la polarisation directe du ^{13}C et du ^2D sont peu efficaces comparées à la CP. Ceci prouve que les produits d'opérateurs hétéronucléaires dans les groupes CD_2 et CD_3 ne sont pas dus à des processus de PDN mais sont bel et bien créés pendant la polarisation croisée à basse température, le champ RF appliqué au ^{13}C n'étant pas assez intense pour découpler les spins des carbones et des deutériums. C'est la raison pour laquelle

ces effets sont difficiles à détecter en RMN conventionnelle lorsque le système n'a pas été hyperpolarisé. Les simulations effectuées avec SpinDynamica reproduisent particulièrement bien l'évolution temporelle du signal du carbone observée dans les différents cas expérimentaux.

Pour conclure, nous démontrons que l'efficacité de la polarisation croisée peut être grandement améliorée par l'extinction de l'irradiation microonde avant d'effectuer la polarisation croisée à 1.2 K. Nous avons également démontré comment un noyau de deutérium couplé à un ^{13}C peut être indirectement polarisé par la CP à cause des impulsions radiofréquence faibles dans le cas des groupements CD_2 et CD_3. Ces observations offrent de nouvelles perspectives à la PDN en ajoutant un nouveau noyau à la liste de nos noyaux observables. Ainsi, la RMN du deutérium avec une sensibilité accrue et des échelles de temps plus longues devient possible.

Références

1.   Rabi, I. I.; Millman, S.; Kusch, P.; Zacharias, J. R., The Molecular Beam Resonance Method for Measuring Nuclear Magnetic Moments. The Magnetic Moments of 3Li6, 3Li7 and 9F19. *Phys. Rev.* **1939,** *55* (6), 526-535.

2.   Kellogg, J. M. B.; Rabi, I. I.; Ramsey, N. F.; Zacharias, J. R., The Magnetic Moments of the Proton and the Deuteron. The Radiofrequency Spectrum of ${\mathrm{H}}_{2}$ in Various Magnetic Fields. *Phys. Rev.* **1939,** *56* (8), 728-743.

3.   Bloch, F.; Hansen, W. W.; Packard, M., Nuclear Induction. *Phys. Rev.* **1946,** *69* (3-4), 127-127.

4.   Purcell, E. M.; Torrey, H. C.; Pound, R. V., Resonance Absorption by Nuclear Magnetic Moments in a Solid. *Phys. Rev.* **1946,** *69* (1-2), 37-38.

5.   Overhauser, A. W., Polarization of Nuclei in Metals. *Phys. Rev.* **1953,** *92* (2), 411-415.

6.   Carver, T. R.; Slichter, C. P., Polarization of Nuclear Spins in Metals. *Phys. Rev.* **1953,** *92* (1), 212-213.

7.   Hall, D. A.; Maus, D. C.; Gerfen, G. J.; Inati, S. J.; Becerra, L. R.; Dahlquist, F. W.; Griffin, R. G., Polarization-Enhanced NMR Spectroscopy of Biomolecules in Frozen Solution. *Science* **1997,** *276* (5314), 930.

8.   Griffin, R. G.; Prisner, T. F., High field dynamic nuclear polarization-the renaissance. *Phys. Chem. Chem. Phys.* **2010,** *12* (22), 5737-5740.

9.   Ardenkjaer-Larsen, J. H.; Leach, A. M.; Clarke, N.; Urbahn, J.; Anderson, D.; Skloss, T. W., Dynamic nuclear polarization polarizer for sterile use intent. *NMR Biomed.* **2011,** *24* (8), 927-932.

10.   Hartmann, S. R.; Hahn, E. L., Nuclear Double Resonance in the Rotating Frame. *Phys. Rev.* **1962,** *128* (5), 2042-2053.

11.   Pines, A.; Gibby, M. G.; Waugh, J. S., Proton-Enhanced Nuclear Induction Spectroscopy. A Method for High Resolution NMR of Dilute Spins in Solids. *J. Chem. Phys.* **1972,** *56* (4), 1776-1777.

12.   Pines, A.; Gibby, M. G.; Waugh, J. S., Proton-enhanced NMR of dilute spins in solids. *J. Chem. Phys.* **1973,** *59* (2), 569-590.

13.   Carravetta, M.; Johannessen, O. G.; Levitt, M. H., Beyond the T1 limit: singlet nuclear spin states in low magnetic fields. *Phys. Rev. Lett.* **2004,** *92* (15), 153003.

14.   Carravetta, M.; Levitt, M. H., Theory of long-lived nuclear spin states in solution nuclear magnetic resonance. I. Singlet states in low magnetic field. *J. Chem. Phys.* **2005,** *122* (21), 214505.

15.   Bowen, S.; Hilty, C., Rapid sample injection for hyperpolarized NMR spectroscopy. *Phys. Chem. Chem. Phys.* **2010,** *12* (22), 5766-5770.

16.   Kurzbach, D.; Weber, E. M.; Jhajharia, A.; Cousin, S. F.; Sadet, A.; Marhabaie, S.; Canet, E.; Birlirakis, N.; Milani, J.; Jannin, S.; Eshchenko, D.; Hassan, A.; Melzi, R.; Luetolf, S.; Sacher, M.; Rossire, M.; Kempf, J.; Lohman, J. A.; Weller, M.; Bodenhausen, G.; Abergel, D., Dissolution dynamic nuclear polarization of deuterated molecules enhanced by cross-polarization. *J. Chem. Phys.* **2016,** *145* (19), 194203.

17.   Jhajharia, A.; Weber, E. M.; Kempf, J. G.; Abergel, D.; Bodenhausen, G.; Kurzbach, D., Communication: Dissolution DNP reveals a long-lived deuterium spin state imbalance in methyl groups. *J. Chem. Phys.* **2017,** *146* (4), 041101.

18.   Schmidt-Rohr, K.; Spiess, H. W., *Multidimensional Solid-state NMR and Polymers*. Academic Press: 1994.

19.   Bernatowicz, P.; Kruk, D.; Kowalewski, J.; Werbelow, L., 13C NMR lineshapes for the 13C2H2H' isotopomeric spin grouping. *Chemphyschem* **2002,** *3* (11), 933-8.

20.   Milani, J.; Vuichoud, B.; Bornet, A.; Mieville, P.; Mottier, R.; Jannin, S.; Bodenhausen, G., A magnetic tunnel to shelter hyperpolarized fluids. *Rev. Sci. Instrum.* **2015,** *86* (2), 024101.

21.   Werbelow, L. G.; Morris, G. A.; Kumar, P.; Kowalewski, J., Cross-correlated quadrupolar spin relaxation and carbon-13 lineshapes in the (13)CD(2) spin grouping. *J. Magn. Reson.* **1999,** *140* (1), 1-8.

22.   Kowalewski, J.; Mäler, L., *Nuclear spin relaxation in liquids : theory, experiments, and applications.* New York (N.Y.) : Taylor & Francis: 2006.

23.   Kurzbach, D.; Weber, E. M. M.; Jhajharia, A.; Cousin, S. F.; Sadet, A.; Marhabaie, S.; Canet, E.; Birlirakis, N.; Milani, J.; Jannin, S.; Eshchenko, D.; Hassan, A.; Melzi, R.; Luetolf, S.; Sacher, M.; Rossire, M.; Kempf, J.; Lohman, J. A. B.; Weller, M.; Bodenhausen, G.; Abergel, D., Dissolution Dynamic Nuclear Polarization of Deuterated Molecules Enhanced by Cross-Polarization *J. Chem. Phys.* **2016** *145* (19), 194203*.*

24.   Feng, Y.; Davis, R. M.; Warren, W. S., Accessing long-lived nuclear singlet states between chemically equivalent spins without breaking symmetry. *Nat. Phys.* **2012,** *8* (11), 831-837.

25.   Pileio, G.; Carravetta, M.; Levitt, M. H., Storage of nuclear magnetization as long-lived singlet order in low magnetic field. *Proc. Natl. Acad. Sci. U.S.A.* **2010,** *107* (40), 17135-9.

26.   Pileio, G.; Levitt, M. H., Theory of long-lived nuclear spin states in solution nuclear magnetic resonance. II. Singlet spin locking. *J. Chem. Phys.* **2009,** *130* (21), 214501.

27.   Kiryutin, A. S.; Zimmermann, H.; Yurkovskaya, A. V.; Vieth, H. M.; Ivanov, K. L., Long-lived spin states as a source of contrast in magnetic resonance spectroscopy and imaging. *J. Magn. Reson.* **2015,** *261*, 64-72.

1. Introduction: NMR to Dissolution DNP

1.1 General Introduction

NMR spectroscopy nowadays is one of the most useful techniques for the investigation of the structure, dynamics, physical and chemical properties of molecules in solution and in solids. Additionally, it has a vast range of applications in magnetic resonance imaging (MRI). However the technique is limited by its low sensitivity and consequently weak NMR signals that lead to long experimental times. Some important magnetically active spins like ^{13}C and ^{15}N are difficult to observe with sufficient sensitivity, due to their low gyromagnetic ratios (γ) and low natural abundance. To avoid the long experimental times and to improve the sensitivity, several improvements have been realized in the past, e. g., by increasing the magnetic field of the NMR instrument or by using so-called cryo-probes that reduce the electronic noise in the spectrometer's receiver circuits. Yet, the nuclear polarization, which underlies signal intensity in NMR, was still limited by low gyromagnetic ratios. A frequently used "bypass" around this problem is heteronuclear correlation spectroscopy, where one uses high-γ nuclei like protons to indirectly detect other nuclei that have weaker magnetic moments. A prominent example is the

heteronuclear single quantum correlation (HSQC) experiment, introduced by Ruben and Bodenhausen in 1980,[1] in which the relatively large proton magnetization is transferred to another nucleus to "read" its properties and subsequently back-transferred for detection to the protons, the signals of which are modulated by the frequency of the heteronuclei.

This thesis focuses on yet another technique aiming at signal enhancement. A dramatic effect can be achieved by using a technique called "*dynamic nuclear polarization*" (DNP). The principle idea of this technique is to use the huge magnetic moment of unpaired electrons - compared to nuclear spins - and to transfer it to the nuclear spins to achieve a large nuclear magnetization. A significant enhancement can be achieved for ^{1}H and as well for low-γ nuclei such as ^{13}C, ^{15}N, etc.. In 2003, a novel technique that became known as dissolution-DNP was developed by Ardenkjaer-Larsen and co-workers.[2] This method can provide enhancements by a factor of up to four orders of magnitude for ^{13}C in liquid state at room temperature. ^{13}C is present in most biological molecules and features favorable relaxation properties rendering it a suitable candidate for DNP. There are several DNP systems available to hyperpolarize ^{13}C, e. g., the Hypersense™,[3] a commercially available dissolution-DNP setup working at 3.5 T, or the so-called Spinlab system. For these commercially available systems, Trityl, a radical with a narrow electron paramagnetic resonance (EPR) line, is used as a polarizing agent,[4-5] which can efficiently polarize low-γ nuclei like ^{13}C but the time necessary to achieve the highest polarization levels can be quite long.

To overcome the latter problem, some polarizers have been designed[6-8] that allow the use of derivatives of 2,2,6,6-tetramethyl piperidine-1-oxyl (TEMPO) radical to hyperpolarize the high-γ nuclear spins and transfer their polarization to low-γ nuclear spins. To this end, Jannin and co-workers have introduced a combination of cross polarization (CP) with dissolution-DNP,[9-14] where proton spins are polarized directly and their polarization is subsequently transferred to ^{13}C at cryogenic temperatures near 1.2 K. Dissolution-DNP can be very efficient using CP to polarize ^{13}C nuclei, much faster than with Trityl radicals. Chapter 2 will briefly discuss the already implemented ideas of cross polarization and their

combination with dissolution-DNP. A later discussion will show how to improve CP at 1.2 K to enhance the polarization, i. e., the signal intensity of low-γ nuclear spins. To further optimize CP, this thesis will discuss an interruption of the microwave irradiation prior to the CP to allow the electron's polarization to relax back to the Boltzmann thermal equilibrium. This allows for an increase in the nuclear relaxation time in the rotating frame and therefore for extended CP contact times, which can enhance the CP efficiency, so that more ^{13}C polarization can be achieved.

Even though dissolution-DNP can provide a huge enhancement of NMR signals it is still limited by the lifetime of the hyperpolarized state of the molecules, which is determined by the spin-lattice relaxation time constant T_1, which is usually rather short, on the order of seconds or minutes. Hence, either the use of molecules that have longer T_1 values, i. e., low-γ nuclei like ^{13}C and ^{15}N, or storage of the hyperpolarized state can make dissolution-DNP (D-DNP) into a more efficient method. To this end, long-lived states (LLS), first demonstrated by Levitt and co-workers,[15-16] can be employed as they can survive for longer time periods, usually defined as T_{LLS}. The application of LLS has already been demonstrated successfully for two spin-½ nuclei in combination with D-DNP to enhance the sensitivity in drug screening experiments by Buratto et al.[17] but beyond spin-½ nuclei, this thesis focuses on quadrupolar nuclei, i. e., deuterium with spin 1. We introduce a new class of long-lived states involving two or three deuterium spins, which can extend the lifetime of the deuterium Zeeman magnetization by a factor up to 20. This can help the investigation of deuterium properties indirectly via ^{13}C liquid state NMR.

Chapter 3 will discuss the theory and observations of long-lived states involving deuterium nuclei in ^{13}CD$_2$ groups. This is based on our observation that applying ^{1}H-^{13}C cross-polarization to deuterated methylene groups using DNP at 1.2 K yields an asymmetry in ^{13}C NMR multiplets in liquid-state NMR after dissolution. We could trace this asymmetry back to a population imbalance between symmetric and antisymmetric spin manifolds, which is hardly possible to be populated without DNP. An imperfection in the CP process gives rise to multispin

terms during CP that can be projected onto states that have longer lifetimes than deuterium Zeeman magnetization and that can be observed indirectly through ^{13}C NMR. Simulations have been performed by using the SpinDynamica software package to monitor the evolution of the asymmetry of the multiplet patterns as a function of time. Both experimental observations and simulations show that after a sufficiently long time interval, the asymmetry of the ^{13}C spectra vanishes because of relaxation of the non-equilibrium deuterium states. We describe these long-lived states in $^{13}CD_2$ groups as sextet-triplet imbalance (STI).[18]

As an imbalance between symmetric and antisymmetric spins states, described as A/E imbalance in $^{13}CH_3$ has also been discussed earlier by Levitt, Dumez and co-workers.[19-20] We subsequently discussed a similar phenomenon for deuterated methyl groups that will be discussed in chapter 4. For a $^{13}CD_3$ group, the long-lives states can be defined as a spin state imbalance (SSI), based on population imbalances between different irreducible representations of the C_{3v} point group. The lifetimes of the long-lives states can provide information about the activation energy of methyl group rotation. Long-lived states involving deuterium spins can overcome limitations of quadrupolar NMR.

In the following, I will briefly introduce the relevant theories for the description of the findings reported herein, including a historical perspective of DNP. Subsequently, I will present and discuss the results I gathered and I will conclude the thesis with some related future perspectives.

1.2 Theory

Nuclear magnetic resonance (NMR) is based on the concept of a nuclear spin ensemble immersed in a magnetic field. In 1922, Otto Stern and Walther Gerlach observed that in an inhomogeneous magnetic field, beams of silver atoms could be separated according to the orientations of their electronic angular momentum. This experimental demonstration of quantization of the angular momentum is known as the Stern-Gerlach experiment. Later in 1938, Isidor Rabi modified the beam technique to study the magnetic properties of atoms, i.e., their

magnetic moments.[21] A lithium chloride (LiCl) molecular beam was passed through a vacuum chamber and Rabi named the observed phenomenon "Nuclear magnetic resonance".[22] In 1946, Bloch[23] and Purcell [24] independently improved this technique by applications to liquids and solids in bulk . The following section includes the discussion of spin polarization, which underlies spin magnetization in NMR, and how DNP can enhance this polarization.

1.2.1 Nuclear spin polarization:

Spin is an intrinsic property of elementary particles, which can be more precisely called spin angular momentum. The spin angular momentum is characterized by the nuclear spin quantum number I. The magnitude of I is given as:

$$|I| = \hbar\sqrt{I(I+1)} \qquad (1.1)$$

where $\hbar = h/2\pi = 1.054 \times 10^{-34}$ Js is the reduced Planck constant. The nuclear spin quantum number I can either be integer or half integer. Nuclei with a spin quantum number $I = \frac{1}{2}$ are the most frequent subject of investigation in NMR spectroscopy and are well understood. This includes, e. g., the stable isotopes ^{1}H, ^{13}C, ^{15}N and ^{19}F. In contrast, nuclei with a spin quantum number $I = 0$ are not detectable by NMR. A third case is constituted by nuclei with $I > \frac{1}{2}$, which are often called quadrupolar nuclei. These quadrupolar nuclei feature a non-spherical charge distribution, which produces an electric quadrupolar moment. As a result, quadrupolar spins display fast relaxation towards equilibrium after excitation - a phenomenon which will be of central importance for this thesis.

We may introduce an arbitrary direction z, along which we align the static magnetic field B_0 present in any NMR spectrometer. I is quantized along this direction. This quantization of the spin angular momentum allows for discrete values of the so-called z-component of the nuclear magnetic moment. The z-component of I may be expressed as:

$$I_z = m_I \hbar \qquad (1.2)$$

where $m_I = -I, -I+1, \ldots, I-1, I$ represents the magnetic quantum number

with 2I+1 possible discrete values.

Nuclei with non-zero spin posses nuclear magnetic moments μ given by

$$\mu_I = g_n\beta_n\vec{I} = \gamma_I\vec{I} \quad (1.3)$$

with the nuclear magneton β_n = 5.051×10^{-27} J/T, γ_I and g_n denote the characteristic properties of the nuclear gyromagnetic ratio and the nuclear g-factor, respectively. The gyromagnetic ratio is a constant quantity for each spin and can have a positive or negative value, so that μ_I and I can be oriented parallel or antiparallel along the z-direction.

The interaction of a magnetic substance with the external magnetic field $\vec{B}_0 = B_0\hat{z}$, is expressed in terms of the magnetic moment μ. It is called Zeeman interaction and the corresponding Hamiltonian is given by:

$$H_{nz} = -\vec{\mu}_I \cdot \vec{B}_0 = -g_n\beta_n\vec{I}_zB_0 = -\gamma_I\vec{I}_zB_0 \quad (1.4)$$

Since I_z is quantized, the allowed energy states can only have certain discrete values, too. The energy states are given by the expression:

$$E_m = -\gamma_I\vec{I}_zB_0 = -\gamma_I m_I\hbar B_0 = -\hbar\omega_I m_I \quad (1.5)$$

where $\omega_I = \gamma_I B_0$ is the Larmor precession frequency of the nuclei. There are 2I+1 (-I to I) possible energy levels, denoted as Zeeman energy states.

Magnetic moments μ precess around a magnetic field B_0 aligned along the z-direction with an angular frequency ω_I such that the energy of the states depends on the relative orientation of B_0 and μ. An energetic minimum is reached when the magnetic moment μ is parallel (or antiparallel if γ_I <0) to the field B.

If we consider a system of N_I identical nuclei with non-zero spins, all spins are randomly oriented in absence of a magnetic field. When a magnetic field B_0 is applied, this give rise to the abovementioned 2I+1 non-degenerate energy levels and the nuclear spins adopt preferred orientations. As an example, nuclei with spin ½ in the presence of the magnetic field are distributed between two Zeeman

energy levels corresponding to $m_I = \pm\ \frac{1}{2}$ with energy $E_{\pm 1/2} = \mp\hbar\omega_I/2$. These energy levels can be denoted as α and β corresponding to low and high energies,. At thermal equilibrium, the Boltzmann distribution between the two levels is given by:

$$\frac{N_\beta}{N_\alpha} = \exp\left(-\frac{(E_\beta - E_\alpha)}{k_B T}\right) = exp\left(\frac{\hbar\omega}{k_B T}\right) \quad (1.6)$$

where E_α and E_β represent the spin energy in the α and β states and N_α, N_β corresponds to the populations in the α and β states, respectively. The Boltzmann constant is $k_B = 1.38\times10^{-23}$ J/K and T is the temperature of the spin system.
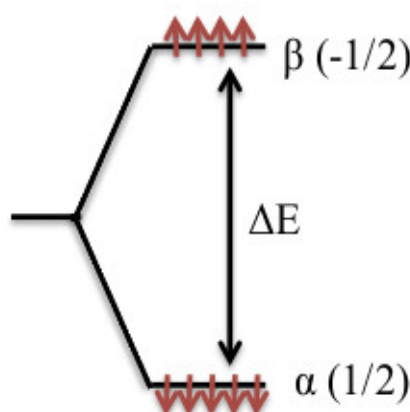
Figure 1.1. Energies of the two states of a spin 1/2 in the presence of an external magnetic field.

Figure 1.1 exemplifies the distribution of nuclei between the two states in a system with spin- ½ in the presence of external magnetic field.

The energy difference between α and β states is:

$$\Delta E_m = \gamma_I \hbar B_0 \quad\quad\quad (1.7)$$

The difference between the populations of any two adjacent energy levels provides the polarization of the spin system. As the magnetic moment of nuclear spins is quite small, the polarization levels obtainable in modern NMR spectrometers operating at some tens of Tesla is quite small - in the range of a

few parts per million (ppm).

In the framework of statistical thermodynamics, the equilibrium Boltzmann distribution that defines the population of the energy states can be expanded:

$$\frac{N_{\mathrm{m}}}{N} = \frac{\exp(-E_m/k_{\mathrm{B}}T)}{\sum_{m=-I}^{I}\exp(-E_m/k_BT)} = \frac{\exp(-\gamma_I m_{\mathrm{I}}\hbar B_0/k_{\mathrm{B}}T)}{\sum_{m=-I}^{I}\exp(-\gamma_I m_{\mathrm{I}}\hbar B_0/k_{\mathrm{B}}T)}$$

$$\approx \frac{1}{(2I+1)}\left(1 + \frac{\gamma_I m_{\mathrm{I}}\hbar B_0}{k_{\mathrm{B}}T}\right) \qquad (1.8)$$

where N_{m} is the number of spins in the mth energy state, N is the total number of spins and T is the temperature in Kelvin. The denominator defines the state function of the thermodynamic system. By applying a Taylor series expansion, we can thus obtain the expression for the spin polarization.

The spin polarization of a system with N_{I} spins is defined as:

$$P_{\mathrm{I}} = \frac{N_+ - N_-}{N_+ + N_-} \qquad (1.9)$$

where N_+ and N_- are number of spins in lower and higher energy states. Using the Boltzmann distribution we find for the nuclear polarization:

$$P_I = \frac{1}{I}\frac{\sum_{m=-I}^{I} m_I \exp(-E_m/k_BT)}{\sum_{m=-I}^{I}\exp(-E_m/k_BT)} \qquad (1.10)$$

We see directly that the population of states depends on the magnetic field strength and the temperature of the system. Population differences between the two states increase with higher magnetic fields and at lower temperatures.

Thus, in cases of a system with spin- ½, $m_{\mathrm{I}} = \pm½$ with energy levels $E_{\pm 1/2} = \mp\hbar\omega_I/2$, the polarization (using equations 1.6 and 1.9) is:

$$P_{\mathrm{I}} = \frac{N_\alpha - N_\beta}{N_\alpha + N_\beta} = \frac{1 - N_\beta/N_\alpha}{1 + N_\beta/N_\alpha}$$

$$= \tanh\left(\frac{\hbar\omega_{\mathrm{I}}}{2k_{\mathrm{B}}T}\right) = \tanh\left(\frac{\hbar\gamma_I B_0}{2k_{\mathrm{B}}T}\right) \qquad (1.11)$$

It is important to note that the NMR signal intensity is proportional to the

polarization of the spin system so that high polarization levels lead to high signal intensities. Indeed, the longitudinal magnetization M_Z, which is read by radio frequency pulses in NMR is directly proportional to P_I.

At very high temperatures close to infinity, all the energy levels are equally populated and the polarization is zero. In contrast, at very low temperatures near to zero Kelvin, the lower energy state will be more populated compared to the higher states and the polarization will be close to 1.

The magnetic field dependence of the polarization can be traced back to its dependence on the gyromagnetic ratio of spins as evident from eq. 1.11. As a strong signal intensity is very desirable in NMR, improvement of the polarization is a common target. To this end, a plethora of ingenious techniques have been imagined in the past. As mentioned in the general introduction it is possible to transfer the polarization from a spin with a high gyromagnetic ratio to low gyromagnetic ratio spins. Under typical experimental conditions, this can be from ^1H to ^{13}C or ^{15}N. In liquid state NMR this transfer can be done via insensitive nuclei enhanced by polarization transfer (INEPT)[25-26] or nuclear Overhauser enhancement (NOE)[27-28] and in solid state NMR by cross polarization (CP)[29]. Yet, the maximum enhancement is always determined by the spin with the highest γ value. Therefore, DNP makes use of electron spins as these feature a very high gyromagnetic ratio in comparison to any nuclei as electrons are much lighter and $\gamma = q/2m$. The gyromagnetic ratio of an electron is 668 times larger than that of a proton. Hence, at cryogenic temperatures 1.2 K and magnetic field at 6.7 T, the thermal equilibrium polarizations of unpaired electrons, protons and ^{13}C nuclei are 99.89%, 0.57% and 0.020% respectively. Due to the low energy of nuclear spins, the high temperature approximation can be applied to equation 1.11 leading to:

$$P_I = \tanh\left(\frac{\hbar\omega_I}{2k_B T}\right) \approx \frac{\hbar\omega_I}{2k_B T} \qquad (1.12)$$

The bulk nuclear magnetic moment M can be defined as the vector sum of μ_i of all individual nuclei

$$\vec{M} = \sum_{i=1}^{N} \mu_i \quad (1.13)$$

Table 1.1. The characteristic parameters of a few spins are shown.

Spin system	Spin	Natural Abundance	Gyromagnetic ratio $\gamma/2\pi$ (MHz/T)
Electron (e^-)	1/2		-28024.954
^{1}H	1/2	99.98%	42.576
^{2}D	1	0.02%	6.536
^{13}C	1/2	1.1%	10.705

Table 1.1 shows some characteristic parameters such as spin quantum numbers, natural abundances and gyromagnetic ratios of a few selected spins.

In the presence of a magnetic field B_0, the z-component of the magnetization M_0 is given by:

$$M_0 = \gamma\hbar \sum_{m=-I}^{I} m_I N_I \approx N_I \gamma^2 \hbar^2 B_0 I(I+1)/3k_B T \propto P_I \qquad (1.14)$$

The orientation of the bulk magnetization M is the same as the direction of the static magnetic field. In NMR we detect the sum of the transverse components of the magnetic moment, $M_x + iM_y$, after rotation of M_0 through an angle 90 °, so that the NMR signal intensity is linearly proportional to the polarization.
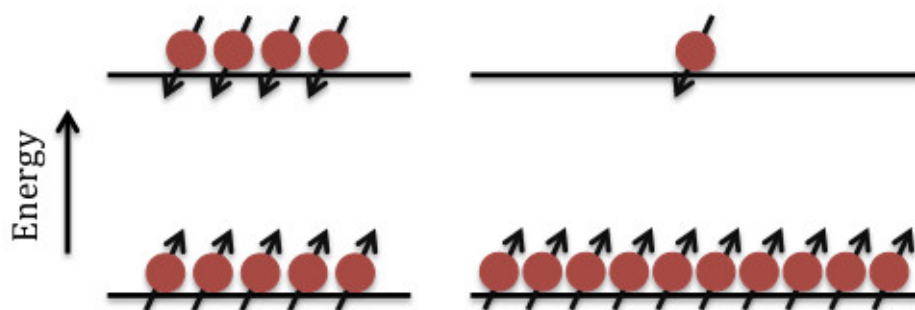

Figure 1.2. Orientation of the spins at thermal equilibrium (left) and in a

hyperpolarized state (right).

In the presence of a typical magnetic field of several tens of Teslas, the nuclear spin polarization is normally very poor as the population difference between two Zeeman energy states is small, and as a result there is a small net magnetization, which is often too weak to be observed. There are several techniques in magnetic resonance to improve the polarization at thermal equilibrium, such as an increase of the magnetic field. The highest commercially available magnetic field will soon be 28.2 T (1.2 GHz for protons), and the polarization of the protons at this field is $P(^1H)$ = 0.0096% at a temperature of 300 K. It is difficult to achieve a proton polarization higher than 0.01% at room temperature by further increasing the magnetic field of the spectrometer, since this becomes extremely expensive. However, an increase in the magnetic field is more useful to improve resolution rather than the polarization.

Additionally, the limitation of NMR by its poor sensitivity is reflected in the signal-to-noise ratio (SNR) of an experiment, which is proportional to $(B_0)^{3/2}$ rather than B_0 but small gains in sensitivity through high field spectrometers are often not worth of cost. These technical and instrumental drawbacks push towards the study of hyperpolarization techniques. Hyperpolarization produces a huge difference in populations between two Zeeman energy states in a nuclear spin system, resulting in an enhancement of the NMR signal. Figure 1.2 exemplifies the differences in populations of Zeeman energy states for an ensemble of spin- ½ nuclei at thermal equilibrium and in a hyperpolarized state.

Additionally, hardware factors can affect the sensitivity, such as improvements of electronics, optimization of the sample volume and concentration, or optimization of cross-polarization pulse sequences that are often used for low-γ nuclei. Combinations of these factors and spin physics can significantly improve the signal-to-noise ratio.

There are several known hyperpolarization methods such as the "brute force" approach[30] (BF), spin exchange optical pumping[31] (SEOP), para-hydrogen induced polarization[32-33] (PHIP), apart from DNP.[34] In the next section, I will focus on dynamic nuclear polarization.

1.2.2 Basic principles of DNP

The aim of dynamic nuclear polarization is to transfer the large Boltzmann equilibrium electron polarization to nuclei under continuous wave (CW) microwave irradiation. Electrons have a high gyromagnetic ratio compared to any nucleus and, thus, under similar experimental conditions, electrons will have a larger Boltzmann polarization than any nucleus. When a nucleus is coupled to electron spins (via so-called hyperfine couplings), the polarization can readily be transferred to the nuclear spins.

The idea of transferring electron polarization to nuclei was first proposed by Overhauser in 1953,[28] and subsequently verified by Carver and Slichter,[35] the phenomenon is nowadays called the Overhauser effect. They demonstrated it experimentally in lithium metals by enhancing intensities of ^{6}Li NMR signals. In the 1950's, many DNP theories were investigated and developed; from a methodological as well as from an experimental perspective. Later in 1957, DNP was also employed for non-conducting solids at low temperatures by Jeffries[36]. In 1958, Abragam and Proctor described the effect of DNP for these non-conducting solids, experimentally and theoretically, calling the described effect the solid effect.[37] During 1960's and 1980's, theories of DNP in solids were explored by Provotorov,[38] Borghini,[39] and Abragam and Goldman[40] leading to the discovery of a new DNP mechanism called thermal mixing.[41] Yet another DNP mechanism, called cross effect, was observed by Hwang and Hill in 1967.[42-43]

In the 1980's and early 90's Wind and Yannoni explored high-resolution experiments in solid-state NMR combining it with DNP. DNP was merged with solid state NMR to achieve enhanced sensitivity and highly resolved spectra of polymers and carbonaceous materials.[44-45] Polymers doped with free radicals and coals or diamonds containing endogenous unpaired electrons showed quite large signal enhancements at a magnetic field near 1.4 T (40 GHz EPR and 60 MHz ^{1}H NMR). Wind and co-workers[44] initially developed DNP for solids in 1985 but it only became known after Griffin's work in 1993. Griffin developed a new

way of DNP at low temperatures using a gyrotron (a stable microwave source), called magic angle spinning (MAS)-DNP.[46-47] MAS-DNP experiments are usually performed at temperatures of approximately 100 K. Subsequently, DNP was augmented when Ardenkjær-Larsen proposed solid-state DNP in combination with liquid-state detection to produce hyperpolarization in liquids[2]. This invention made DNP possible in the field of magnetic resonance imaging (MRI). This method is known as Dissolution-DNP and it has a lot of applications, not only in MRI, but also in liquid-state NMR[48]. As shown in the Figure 1.3 and Table 1.1, electron polarizations are much larger in comparison to nuclear polarizations, so that enhancement factors are significantly improved when temperatures drop below 10 K. Therefore, typical dissolution DNP experiments are performed at cryogenic temperatures between 1.2-4.2 K. In the last decade,[3, 7-8, 49] several dissolution-DNP machines were inspired by and built based on the principles of Ardenkjær-Larsen's design. In our laboratory, we have two dissolution DNP and a MAS-DNP setup. A dissolution DNP Bruker prototype is available with a magnetic field of 6.7 T, a microwave irradiation center frequency of 188.2 GHz with a maximum microwave power 350 mW (provided by an ELVA microwave source). In MAS-DNP, a gyrotron is used to generate microwave fields that saturate the EPR transitions with a microwave power of about 5 W. Our gyrotron is functional at a microwave frequency of 527 GHz optimized for usage with an NMR spectrometer working at a proton Larmor frequency of 800 MHz.

In the following, I will briefly describe the theory of DNP mechanisms such as the solid effect, the cross effect and thermal mixing.

1.2.3 DNP Mechanisms

Several mechanisms of polarization transfer from electrons to nuclear spins can be distinguished according to the source of the electron spin polarization. In a coarse-grained manner we may distinguish: the solid effect (SE), the cross effect (CE) and thermal mixing (TM), although the CE is often described as a special form of TM.
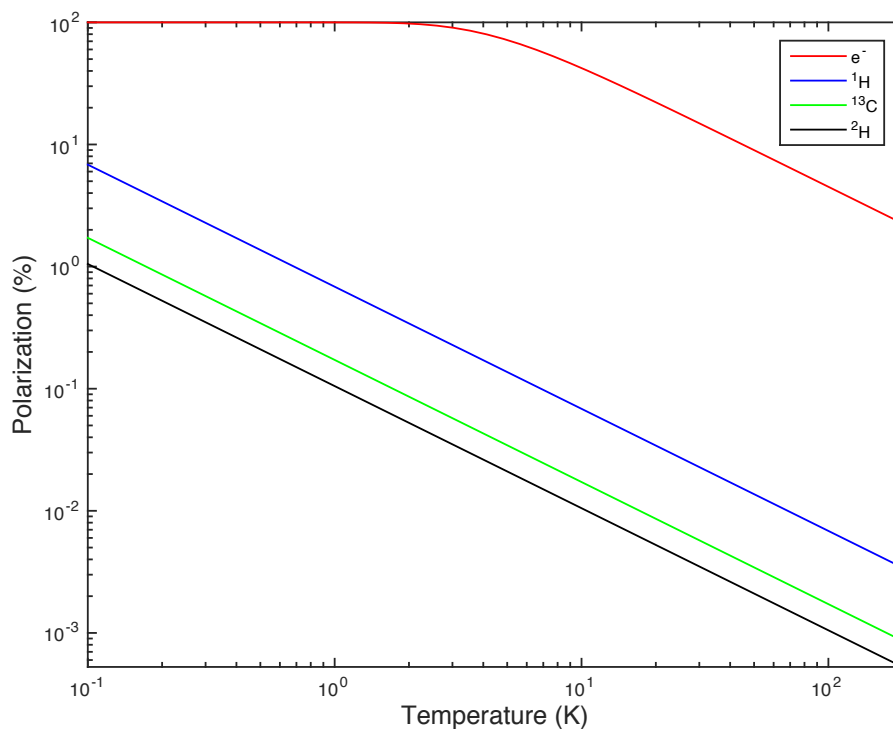
Figure 1.3. Electronic and nuclear (^{1}H, ^{13}C, ^{2}H) polarizations in red, blue, green and black respectively calculated as a function of the temperature at B_0 = 6.7 T.

In my work, I have used TEMPOL as a polarizing agent. Due to its broad EPR line, the most probable dominant mechanism for TEMPOL is a combination of differential solid effect and of the cross effect, as pointed out by Vega and co-workers[50-51]. However other mechanisms, like thermal mixing (TM) can also contribute but are less intense.

Solid Effect

In 1957, Jeffries proposed the transfer of electron polarization to nuclei via the irradiation of forbidden transition[36], which was experimentally demonstrated by Abragam and Proctor in 1958.[37] This is the solid effect (SE) that has been further developed over the following decades.[52-53] The SE is the main mechanism for polarization transfer if the nuclear Larmor frequency ω_n is larger than the

homogeneous (δ) and inhomogeneous EPR line widths (Δ), such that $\omega_n > \delta, \Delta$.[37] For the solid effect, the frequencies of maximum positive and negative polarization enhancement are separated by $2\omega_n$. Significant recent theoretical contributions can be attributed to Wenckebach,[54] Griffin[55] and Vega[50, 56-57] who explains the SE from a quantum mechanical point of view.
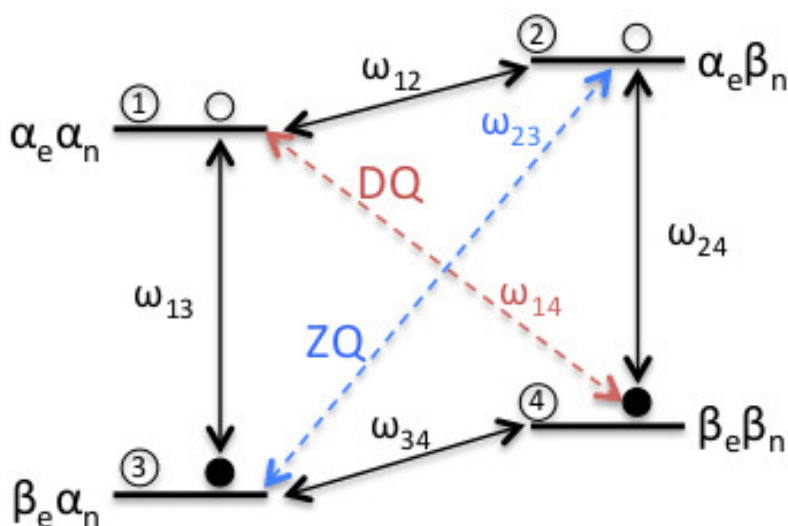

Figure 1.4. Energy-level diagram of a coupled electron-nucleus spin pair ($S = I = \frac{1}{2}$, where S and I corresponds the electron and nuclear spins) to illustrate the solid effect. Solid arrows indicate allowed transitions, and "forbidden" ZQ and DQ e-n transitions are shown by red and blue arrows respectively. Filled and hollow circles represent Boltzmann populations of the system.

The SE[56] involves two spins including an electron and a nuclear spin; the two are coupled by magnetic dipole-dipole interactions. An energy level diagram is shown for the coupled e-n spin system in Figure 1.4. The figure displays an excess or deficit of populations with respect to the saturated state. In case of saturation, the populations of the excited and ground states tend to equalize, and NMR gives no signal. At low temperatures, the electrons are highly polarized ($P(e) \approx 99\%$) in comparison to nuclear spins. ZQ or DQ electron transitions are excited at frequencies of $\omega_{\mu w} = \omega_e + \omega_n$ or $\omega_e - \omega_n$, where ω_e and ω_n denote the electron and nuclear Larmor frequencies, respectively. Through this, the large electron spin polarization can be transferred to the dipole-coupled nucleus. Irradiating at a microwave frequency $\omega_{\mu w} = \omega_e - \omega_n$ will excite the double

quantum (DQ) transition of the e-n spin system. On the other hand, microwave irradiation at a frequency $\omega_{\mu w} = \omega_e + \omega_n$ will excite the zero quantum (ZQ) transition of the spin system. DQ and ZQ transitions are also often called flip-flip and flip-flop transitions, respectively. These transitions are further called "forbidden transitions". However, due to non-secular components of the hyperfine coupling that can become non-negligible if the EPR line width is significantly smaller than the nuclear Larmor frequency, the violation of the law of conservation due to the double spin flips is compensated and these transitions become (partly) allowed.[36, 40] Consequently, a prerequisite for the solid effect to occur is quite a strong microwave irradiation, as second-order transitions are less probable than single-quantum EPR transitions.

For SE, the occurrence of positive, negative or zero enhancements depends on the microwave irradiation frequency. In Figure 1.4, saturation of the DQ transition gives rise to a positive nuclear polarization for both nuclear transitions; similarly, the saturation of the ZQ transition gives rise to a negative nuclear polarization. In principle, it is the superposition of the DQ and ZQ contributions that leads to the overall DNP enhancement at a given microwave frequency. That is why the solid effect only occurs for narrow electron line widths compared to nuclear Larmor frequency, as in such a case the DQ and ZQ transitions cannot be excited at the same time.[40-41] On the other hand, superpositions can entail quite complicated consequences if the line width of the EPR spectrum becomes broader than nuclear Larmor frequency and one needs to employ more complicated models such as the "Differential Solid Effect".[54] Typically, the SE mechanism is the main mechanism for narrow-band polarizing agent such as TAM (triarylmethyl) radicals (often referred to as trityl in the laboratory jargon).

Cross Effect

In the presence of high concentrations of electrons, Hwang and Hill observed another DNP polarization mechanism, called cross effect.[42-43] Both the solid effect and the cross effect can take place under the same experimental

conditions, but unlike the solid effect, the cross effect (CE) is based on allowed transitions instead of forbidden transitions.[58-59] The cross effect mechanism involves a three spin process (two electron spins and one nuclear spin) involving the irradiation of a dipolar coupled electron spin system. For CE we need to fulfill two prerequisites, the electron-electron interactions have to be strong and the homogenous EPR line must be larger than nuclear Larmor frequency. The cross effect can become the dominant mechanism if $\Delta > \omega_n > \delta$, where δ and Δ denotes the homogeneous line width (δ) and inhomogeneous spectral width (Δ) of the EPR line, respectively, and ω_n is nuclear Larmor frequency. A triple spin flip becomes probable if the following condition is fulfilled:

$$|\omega_{e1} - \omega_{e2}| \approx \omega_n \quad (1.15)$$

where ω_{e1} and ω_{e2} are Larmor frequencies of two different electron spins e_1 and e_2. This is possible for example if the orientations of the two electrons (e_1, e_2) are different, which gives rise to distinct EPR frequencies for both electrons. An example of the distribution of energy levels for such a system is shown in Figure 1.5.
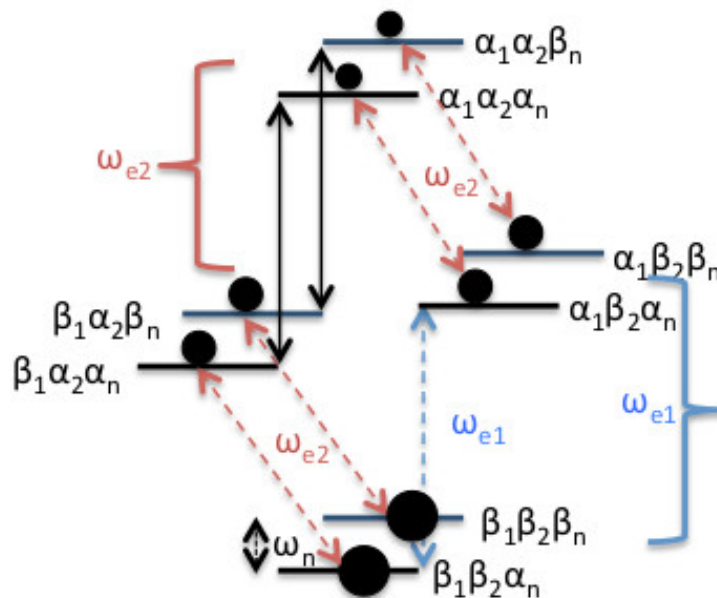

Figure 1.5. Energy level diagram for a three-spin system e_1-e_2-n. Conditions for the cross effect to occur $\omega_{e1} - \omega_{e2} \approx \omega_n$.

Nowadays, in high-field MAS-DNP experiments, the cross effect is a dominant mechanism around 100 K. The probability to match cross effect conditions are higher for bi-radicals or in a concentrated mixture of several radicals as chances to find the electron pair matching condition eq. 1.15 are improved.[59-60] Recent contributions to the understanding of CE-based DNP can be found at K.N. Hu[61], and Hovav and Vega[59] who explain the cross effect from a quantum mechanical point of view.

Thermal Mixing

DNP processes can happen via the CE mechanism if the EPR line width is comparable or broader than the nuclear Larmor frequency. The CE mechanistically underlies the so-called theory of thermal mixing (TM), which denotes a regime in which the spin temperatures of all partaking spins are equal. In our laboratory, dissolution DNP experiments typically do not match the conditions of the solid effect mechanism, so that TM has to be considered. This is the case because we perform our experiments that aim at polarizing ^{1}H or ^{13}C nuclei mostly with derivatives of TEMPO radicals.[62] Yet, dissolution experiments are also possible with trityl or BDPA radicals[2, 63] matching SE conditions as they feature quite narrow EPR line widths. For X-nuclei like ^{13}C, ^{15}N, ^{129}Xe the essential requirement of TM is fulfilled as the small gyromagnetic ratios of these nuclei fulfill the condition $\delta > \omega_n$.

The thermal mixing mechanism can be thermodynamically described by the thermal interaction of three systems that we consider to have distinct heat capacities: *i*) the nuclear Zeeman reservoir (NZ), *ii*) the electron Zeeman reservoir (EZ), and *iii*) the electron spin-spin interaction reservoir (SS). Each of these systems can be described by its own spin temperatures, which converge as one approaches the regime of TM. Hence, the spin temperature can be considered as the key concept underlying TM-based DNP.[41, 64-65]

In some cases, the condition that the nuclear Larmor frequency ω_n must be comparable to the EPR linewidth δ is only met by inhomogeneous EPR line

broadening. TM requires that the radical concentration be sufficiently high so that the system features strong electron dipolar interactions, which will couple the different inhomogenously broadened "spin packets" of the EPR line. Under these conditions, the NZ reservoir and electron dipolar reservoir are thermally coupled via triple spin (SSI) flips where two electron spins with an energy difference matching the nuclear transition undergo a flip-flop transition while the nuclear spin is inverted.[40, 66] The TM mechanism take places in two steps[40, 67]: *i*) *Dynamic cooling* of the electron dipolar system via incident continuous-wave microwave irradiation that couples it to the electron Zeeman bath. The concept of dynamic cooling is based on an idea developed by Redfield[64] for NMR under strong radio field frequency irradiation and was later applied to the field of electron paramagnetic resonance (EPR) and DNP[39] *ii*) The above-mentioned *SSI triple spin flips*, i.e., the CE case. In cases where the nuclear Larmor frequency is larger than the EPR linewidth, the nuclear Zeeman and electron SSI reservoirs will not be thermally coupled as the energy difference between any two electrons will be to small. In this case, the solid effect might take place instead.

Spin temperature theory

To understand TM, we will briefly introduce the concept of spin temperature. Redfield introduced the spin temperature theory in 1955.[64] The main hypothesis of the theory is based on the evolution of a large isolated spin system under strong irradiation (see also Provotorov[38]). This theory describes the population of the nuclear spin states of solids in the rotating frame.

Suppose a system with N spins (I) isolated from the lattice (surroundings); its interactions are time-independent. Transitions between its eigenstates are energy conservative. In the case of internal equilibrium, the system follows the Boltzmann law, as described above (see section 1.2.1):

$$p_i \propto \exp\left(\frac{-E_i}{k_B T}\right) = \exp(-\beta \omega_i) \qquad (1.16)$$

where $\beta = \hbar / k_B T$ is defined as the inverse temperature coefficient (ref[40], p. 401)

and $E_i = \hbar\omega_i$. Therefore, the ratio between the populations of the energy levels E_i and E_{i+1} is given by:

$$\frac{n_i}{n_{i+1}} = \exp\left(\frac{-\Delta E}{k_B T}\right) \qquad (1.17)$$

where the energies E_i and E_{i+1} correspond to the ith and $i+1^{th}$ energy states of the system and ΔE is the energy difference between them. Therefore, the temperature T can be expressed in terms of populations:

$$T = -\frac{\Delta E}{k_B(\ln(n_i) - \ln(n_{i+1}))} \qquad (1.18)$$

Practically, a spin system cannot be fully isolated and always tries to reach equilibrium with the lattice. Thermal coupling between a spin reservoir and the lattice thus allows one to attain an equilibrium between spin temperature T_S and lattice temperature T_L. In thermal equilibrium in contact with the lattice, T is given by the "lattice temperature" T_L (temperature of the surrounding heat bath) as the two temperatures will be converging to a single value. If the system strives away from the equilibrium, the spin temperature T_S will be different from T_L.

In a next step, we formulate the density matrix of the system σ that can be written as[34]

$$\sigma = \frac{exp(-\beta H)}{Tr(exp(-\beta H))} \qquad (1.19)$$

where H is the spin system's Hamiltonian and β corresponds to the inverse spin temperature coefficient. In the steady state, for a system with positive energy, the population will be larger for lower energy levels leading to a positive value of β. In contrast, populations will be higher for a high-energy level if the value of β is negative, which means that a negative value of the spin temperature is possible. Figure 1.6 illustrates population distributions of a dipolar electronic system with respect to spin temperature.
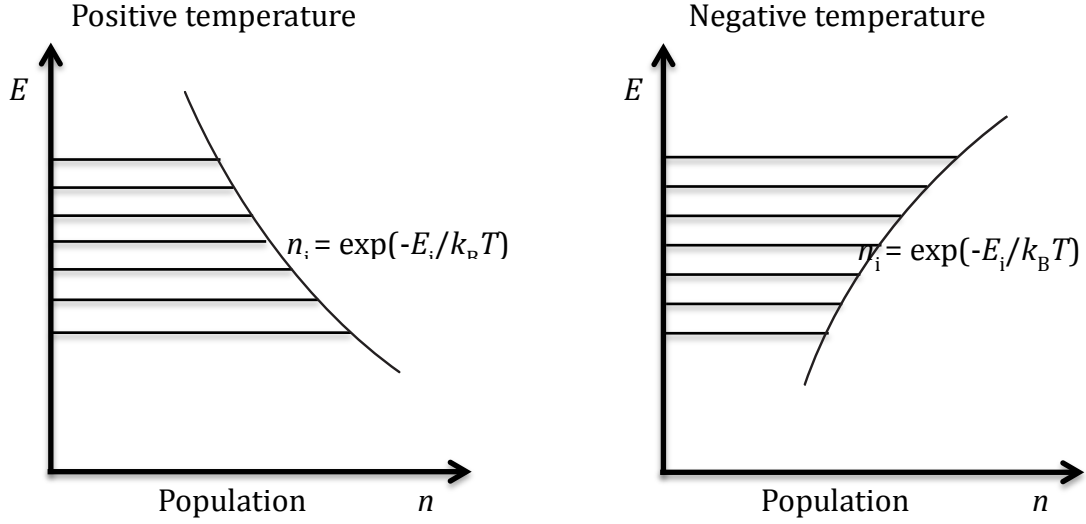
Figure 1.6. An illustration of population distributions of a spin system with dipolar couplings for positive (left) and negative (right) spin temperatures. In the picture, horizontal lines represent spin quantum states while the vertical position (y-axis) of the lines correspond to the energy E. The lengths of these lines (along the x-axis) represent their relative populations (n). All energy levels are equally spaced.

The spin temperature theory is important if the system acquires its internal equilibrium much faster than the spin-lattice relaxation rate $1/T_1$ leads to a loss of polarization, therefore $T_1 \gg t$, where t is the time for achieving the internal equilibrium of the spin system. The theory considers only populations of eigenstates while neglecting coherences. Therefore, any off-diagonal element of the density operator should be zero. Usually this condition is not entirely satisfied in a non-equilibrium situation. However, if coherences decay to zero before all heat reservoirs are equilibrated, we can still apply the spin temperature theory. Hence, spin temperature theory should be applied on a time scale of $t > T_2$ as coherences decay with the transverse relaxation time T_2. This signifies that the spin temperature is restricted to the condition $T_1 \gg T_2$.[68]

In the next step, we investigate the influence of microwave irradiation. Suppose that an ensemble of N_S electron spins is in equilibrium with the lattice at a temperature T_L in the presence of a static magnetic field B_0 and that the electrons are coupled through dipole-dipole interactions.

When a microwave field is applied near to the electron Larmor frequency ω_e, the residual effective magnetic field B_{eff} is strongly reduced, a phenomenon that can be explained in a reference frame rotating with B_1. In this situation, the electron Zeeman energies become comparable to the dipole-dipole interactions and therefore both reservoirs can exchange their energy. We speak of a coupling of both reservoirs through the microwaves. The reduced effective magnetic field B_{eff}, which is parallel to the static magnetic field B_0, is given by the vector sum of the longitudinal field B_0 and offset $\Delta = \omega_e - \omega_{mw}$ of the microwave field. Hence, in the presence of microwave irradiation at a frequency ω_{mw} close to the electron Larmor frequency ω_e, the spin temperature of the electron Zeeman reservoir is therefore reduced by a factor $(\omega_e - \omega_{mw}/\omega_e)$. Likewise, the electron spin temperature is equal to the electron Zeeman temperature:

$$T_L^{rot} = T_{EZ}^{rot} = \frac{\omega_e - \omega_{mw}}{\omega_e} T_L = \frac{\Delta}{\omega_e} T_L = \frac{B_{eff}}{B_0} T_L \qquad (1.20)$$

Provotorov described a theory of saturation for a continuous microwave field in the high temperature limit.[68-69] In this approximation, the system can be represented by two distinct reservoirs: the electron Zeeman reservoir (EZ) and the spin-spin interaction or dipolar reservoir (SS)[68] as defined earlier each reservoir is characterized by its own spin temperature, T_{EZ} and T_{SS}. In thermal equilibrium, all kinds of spin temperatures tend to the lattice temperature, which implies $T_{EZ} = T_{SS} = T_L$ and their relaxation rate can be notated as R_{1e} and $R_{1,SS}$ for the EZ and SS reservoir, respectively. Yet, T_{SS} can be reduced with respect to T_{EZ}, if the applied microwaves are slightly off-resonance at a frequency $\omega_{mw} = + \omega_e - \Delta$. The electron Zeeman transitions absorb quanta of energy $h\nu_{mw}$ resulting in the saturation of a spin packet at the offset frequency Δ, and thus is the heating of the electron Zeeman bath, while the spin-spin interaction reservoir starts to cool down. Both processes are restrained by spin lattice relaxation. In total, energy is taken from the SS reservoir and transmitted to the lattice. In the high temperature approximation, the temperature of the lattice does not change as the latter is assumed to have infinitive heat capacity. T_{SS} can be positive or negative, depending on the sign of the offset frequency $\Delta = \omega_e - \omega_{mw}$. Figure 1.7 illustrates the populations as a function of energy for positive and negative spin

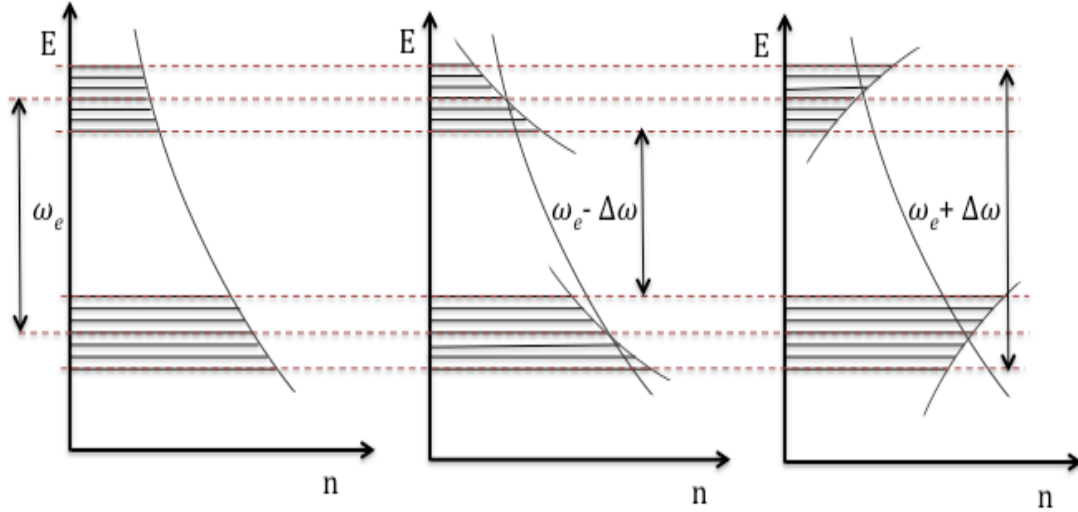temperatures, where microwaves are applied at different frequencies near to the electron Larmor frequency.

Figure 1.7. Population distributions of the electron spin system at thermal equilibrium with the lattice ($T_{EZ} = T_{SS} = T_L$) (far left), under microwave irradiation at frequency $\omega_{mw} < \omega_e$ (middle), under microwave irradiation at frequency $\omega_{mw} > \omega_e$ (right). In the pictorial representations, horizontal lines correspond to spin quantum states while the vertical positions (y-axis) of the lines represent their energy E. The length of these lines (x-axis) represent their relative populations (n).

Provotorov described the evolution of the inverse spin temperatures of the EZ and SS reservoirs in the rotating frame with respect to the inverse spin temperature coefficient of the lattice $\beta_L = \hbar/k_B T_L$. Thus, the inverse spin temperatures of the EZ and SS reservoirs were similarly defined as $\beta_{EZ} = \hbar/k_B T_{EZ}$ and $\beta_{SS} = \hbar/k_B T_{SS}$. Provotorov described the evolution of the spin temperature coefficients β_{EZ} and β_{SS} [34, 68] yielding a theoretical framework for dynamic cooling of the spin-spin interactions.

So far, there was no nuclear spin included in our description, but if the nuclear Larmor frequency is comparable to or smaller than the line-width of the electron EPR spectrum ($\Delta\omega_e \geq \omega_n$), nuclei can be involved and energy can flow between the non-Zeeman electronic and nuclear Zeeman baths. These bathes are coupled via hyperfine interactions. Thus, a third reservoir, called nuclear Zeeman

reservoir (NZ) can be added to the system. Cooling down the SS reservoir at slightly off-resonance microwave frequency will also cool down the NZ reservoir as in the regime of TM these bathes tend to be in equilibrium with the lattice, where longitudinal spin-lattice relaxation proceeds with a rate R_{1n}. Note that a reduction of the temperature of the NZ reservoir (T_{NZ}) denotes an increase in the nuclear polarization.
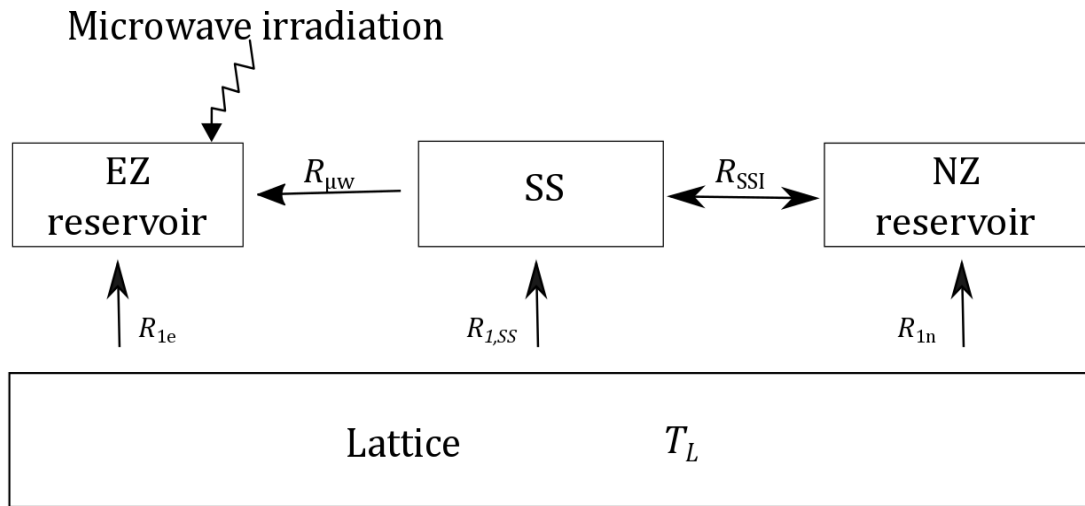

Figure 1.8. Illustration of thermal mixing. The different heat reservoirs are displayed as boxes and characteristic transition times are indicated.

In thermal mixing processes, different systems achieve a common temperature. As TM processes are favored for the condition $T_{1e} \gg T_{2e}$,[68] the mechanism is most likely to occur at low temperatures and high electron concentrations (Figure 1.8 illustrates the thermal mixing process).

1.2.4 DNP Interactions

Hyperfine interactions

The interaction between a single electron and a single nucleus is described as hyperfine interaction (*hfi*). This interaction includes two different contributions: *i)* the Fermi contact interaction, *ii)* the electron-nuclear dipole-dipole

interaction; therefore Hamiltonian of the hyperfine interaction (H_{hfi}) can be expressed by the sum of the Fermi contact interaction H_F and the electron-nuclear dipole-dipole interaction H_{DD}.[70-71]

$$H_{hfi} = \vec{S} \cdot \tilde{A} \cdot \vec{I} \qquad (1.21)$$

$\tilde{A}$ represents the hyperfine interaction tensor, which contains an isotropic (or *Fermi contact)* part as well as anisotropic components of the electron-nucleus dipole-dipole coupling.[70] The hyperfine interaction matrix A can be represented as[71]:

$$A = \begin{pmatrix} A_{xx} & A_{xy} & A_{xz} \\ A_{yx} & A_{yy} & A_{yz} \\ A_{zx} & A_{zy} & A_{zz} \end{pmatrix} \qquad (1.22)$$

For each electron-nucleus pair, the Hamiltonian can be expanded in nine terms, be given by $\hat{S}_i A_{ij} \hat{I}_j$ where i, j = x, y, z.

The Fermi contact term can be written as:

$$H_F = a_{\mathrm{iso}} \vec{S} \cdot \vec{I} \qquad (1.23)$$

with the isotropic hyperfine coupling constant[71]

$$a_{\mathrm{iso}} \propto \mu_0 \hbar^2 \gamma_e \gamma_n |\psi_0(0)|^2 \qquad (1.24)$$

with the vacuum permeability constant $\mu_0 = 4\pi \times 10^{-7}$ H/m and $|\psi_0(0)|^2$ denoting the electron spin density probability at the site of the nucleus.

The electron-nuclear dipole-dipole coupling is given by:

$$H_{DD} = \frac{\mu_0}{4\pi} \frac{\hbar^2 \gamma_S \gamma_I}{r^3} \left[\vec{S} \cdot \vec{I} - 3 \frac{(\vec{S} \cdot \vec{r})(\vec{I} \cdot \vec{r})}{r^2} \right] \quad (1.25)$$

where *r* represents the vector connecting the unpaired electron and the nucleus, which shows that the hyperfine interaction is strongly dependent on the distance between the electron spin and the nuclear spin.

1.3 DNP Hardware

This section introduces the hardware required for the dissolution-DNP experiments that I carried out during my studies. For dissolution-DNP, three steps are required, *i*) polarization of the sample at low temperatures, *ii*) dissolution and transfer of the hyperpolarized sample from the polarizer to the detection magnet, and *iii*) detection of the signal in the NMR spectrometer at ambient temperature. This process is schematically depicted in Fig. 1.9.
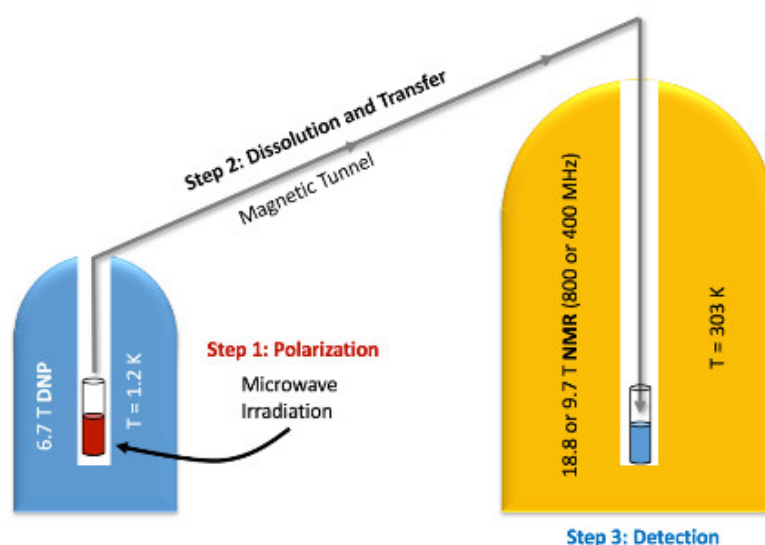
Figure 1.9. The principle of dissolution DNP. A sample that contains radicals frozen at 1.2 K in a magnetic field of 6.7 T is hyperpolarized by means of microwave irradiation at 188.2 GHz (left). Subsequent dissolution and transfer to NMR spectrometers at either 400 or 800 MHz (right) yield NMR spectra that can be enhanced by 4 to 5 orders of magnitude.

The work presented in this thesis has mostly been performed on a Bruker prototype D-DNP system based on the setup proposed by Ardenkjaer-Larsen.[2] Such a system consists of a cryostat with a probe, a superconducting magnet and a microwave irradiation source (see Fig. 1.10).

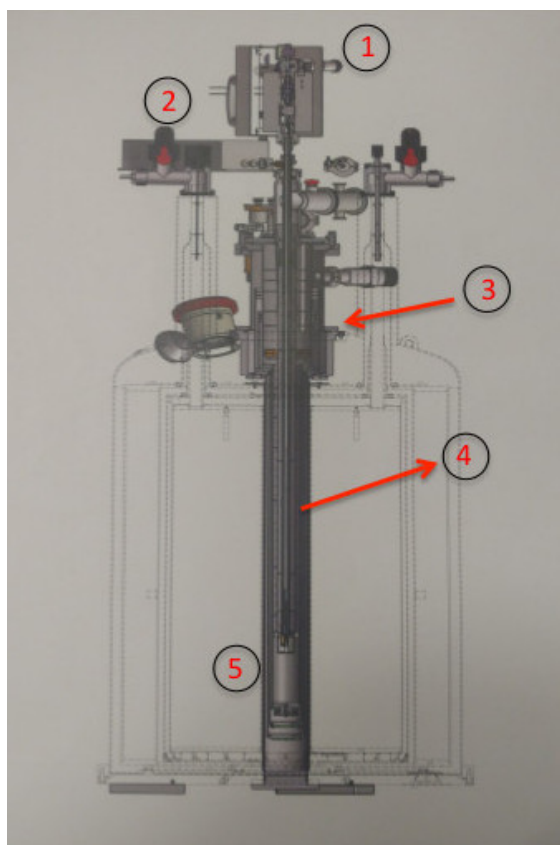**Figure. 1.10.** A schematic view of our DNP apparatus. 1) Dissolution system; 2) microwave source; 3) port for refilling He into the cryostat, which connects with the liquid He dewar; 4) probe for DNP, and 5) sample space, which is irradiated with microwaves. All parts of the setup are explained in the following sections.

1.3.1 Cryostat

In our laboratory, the dissolution-DNP setup is composed of a superconducting wide bore magnet with a field of 6.7 T. A variable temperature insert (VTI) can be cooled with liquid helium such that the temperature of the cryostat can reach 1.2 K. A 100 L liquid He Dewar is normally connected to the system for refilling. The helium is transferred from the liquid He Dewar to a phase separator (PS) where gaseous helium can evaporate. The liquid helium can flow from the phase separator to the sample space via two capillary tubes equipped with software-controlled needle valves. We can monitor the pressure, temperature and helium level of the cryostat with various sensors. Modifying the helium vapor pressure allows one to control the temperature of the helium bath in the cryostat[72]. One

drawback of our setup is a large consumption of the liquid He, which is extremely expensive. We are equipped for the recovery of He gas, which can be converted back to liquid He.
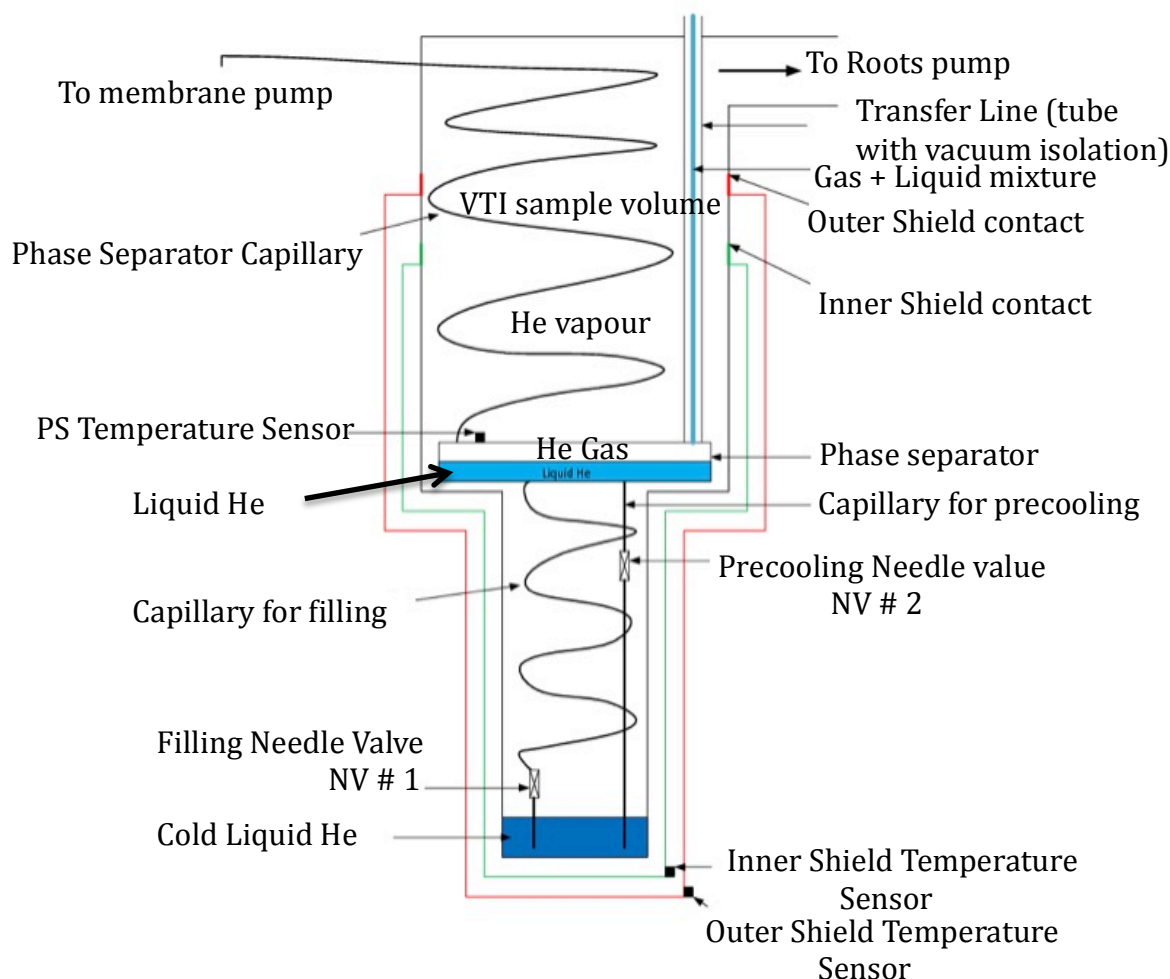
Figure 1.11. A schematic view of the cryostat of the dissolution-DNP setup.

The cryostat is one of the main parts of the polarizer. The sample is immersed in liquid He at temperatures between 1.2 and 4.2 K. A schematic view of the cryostat is shown in figure 1.11.

Figure 1.11 displays how the capillary and the needle valves (NV) connect the phase separator and the VTI. One NV is located close to the bottom of the sample volume as shown in the schematic view. The other is wound around the VTI. Due to the thermal load of the He bath (thermal conductivity of the walls, RF power dissipation, etc.) the liquid He level will continuously decrease during operation so that a permanently renewed supply is necessary. To guide the He flow, the

main volume of the VTI is connected to a pre-vacuum pump, and a membrane pump is connected to the PS volume. When the needle valves are open, the PS and the main volume of the VTI are connected, while the PS and the VTI remain isolated in the opposite case. A so-called root pump is connected to the VTI, to enable us to reach very low temperatures around 1.2 K in the sample volume by reducing the pressure to a few mbar.

1.3.2 Probe

The main body of the probe is composed of a stainless steel pipe, while the top and bottom parts of the probe are made of brass. The RF coils are mounted on a hydrogen-free material (PTFE for example), and are connected to the spectrometer through two rigid coaxial cables as shown in the figure 1.12. The microwaves are carried by a wave-guide, and are reflected by a mirror towards the sample.
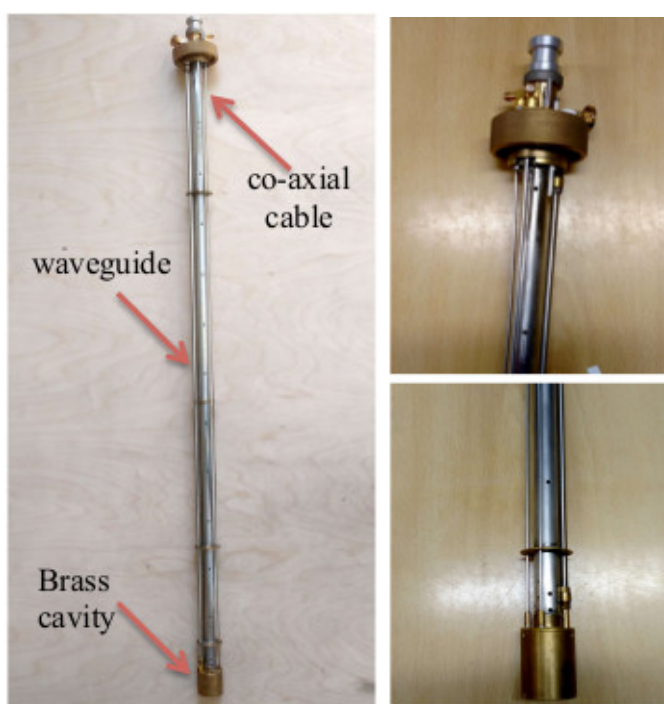

Figure 1.12. A double resonance probe for dissolution DNP. The two rigid coaxial coils connect the upper part and the RF coils. The microwave guide is composed of a circular stainless steel tube. Upper (top right) and bottom (bottom right) parts of the probe.

RF coils

We need a double resonance probe to perform cross polarization (CP) experiments. Bruker provided a suitable ^{1}H-^{13}C CP probe for dissolution-DNP. Sina Marhabaie developed a DNP probe in our laboratory. This probe has been designed for ^{1}H-^{2}D cross polarization. Figure 1.12 shows pictures of the available CP-DNP probes in our laboratory.

During the experiments, these coils are immersed in the liquid He bath in the cryostat, which makes it difficult to place variable tuning and matching capacitors, although tuning and matching of the circuit are required for efficient CP. Therefore, to adjust the tuning and matching for each channel, tuning and matching boxes were added on the top of the ^{1}H-^{2}D DNP probe in contrast to the ^{1}H-^{13}C probe that was already matched and equipped with a tuning knob, positioned close to the top of the polarizer. The tuning and matching box is connected to the coil via coaxial cables. This additionally allows one to compensate for shifts in resonance frequencies of the coil, as these are very sensitive to the temperature so that the resonance conditions can change by a significant amount (a few MHz) between liquid nitrogen and liquid helium temperatures.

Several types of coil designs can be used in NMR spectroscopy depending on the requirements. Usually solenoid coils provide better homogeneity of the B_1 field, but for our polarizer, a coil should be chosen which is suitable for our experiments. As the dissolution system has to be inserted vertically into the VTI from the top of the polarizer, a saddle coil was chosen such that the sample and the dissolution system can be inserted from the top. The design of the saddle coil in our laboratory can be seen in figure 1.13.

Figure 1.13. A saddle coil designed for rapid dissolution. A sample holder can be inserted from the top of the VTI into the active volume of the coil.

1.3.3 Microwave Source

Our DNP experiments are usually performed at frequencies $187.5 < f_{\mu w} < 188.5$ GHz with a maximum microwave power of 350 mW at the output of the microwave source. Microwaves are generated with an ELVA source which provides a frequency span of $f_{\mu w} = 94$ GHz $\pm$ 250 MHz. With the help of a frequency doubler (Virginia diodes) a final frequency of $f_{\mu w} = 188$ GHz $\pm$ 500 MHz can be reached.

To enhance the polarization of the nuclear spins by DNP, a paramagnetic species is required. In our laboratory, we use 4-hydroxy-2,2,6,6-tetramethyl piperidine-1-oxyl (TEMPOL) as a polarizing agent. To saturate a broad spectral width of the EPR line, frequency modulation can be used.[73] Experimentally, we use an amplitude of $\Delta f_{\mu w} = 100$ MHz with a modulation frequency of $f_{mod} \approx 2$ kHz. Frequency modulation provides a better enhancement in dissolution DNP experiments,[73] especially at 1.2 K.

1.3.4 Magnetic tunnel

During the transfer of the hyperpolarized sample, longitudinal magnetization decays back to its equilibrium state. Several mechanisms, e. g., dipole-dipole interactions, chemical shift anisotropy (CSA), scalar coupling and coupling with

the paramagnetic species are responsible for the longitudinal relaxation. These relaxation mechanisms are briefly discussed in chapter 3.

To overcome this problem several solutions have been proposed. In the group of Walter Kockenberger, the DNP setup is based on a dual magnet[74] where the transfer occurs in less than a second. However, most DNP polarizers are placed at a few meters distance from the NMR or MRI instrument and the transfer time can vary from a few seconds[75] to about a minute[76] depending on the hyperpolarized fluid. Recently B. Meier from Levitt's group has proposed rapid transfer DNP,[77] where the transfer of the solid sample can be done in about 100 ms. In our laboratory, the transfer of the sample from the polarizer to the magnet can vary from 1-10 s. During the transfer, the hyperpolarized sample may travel through very low field regions like the Earth's magnetic field. To overcome some of the above-mentioned relaxation effects or, in other words, to preserve the maximum polarization, a magnetic tunnel was designed by Jonas Milani at EPFL[78]. We use the same tunnel in our laboratory. In our setup the hyperpolarized sample is transferred through the magnetic tunnel that maintains a field of 0.9 T between the polarizer at a magnetic field of 6.7 T to the spectrometers at 9.4 T or 18.8 T.

This tunnel was constructed with permanent neodymium boron magnets (Supermagnete Webcraft GmbH, 5x5x100 mm, NdFeB, N52, with Ni-Cu-Ni coating), which are arranged in a Halbach design[79].

1.3.5 Dissolution Setup

In our DNP setup, the highest polarization can be achieved at a temperature of 1.2 K. The hyperpolarized sample can be transferred in our laboratory to a liquid-state NMR spectrometer through the magnetic tunnel by a burst of 5 mL superheated D_2O at 180 °C and 10.5 bar, which is projected into the frozen sample through a so-called dissolution stick. This stick is inserted into the polarizer from the top of the polarizer. The dissolution process happens in three steps: *i)* flushing, the delay for opening the value between the D_2O reservoir and

the frozen sample, *ii)* boosting with He gas at 7 bar, and *iii)* settling time. The whole process is controlled by software.

1.4 References for Chapter 1

1.   Bodenhausen, G.; Ruben, D. J., Natural abundance nitrogen-15 NMR by enhanced heteronuclear spectroscopy. *Chem. Phys. Lett.* **1980,** *69* (1), 185-189.

2.   Ardenkjaer-Larsen, J. H.; Golman, K.; Gram, A.; Lerche, M. H.; Servin, R.; Thaning, M.; Wolber, J., Increase of signal-to-noise of more than 10,000 times in liquid state NMR. *Discov. Med.* **2003,** *3* (19), 37-9.

3.   Hypersense.   Oxford   Instruments.   https://www.oxford-instruments.com/products/spectrometers/nuclear-magnetic-resonance-nmr/hypersense (accessed 40.04.2013).

4.   Ardenkjaer-Larsen, J. H.; Macholl, S.; Jóhannesson, H., Dynamic Nuclear Polarization with Trityls at 1.2 K. *Appl. Magn. Reson.* **2008,** *34* (3), 509-522.

5.   Macholl, S.; Johannesson, H.; Ardenkjaer-Larsen, J. H., Trityl biradicals and 13C dynamic nuclear polarization. *Phys. Chem. Chem. Phys.* **2010,** *12* (22), 5804-17.

6.   Cheng, T.; Capozzi, A.; Takado, Y.; Balzan, R.; Comment, A., Over 35% liquid-state 13C polarization obtained via dissolution dynamic nuclear polarization at 7 T and 1 K using ubiquitous nitroxyl radicals. *Phys. Chem. Chem. Phys.* **2013,** *15* (48), 20819-22.

7.   Comment, A.; van den Brandt, B.; Uffmann, K.; Kurdzesau, F.; Jannin, S.; Konter, J. A.; Hautle, P.; Wenckebach, W. T.; Gruetter, R.; van der Klink, J. J., Design and performance of a DNP prepolarizer coupled to a rodent MRI scanner. *Concepts. Magn. Reson. B,* **2007,** *31B* (4), 255-269.

8.   Jannin, S.; Comment, A.; Kurdzesau, F.; Konter, J. A.; Hautle, P.; van den Brandt, B.; van der Klink, J. J., A 140 GHz prepolarizer for dissolution dynamic nuclear polarization. *J. Chem. Phys.* **2008,** *128* (24), 241102.

9.   Bornet, A.; Melzi, R.; Jannin, S.; Bodenhausen, G., Cross Polarization for Dissolution Dynamic Nuclear Polarization Experiments at Readily Accessible Temperatures 1.2 < T < 4.2 K. *Appl. Magn. Reson.* **2012,** *43* (1), 107-117.

10.   Milani, J.; Vuichoud, B.; Bornet, A.; Melzi, R.; Jannin, S.; Bodenhausen, G., Hyperpolarization of nitrogen-15 nuclei by cross polarization and dissolution dynamic nuclear polarization. *Rev. Sci. Instrum.* **2017,** *88* (1), 015109.

11.   Vuichoud, B.; Milani, J.; Bornet, A.; Melzi, R.; Jannin, S.; Bodenhausen, G., Hyperpolarization of deuterated metabolites via remote cross-polarization and dissolution dynamic nuclear polarization. *J. Phys. Chem. B* **2014,** *118* (5), 1411-5.

12.   Bornet, A.; Melzi, R.; Perez Linde, A. J.; Hautle, P.; van den Brandt, B.; Jannin, S.; Bodenhausen, G., Boosting Dissolution Dynamic Nuclear Polarization by Cross Polarization. *J. Phys. Chem. Lett.* **2013,** *4* (1), 111-4.

13.   Jannin, S.; Bornet, A.; Melzi, R.; Bodenhausen, G., High field dynamic nuclear polarization at 6.7T: Carbon-13 polarization above 70% within 20 min. *Chem. Phys. Lett.* **2012,** *549*, 99-102.

14.   Jannin, S.; Bornet, A.; Colombo, S.; Bodenhausen, G., Low-temperature cross polarization in view of enhancing dissolution Dynamic Nuclear Polarization in NMR. *Chem. Phys. Lett.* **2011,** *517* (4), 234-236.

15.   Carravetta, M.; Levitt, M. H., Theory of long-lived nuclear spin states in solution nuclear magnetic resonance. I. Singlet states in low magnetic field. *J. Chem. Phys.* **2005,** *122* (21), 214505.

16.   Carravetta, M.; Levitt, M. H., Long-lived nuclear spin states in high-field solution NMR. *J. Am. Chem. Soc.* **2004,** *126* (20), 6228-9.

17.   Buratto, R.; Bornet, A.; Milani, J.; Mammoli, D.; Vuichoud, B.; Salvi, N.; Singh, M.; Laguerre, A.; Passemard, S.; Gerber-Lemaire, S.; Jannin, S.; Bodenhausen, G., Drug screening boosted by hyperpolarized long-lived states in NMR. *ChemMedChem* **2014,** *9* (11), 2509-15.

18.   Kurzbach, D.; Weber, E. M.; Jhajharia, A.; Cousin, S. F.; Sadet, A.; Marhabaie, S.; Canet, E.; Birlirakis, N.; Milani, J.; Jannin, S.; Eshchenko, D.; Hassan, A.; Melzi, R.; Luetolf, S.; Sacher, M.; Rossire, M.; Kempf, J.; Lohman, J. A.; Weller, M.; Bodenhausen, G.; Abergel, D., Dissolution dynamic nuclear polarization of deuterated molecules enhanced by cross-polarization. *J. Chem. Phys.* **2016,** *145* (19), 194203.

19.   Dumez, J. N.; Hakansson, P.; Mamone, S.; Meier, B.; Stevanato, G.; Hill-Cousins, J. T.; Roy, S. S.; Brown, R. C.; Pileio, G.; Levitt, M. H., Theory of long-lived nuclear spin states in methyl groups and quantum-rotor induced polarisation. *J. Chem. Phys.* **2015,** *142* (4), 044506.

20.   Tayler, M. C.; Marco-Rius, I.; Kettunen, M. I.; Brindle, K. M.; Levitt, M. H.; Pileio, G., Direct enhancement of nuclear singlet order by dynamic nuclear polarization. *J. Am. Chem. Soc.* **2012,** *134* (18), 7668-71.

21.   Kellogg, J. M. B.; Rabi, I. I.; Ramsey, N. F.; Zacharias, J. R., The Magnetic Moments of the Proton and the Deuteron. The Radiofrequency Spectrum of H_2 in Various Magnetic Fields. *Phys.Rev.* **1939,** *56* (8), 728-743.

22.   Rabi, I. I.; Millman, S.; Kusch, P.; Zacharias, J. R., The Molecular Beam Resonance Method for Measuring Nuclear Magnetic Moments. The Magnetic Moments of $_3Li^6$, $_3Li^7$ and $_9F^{19}$. *Phys. Rev.* **1939,** *55* (6), 526-535.

23.   Bloch, F.; Hansen, W. W.; Packard, M., Nuclear Induction. *Phys. Rev.* **1946,** *69* (3-4), 127-127.

24.   Purcell, E. M.; Torrey, H. C.; Pound, R. V., Resonance Absorption by Nuclear Magnetic Moments in a Solid. *Phys. Rev.* **1946,** *69* (1-2), 37-38.

25.   Freeman, R., *A Handbook of Nuclear Magnetic Resonance.* 2nd Edition ed.; Longman: 1987.

26.   Morris, G. A.; Freeman, R., Enhancement of nuclear magnetic resonance signals by polarization transfer. *J. Am. Chem. Soc.* **1979,** *101* (3), 760-762.

27.   Anderson, W. A.; Freeman, R., Influence of a Second Radiofrequency Field on High-Resolution Nuclear Magnetic Resonance Spectra. *J. Chem. Phys.* **1962,** *37* (1), 85-103.

28.   Overhauser, A. W., Polarization of Nuclei in Metals. *Phys. Rev.* **1953,** *92* (2), 411-415.

29.   Hartmann, S. R.; Hahn, E. L., Nuclear Double Resonance in the Rotating Frame. *Phys. Rev.* **1962,** *128* (5), 2042-2053.

30.   Hirsch, M. L.; Kalechofsky, N.; Belzer, A.; Rosay, M.; Kempf, J. G., Brute-Force Hyperpolarization for NMR and MRI. *J. Am. Chem. Soc* **2015,** *137* (26), 8428-8434.

31.   Walker, T. G.; Happer, W., Spin-exchange optical pumping of noble-gas nuclei. *Rev. Mod. Phys.* **1997,** *69* (2), 629-642.

32.   Bowers, C. R.; Weitekamp, D. P., Transformation of Symmetrization Order to Nuclear-Spin Magnetization by Chemical Reaction and Nuclear Magnetic Resonance. *Phys. Rev. Lett.* **1986,** *57* (21), 2645-2648.

33.   Bowers, C. R.; Weitekamp, D. P., Parahydrogen and synthesis allow dramatically enhanced nuclear alignment. *J. Am. Chem. Soc* **1987,** *109* (18), 5541-5542.

34.   Abragam, A.; Goldman, M., *Nuclear magnetism: order and disorder.* Clarendon Press: 1982.

35.   Carver, T. R.; Slichter, C. P., Polarization of Nuclear Spins in Metals. *Phys. Rev.* **1953,** *92* (1), 212-213.

36.   Jeffries, C. D., Polarization of Nuclei by Resonance Saturation in Paramagnetic Crystals. *Phys. Rev.* **1957,** *106* (1), 164-165.

37.   Abragam, A.; and Proctor, W. G., Une Nouvelle Methode De Polarisation Dynamique Des Noyaux Atomiques Dans Les Solide. *C. R. Hebd. Seanc. Acad. Sci.* **1958,** *246* (15), 2253-2256.

38.   Provotorov, B., Nuclear Magnetic Resonance in Solids. *Optika I Spek- troskopiya* **1961,** *11*, 123-125.

39.   Borghini, M., Spin-Temperature Model of Nuclear Dynamic Polarization Using Free Radicals. *Phys. Rev. Lett.* **1968,** *20* (9), 419-421.

40.   Abragam, A.; Goldman, M., Principles of dynamic nuclear polarisation. *Rep. Prog. Phys.* **1978,** *41* (3), 395.

41.   Goldman, M., *Spin temperature and nuclear magnetic resonance in solids*. Clarendon Press: Oxford, 1970; p ix, 246 p.

42.   Hwang, C. F.; Hill, D. A., New Effect in Dynamic Polarization. *Physical Rev. Lett.* **1967,** *18* (4), 110-112.

43.   Hwang, C. F.; Hill, D. A., Phenomenological Model for the New Effect in Dynamic Polarization. *Phys. Rev. Lett.* **1967,** *19* (18), 1011-1014.

44.   Wind, R. A.; Duijvestijn, M. J.; van der Lugt, C.; Manenschijn, A.; Vriend, J., Applications of dynamic nuclear polarization in 13C NMR in solids. *Prog. Nucl. Magn. Reson. Spectrosc.* **1985,** *17*, 33-67.

45.   Singel, D. J.; Seidel, H.; Kendrick, R. D.; Yannoni, C. S., A spectrometer for EPR, DNP, and multinuclear high-resolution NMR. *J. Magn. Reson. (1969)* **1989,** *81* (1), 145-161.

46.   Hall, D. A.; Maus, D. C.; Gerfen, G. J.; Inati, S. J.; Becerra, L. R.; Dahlquist, F. W.; Griffin, R. G., Polarization-Enhanced NMR Spectroscopy of Biomolecules in Frozen Solution. *Science* **1997,** *276* (5314), 930.

47.   Griffin, R. G.; Prisner, T. F., High field dynamic nuclear polarization-the renaissance. *Phys. Chem. Chem. Phys.* **2010,** *12* (22), 5737-5740.

48.   Davis, A. L.; Day, I. J., Dynamic Nuclear Polarization: Applications to Liquid-State NMR Spectroscopy. *eMagRes*, John Wiley & Sons, Ltd: 2007.

49.   Wolber, J.; Ellner, F.; Fridlund, B.; Gram, A.; Jóhannesson, H.; Hansson, G.; Hansson, L. H.; Lerche, M. H.; Månsson, S.; Servin, R.; Thaning, M.; Golman, K.; Ardenkjær-Larsen, J. H., Generating highly polarized nuclear spins in solution using dynamic nuclear polarization. *Nucl. Instr. Meth. Phys. Res. A* **2004,** *526* (1), 173-181.

50.   Shimon, D.; Hovav, Y.; Feintuch, A.; Goldfarb, D.; Vega, S., Dynamic nuclear polarization in the solid state: a transition between the cross effect and the solid effect. *Phys. Chem. Chem. Phys.* **2012,** *14* (16), 5729-5743.

51.   Hovav, Y.; Levinkron, O.; Feintuch, A.; Vega, S., Theoretical Aspects of Dynamic Nuclear Polarization in the Solid State: The Influence of High Radical Concentrations on the Solid Effect and Cross Effect Mechanisms. *Appl. Magn. Reson.* **2012,** *43* (1), 21-41.

52.   Schmugge, T. J.; Jeffries, C. D., High Dynamic Polarization of Protons. *Phys. Rev.* **1965,** *138* (6A), A1785-A1801.

53.   Leifson, O. S.; Jeffries, C. D., Dynamic Polarization of Nuclei by Electron-Nuclear Dipolar Coupling in Crystals. *Phys. Rev.* **1961,** *122* (6), 1781-1795.

54.   Wenckebach, W. T., The Solid Effect. *Appl. Magn. Reson.* **2008,** *34* (3), 227.

55.   Smith, A. A.; Corzilius, B.; Barnes, A. B.; Maly, T.; Griffin, R. G., Solid effect dynamic nuclear polarization and polarization pathways. *J. Chem. Phys.* **2012,** *136* (1), 015101.

56.   Hovav, Y.; Feintuch, A.; Vega, S., Theoretical aspects of dynamic nuclear polarization in the solid state – The solid effect. *J. Magn. Reson.* **2010,** *207* (2), 176-189.

57.   Hovav, Y.; Feintuch, A.; Vega, S., Dynamic nuclear polarization assisted spin diffusion for the solid effect case. *J. Chem. Phys.* **2011,** *134* (7), 074509.

58.   Hu, K.-N.; Debelouchina, G. T.; Smith, A. A.; Griffin, R. G., Quantum mechanical theory of dynamic nuclear polarization in solid dielectrics. *J. Chem. Phys.* **2011,** *134* (12), 125105.

59.   Hovav, Y.; Feintuch, A.; Vega, S., Theoretical aspects of dynamic nuclear polarization in the solid state – The cross effect. *J. Magn. Reson.* **2012,** *214*, 29-41.

60.   Hu, K.-N.; Yu, H.-h.; Swager, T. M.; Griffin, R. G., Dynamic nuclear polarization with biradicals. *J. Am. Chem. Soc.* **2004,** *126* (35), 10844-10845.

61.   Hu, K.-N., Polarizing agents and mechanisms for high-field dynamic nuclear polarization of frozen dielectric solids. *Solid State Nucl. Magn. Reson.* **2011,** *40* (2), 31-41.

62.   Kurdzesau, F.; Brandt, B. v. d.; Comment, A.; Hautle, P.; Jannin, S.; Klink, J. J. v. d.; Konter, J. A., Dynamic nuclear polarization of small labelled molecules in frozen water–alcohol solutions. *Journal of Physics D: Appl. Phys.* **2008,** *41* (15), 155506.

63.   Sze, K. H.; Wu, Q.; Tse, H. S.; Zhu, G., Dynamic Nuclear Polarization: New Methodology and Applications. *NMR of Proteins and Small Biomolecules*, Ed. Springer Berlin Heidelberg: Berlin, Heidelberg, 2012; pp 215-242.

64.   Redfield, A. G., Nuclear Magnetic Resonance Saturation and Rotary Saturation in Solids. *Phys. Rev.* **1955,** *98* (6), 1787-1809.

65.   Abragam, A.; Proctor, W. G., Spin Temperature. *Phy. Rev.* **1958,** *109* (5), 1441-1458.

66.   Goertz, S. T., The dynamic nuclear polarization process. *Nucl. Instr. Meth. Phys. Res. A* **2004,** *526* (1), 28-42.

67.   Crabb, D. G.; Meyer, W., SOLID POLARIZED TARGETS FOR NUCLEAR AND PARTICLE PHYSICS EXPERIMENTS. *Annu. Rev. Nucl. Part. S.* **1997,** *47* (1), 67-109.

68.   Provotorov, B., Magnetic Resonance Saturation in Crystals. *Sov. Phys. Jetp-USSR* **1962,** *14* (5).

69.   Provotorov, B., 'A quantum-statistical theory of cross relaxation'. *Sov. Phys. JETP* **1962,** *15*.

70.   Murphy, D. M., Principles of pulse electron paramagnetic resonance. By A Schweiger and G Jeschke, Oxford University Press, *J. Chem. Technol. Biotechnol.* **2004,** *79* (1), 103-103.

71.   Weil, J. A.; Bolton, J. R., *Electron Paramagnetic Resonance: Elementary Theory and Practical Applications*. Wiley: 2007.

72.   Durieux, M.; Rusby, R. L., Helium Vapour Pressure Equations on the EPT-76. *Metrologia* **1983,** *19* (2), 67.

73.   Bornet, A.; Milani, J.; Vuichoud, B.; Perez Linde, A. J.; Bodenhausen, G.; Jannin, S., Microwave frequency modulation to enhance Dissolution Dynamic Nuclear Polarization. *Chem. Phys. Lett.* **2014,** *602*, 63-67.

74.   Leggett, J.; Hunter, R.; Granwehr, J.; Panek, R.; Perez-Linde, A. J.; Horsewill, A. J.; McMaster, J.; Smith, G.; Kockenberger, W., A dedicated spectrometer for dissolution DNP NMR spectroscopy. *Phys. Chem. Chem. Phys.* **2010,** *12* (22), 5883-5892.

75.   Bowen, S.; Hilty, C., Rapid sample injection for hyperpolarized NMR spectroscopy. *Phys. Chem. Chem. Phys.* **2010,** *12* (22), 5766-5770.

76.   Nelson, S. J.; Vigneron, D.; Kurhanewicz, J.; Chen, A.; Bok, R.; Hurd, R., DNP-Hyperpolarized 13C Magnetic Resonance Metabolic Imaging for Cancer Applications. *Appl. Magn. Reson.* **2008,** *34* (3), 533-544.

77.   UK Patent Application No 1710181.7. **2017**.

78.   Milani, J.; Vuichoud, B.; Bornet, A.; Mieville, P.; Mottier, R.; Jannin, S.; Bodenhausen, G., A magnetic tunnel to shelter hyperpolarized fluids. *Rev. Sci. Instrum.* **2015,** *86* (2), 024101.

79.   Halbach, K., Design of permanent multipole magnets with oriented rare earth cobalt material. *Nucl. Instr. Meth.* **1980,** *169* (1), 1-10.

2. Microwave Gating in DNP

Dynamic nuclear polarization (DNP)[1-2] has become a useful method to enhance NMR signals by transferring electronic spin polarization to the surrounding coupled nuclear spins. Nuclear spin polarization builds up through DNP in a solid sample doped with paramagnetic polarizing agents (PAs) at suitable temperatures and magnetic fields. Most dissolution-DNP polarizers usually work at 1.2 K, where the electron spin polarization is close to unity. At a magnetic field of 6.7 T and temperatures of 1.2 K the electron spin polarization is ca. 99.89%, almost fully polarized. To improve the DNP efficiency several studies suggest that increasing magnetic fields will provide higher enhancements at the expense of longer build up times.[3] However, one main limitation is the lack of microwave sources at higher frequencies.

Having an eye on D-DNP, it is worthwhile to improve ^{13}C polarization levels due to the long relaxation times of carbon nuclei, which make them promising candidates to survive the transfer delay during a D-DNP experiment. Using radicals such as Trityl that have narrow ESR lines such an experiment can be readily performed. There are many advantages in polarizing ^{13}C nuclear spins as (*i*) they can be enriched, (*ii*) there is no significant background signal, (*iii*) and the longitudinal relaxation times can be as long as $T_1(^{13}C) > 50$ s in carboxylic, carbonylic, or quaternary sites. This allows a significant part of the hyperpolarized magnetization of metabolites such as [1-^{13}C]pyruvate to survive

the transfer from the polarizer to the detection magnet, including injection into animals or patients. This method can be used in the field of MRI where hyperpolarized [1-^{13}C]pyruvate or other metabolites can be used to monitor enzymatic conversion rates. This enables real-time localized ^{13}C spectroscopy for tumor characterization in patients.[4] Several other low-γ nuclei such as ^{15}N or ^{129}Xe are also amenable.[5,6]

To speed up the ^{13}C polarization process, proton polarization can be transferred to this low-γ nuclei, by using cross polarization methods such that enhancements can be achieved up to a factor of 10^4 using dissolution-DNP.[7] Recently, Jannin and co-workers proposed to combine D-DNP with cross-polarisation (CP).[8-10] The abundant proton spins are first rapidly polarized using PAs with broad EPR lines such as TEMPO. The proton polarization can be as high as $P(^1H) > 90\%$ at $T = 1.2$ K and $B_0 = 6.7$ T. This polarization can subsequently be transferred to ^{13}C. This indirect strategy provides high polarizations $P(^{13}C)$ with short build-up times.

Here we show that this method can been improved by using microwave gating during the cross polarization experiment. By switching the microwave irradiation off prior to CP, the electron polarization returns to a highly polarized Boltzmann thermal equilibrium P_e^{TE} on the time-scale of $T_1(e)$ which is on the order of 100 ms in our systems. As a result, the proton relaxation time in the rotating frame in the presence of a radiofrequency field, $T_{1\rho}(^1H)$, can be extended by as much as an order of magnitude, while $T_{1\rho}(^{13}C)$ also increases by a smaller factor. This allows the CP contacts to be extended, thus significantly improving CP efficiency. By gating the microwave irradiation, a polarization $P(^{13}C) = 64\%$ could be achieved in [1-^{13}C]acetate with build-up time constants as short as 160 s. A record polarization of $P(^{13}C) = 78\%$ could be reached in [^{13}C]urea, albeit with a somewhat longer build-up time constant of 470 s. Experimental details and observations of the impact of microwave gating on CP-DNP combinations will be discussed in detail in this chapter.

2.1 Nuclear polarization transfer

Polarization transfer techniques are used in magnetic resonance to transfer the magnetization between two different spins to enhance the polarization of low-γ nuclei.[8] This method can also be used in DNP, for both, MAS-DNP and dissolution-DNP. In this section, I will briefly discuss the implementation of the CP method in dissolution-DNP at 6.7 T as performed in our laboratory.

2.1.1 Cross Polarization

Using cross polarization (CP) methods, the polarization of low-γ nuclei can be enhanced by the factor γ_I/γ_X, where γ_I and γ_x denote the gyromagnetic ratios of spins *I* and *X,* respectively.

Cross polarization techniques were first introduced by Hartmann and Hahn in 1962.[8] Usually, the idea of CP is to transfer the polarization from high-γ nuclei to low-γ nuclei through strong dipolar interactions between ^{1}H and nuclei *X*. A typical CP pulse sequence is shown in Fig. 2.1. Cross-polarization is reviewed in detail by Rovnyak[11] and can also be found in the monograph by Ernst et al.[12]
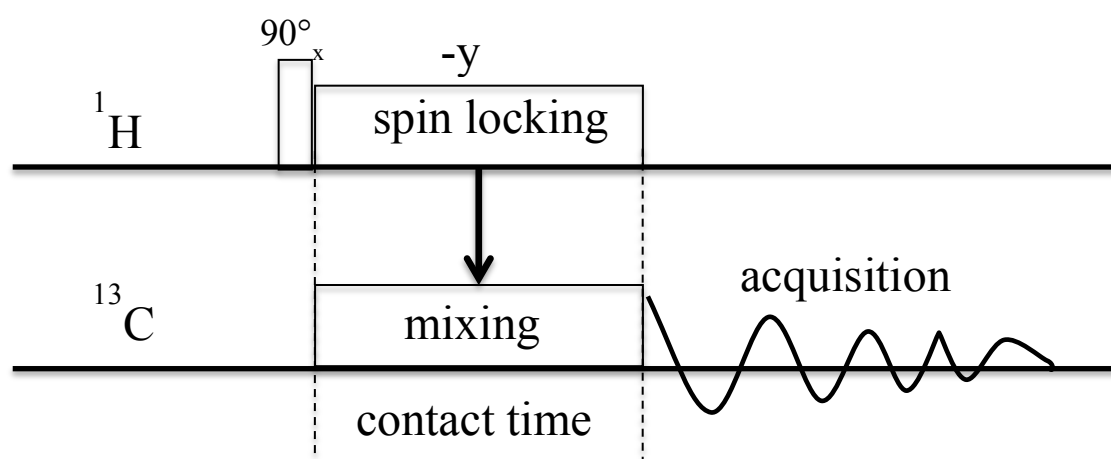

Figure 2.1. Cross Polarization (CP) pulse sequence. A $\pi/2$ pulse is applied to the *I* spin along the x-axis of the rotating frame and followed by spin locking fields on both

channels. During the spin locking time period cross polarization takes place and finally ^{13}C spin is observed.

The sequence in Fig. 2.1 shall exemplify how proton spins are excited via a 90° pulse and how their energy is then transferred to the observed ^{13}C nucleus by using a long low-power pulse on both channels (usually called spin locking pulse or contact pulse). Fast spin lattice relaxation of the protons allows repeating the sequence in short intervals. During the experiment, the magnetization is exchanged through mutual energy conserving spin flips in homonuclear systems, but for systems with heteronuclei, the exchange of magnetization must be driven externally, through RF fields. Thus, the CP methods require two continuous RF fields at the resonance frequencies of spins *I* and *X*.

The RF power ratio between the contact pulses needs to be tuned so that the transition energy for both nuclei become similar. The RF field rotates the magnetization around the axis of the applied field such that the rotation frequency depends on the frequency and amplitude of the RF field. When the rotation frequencies of I and X spins are equal, an energy-conserving dipolar contact between the two spin systems is created, which results in an energy exchange between them. This condition is often denoted as Hartmann–Hahn condition. It can be expressed via the amplitudes of the two spin locking fields:

$$\gamma_I B_{1I} = \gamma_X B_{1X} \qquad (2.1)$$

Under such conditions, differences between their respective energy levels in the rotating frame are equalized and a transfer of energy through the dipolar couplings is allowed.

2.1.2 Combination of CP and dissolution-DNP

Radicals with narrow line-width, e.g, trityl, are efficient to polarize directly ^{13}C

even though it takes a long time to achieve high steady state polarization levels at 1.2 K.[13] However, the long build up time for ^{13}C does not allow performing DNP experiments frequently such that DNP was combined with CP to circumvent this problem. Using TEMPOL as a radical, DNP with CP methods was optimized by Bornet at a magnetic field 3.35 T and temperatures near at 1.2 K (for more details see ref. [14]). TEMPOL has a rapid buildup time constant for protons and combining cross polarization with dissolution-DNP can be very efficient.[9-10] In the following I will outline a work including some theoretical background that we have carried out at EPFL Lausanne and which has been published as Ref [15]. It aims at enhancing the CP efficiency by employing the abovementioned microwave gating or interruption approach.

2.2 Boosting CP Efficiency by Microwave Gating

2.2.1 Paramagnetic Relaxation

A nuclear spin at a distance *r* from an electron spin relaxes in the rotating frame at the rate constant $R_{1,\rho}$ as a function of time

$$R_{1,\rho}(t) = \frac{1}{T_{1\rho}(t)} \qquad (2.2)$$

Under conditions that are suitable for DNP, a significant contribution to the relaxation rate constant in the rotating frame $1/T_{1\rho}(^1H)$ can arise from the presence of PAs. This has been extensively studied in the presence and absence of spin diffusion,[16-17] albeit using a theoretical treatment that is valid in the high temperature limit only. The spin-locked magnetization of a nuclear spin *I* at a distance *r* from an electron spin S = ½ relaxes with the following rate constant

$$\frac{1}{T_{1\rho}} = \frac{C}{r^6} \frac{\tau}{1+\omega_1^2 \tau^2} \qquad (2.3)$$

where r is the distance between the electron and nuclear spin, ω_1 the nuclear angular nutation frequency in the rotating frame, and τ the rate of fluctuations of the electron dipolar field seen by the nuclear spins, and C a constant (see supplement of reference[15] for details on τ and C). This equation is however only valid in the high-temperature approximation where the electron spin polarization is negligible.

2.2.2 Microwave irradiation can shorten $T_{1\rho}$

Typically, at cryogenic temperatures and high fields, the electron spin polarization in thermal equilibrium P_e^{TE} can be close to unity (so that the electron polarization cannot be neglected in theoretical treatments), which leads to an attenuation of the transition rates within the electron spin manifold by a factor of[18]

$$\kappa = 1 - P_e^{\mu w} \cdot P_e^{TE} \tag{2.4}$$

where $P_e^{\mu w}$ is the partly saturated electron spin polarization in the presence of microwave irradiation. This leads to an acceleration of the relaxation rate constant in the rotating frame:

$$\frac{1}{T_{1\rho}} = \frac{C}{r^6} \frac{\kappa\,\tau}{1+\omega_1{}^2\,(\kappa\,\tau)^2}$$

$$= \frac{C}{r^6} \frac{\tau(1-P_e^{\mu w}\cdot P_e^{TE})}{1+\omega_1{}^2\,\tau^2(1-P_e^{\mu w}\cdot P_e^{TE})^2} \tag{2.5}$$

Under magic angle spinning (MAS) conditions, typically T = 100 K and B_0 = 9.4 T, the electron spin polarization in thermal equilibrium is relatively low with P_e^{TE} = 6.3%, which translates into $0.996 < \kappa < 1$, so that $1/T_{1\rho}$ remains essentially the same with or without electron spin saturation by microwave irradiation. However, under D-DNP conditions, typically at T = 1.2 K and B_0 = 6.7 T, the electron spin polarization in thermal equilibrium is close to unity with P_e^{TE} = 99.89%, which translates into $2.1 \cdot 10^{-3} < \kappa < 1$. Therefore one can

expect an increase in $1/T_{1\rho}$ by several orders of magnitude when microwave irradiation is applied to saturate the electron spin transition.

To verify this, $T_{1\rho}(^1\text{H})$ relaxation curves of the proton spins were measured with a suitable pulse sequence (Fig. 2.2) at B_0 = 9.4 T and T = 100 K (Fig. 2.3a) and B_0 = 6.7 T and T = 1.2 K (Fig. 2.3b) with and without microwaves at 263 GHz and 188.3 GHz respectively (in the latter case, frequency modulation over a range $\Delta f_{\mu w}$ = 50 MHz at a rate f_{mod} = 10 kHz[19] was applied) in a frozen glassy sample containing 3 M [1-^{13}C]acetate in H_2O:D_2O:glycerol-d_8 (v:v:v = 1:4:5) doped with 40 mM TEMPOL as a polarizing agent. As can be explained by theory (see equation 2.5), the effect of microwave irradiation on $1/T_{1\rho}$ is not significant at B_0 = 9.4 T and T = 100 K, but it can dramatically change the $1/T_{1\rho}$ at B_0 = 6.7 T and T = 1.2 K.

As expected, the effect of microwave irradiation on $1/T_{1\rho}$ is insignificant at B_0 = 9.4 T and T = 100 K, but is dramatic at B_0 = 6.7 T and T = 1.2 K.
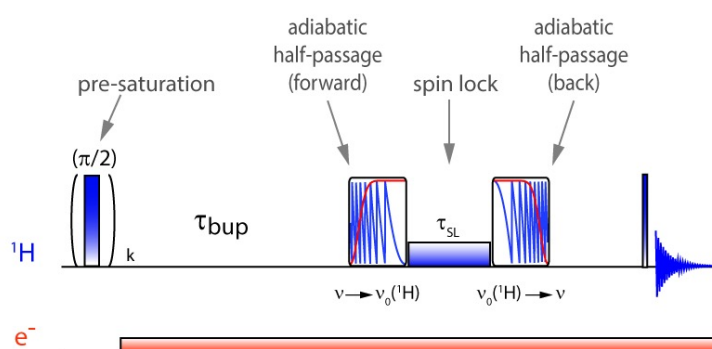
a   Spin-locking pulse sequence

Figure 2.2. Pulse sequence used to measure $T_{1\rho}(^1\text{H})$ where the proton spins are saturated by a train of 90° pulses, and subsequently evolve during a fixed delay τ_{bup} = 2 s, either relaxing to their equilibrium if there is no microwave irradiation, or building up towards their DNP steady-state in the presence of microwave irradiation. After τ_{bup} has elapsed, a half-chirp pulse (swept from -100 kHz to the centre of the line in 175 μs, with a sweep rate of 0.57 kHz/μs and an amplitude $\gamma B_1/(2\pi)$ = 20 kHz) is applied to the

protons to bring their magnetization into the transverse plane. This is followed by a spin-lock pulse with the same amplitude of 20 kHz and a variable duration τ_{SL}. Finally, the magnetization is flipped back along the longitudinal axis with another half-chirp pulse (swept from the center of the line to -100 kHz in 175 μs, all other parameters being identical) and the proton NMR signal is observed following a 10° excitation pulse.

a $T_{1\rho}$ with and without microwave irradiation at 100 K
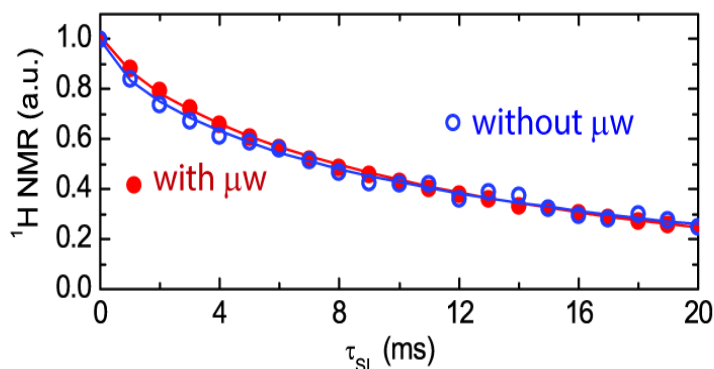
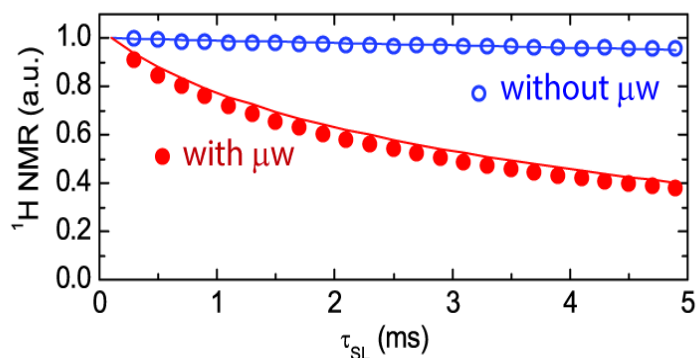**b** $T_{1\rho}$ with and without microwave irradiation at 1.2 K

Figure 2.3. (a) Proton $T_{1\rho}$ decay measured at B_0 = 9.4 T and T = 100 K in a frozen glassy sample containing 3 M [1-^{13}C]acetate in H_2O:D_2O:glycerol-d_8 (v:v:v = 1:4:5) doped with 40 mM TEMPOL, with (●) and without (○) microwave irradiation with $P_{\mu w}$ = 4 W and $f_{\mu w}$ = 263 GHz. **(b)** Proton $T_{1\rho}$ decay measured at B_0 = 6.7 T and T = 1.2 K in the same sample, with (●) and without (○) microwave irradiation with $P_{\mu w}$ = 87.5 mW and $f_{\mu w}$ = 188.3 GHz modulated over a range $\Delta f_{\mu w}$ = 50 MHz at a rate f_{mod} = 10 kHz.

In the absence of microwave irradiation, the thermal equilibrium polarization P_e^{TE} depends only on the sample temperature, i.e., $P_e^{TE} = 99.89\%$ at 1.2 K. In the presence of microwave irradiation, the electron polarization $P_e^{\mu w}$ was treated as an adjustable temperature-dependent parameter and was estimated to be $P_e^{\mu w} = 48\%$ at 1.2 K, bearing in mind that $P_e^{\mu w} = 0\%$ would describe complete saturation. Even a partial saturation of the electron spin polarization of $P_e^{\mu w} = 48\%$ severely affects the proton relaxation rate constant in the rotating frame $1/T_{1\rho}(^1\text{H})$. This in turn determines how much magnetization remains after spin locking during an interval τ_{SL}. When the microwaves are switched off, we determined $T_{1\rho}(^1\text{H}) \approx 200$ ms, so that more than 90% of the spin-locked proton magnetization survives after spin-locking for τ_{SL} = 10 ms, but this value drops to 20% when the microwaves are switched on, since $T_{1\rho}(^1\text{H}) \approx 10$ ms in this case.

a $T_{1\rho}$ curves varying microwave power

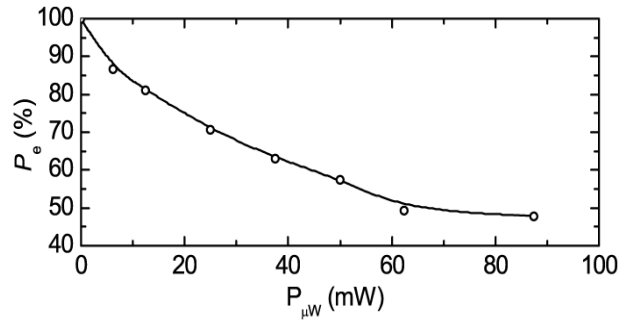**b** Average electron spin polarization
under microwave irradiation

71
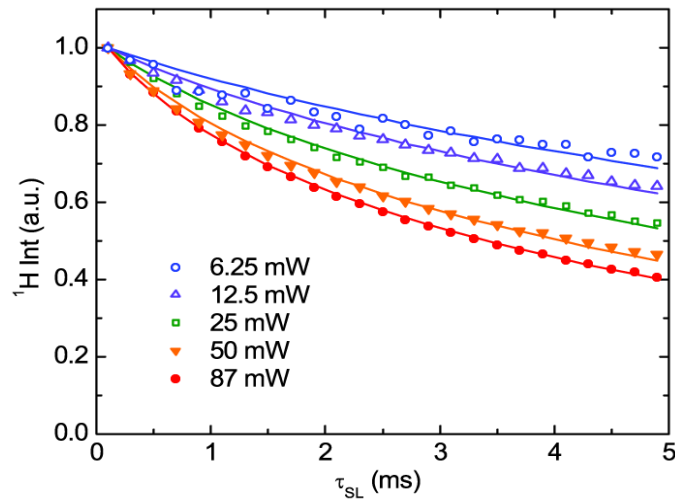
Figure 2.4: a) $T_{1\rho}(^1H)$ decay of the proton magnetization measured with the sequence of Fig. 1a as a function of the applied microwave power $P_{\mu w}$ (with $f_{\mu w} = 188.3$ GHz, $\Delta f_{\mu w} = 50$ MHz, $f_{mod} = 10$ kHz) in 3 M [1-^{13}C]acetate in D_2O:H_2O:glycerol-d_8 (v:v:v = 1:4:5) doped with 40 mM TEMPOL, at 1.2 K and 6.7 T. This behavior reflects varying degrees of saturation of the electron polarization. **b**) Average electron spin polarisations under microwave irradiation $P_e^{\mu w}$ (averaged over the whole ESR line) as a function of the power $P_{\mu w}$ of the microwave irradiation, estimated by numerical fits (for simulation details see the reference[15]) (the line is drawn to guide the eye).

Fitting the $T_{1\rho}$ relaxation curves with home-written MATLAB routines, performed by Bornet, (see reference[15] for details) offers a way to estimate the electron spin polarization $P_e^{\mu w}$. Figure 2.4a shows seven $T_{1\rho}$ relaxation curves measured with the sequence of Fig. 2.2 with different microwave powers $P_{\mu w}$ ranging from 6.25 to 87 mW. The only parameter that varies between these experiments is the extent of saturation of the electron spin resonance, and hence the electron-spin polarization under microwave irradiation $P_e^{\mu w}$. The electron spin polarizations $P_e^{\mu w}$ deduced from the fits are reported in Fig. 2.4b as a function of the applied microwave power $P_{\mu w}$.

2.2.3 Microwave gating extends $T_{1\rho}$

Microwave irradiation is essential for DNP experiments but as seen above the partial saturation of the electron spins leads to shortening of the nuclear $T_{1\rho}$. We propose here to interrupt the microwave irradiation during a time $\tau_{gate} \sim 5\,T_{1e}$ prior to spin-locking, in order to allow the electrons to relax to their highly polarized thermal equilibrium P_e^{TE} at 1.2 K and 6.7 T. Fig. 2.5a shows the spin-locking sequence with microwave gating (the pulse parameters for the protons are the same as in Fig. 2.2). Fig. 2.5b displays the proton signal integral measured after spin locking ($\gamma B_1(^1H)/(2\pi) = 20$ kHz, $\tau_{SL} = 5$ ms) as a function of the microwave gating interval τ_{gate}. Clearly, the relaxation time $T_{1\rho}(^1H)$ is extended as the electron spin polarization relaxes back to its highly polarized state after

switching off the microwave irradiation. As a result, the proton signal that survives the spin locking experiment increases when the gating period is extended, until it reaches a plateau. The experimentally observed relaxation time $T_{1\rho}$ (^{1}H) allows one to estimate the electron T_{1e} under our experimental conditions. In this work, comparison between experiments and simulations (for details see reference[15]) allowed us to estimate the electron spin-lattice relaxation time $T_{1e} = 48 \pm 1$ ms. We systematically used a microwave gating interval $\tau_{gate} = 500$ ms ($\gg T_{1e}$) in all subsequent experiments.

a Gated spin-locking pulse sequence

b ^{1}H signal varying τ_{gate}
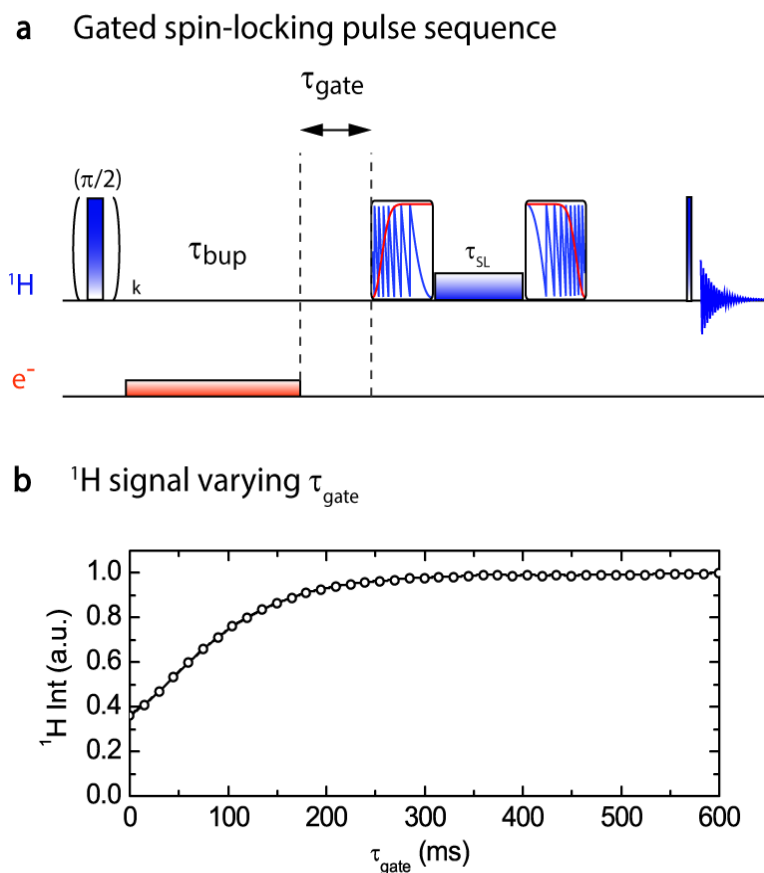
Figure 2.5. a) Pulse sequence used to determine $T_{1\rho}(^1$H) with microwave gating. **b**) Proton signal integrals in 3 M [1-^{13}C]acetate in $D_2O:H_2O$:glycerol-d_8 (v:v:v = 1:4:5) doped with 40 mM TEMPOL measured at B_0 = 6.7 T and T = 1.2 K after spin locking ($\gamma B_1 = 20$ kHz, $\tau_{SL} = 5$ ms) as a function of the gating interval τ_{gate} with the microwave parameters $P_{\mu w} = 87.5$ mW, $f_{\mu w} = 188.3$ GHz, $\Delta f_{\mu w} = 50$ MHz, and $f_{mod} = 10$ kHz, (a line was drawn to guide the eye).

2.2.4 The advantages of microwave gating are substantial at low temperatures

Fig. 2.6 shows the $T_{1\rho}$ relaxation curves measured at different temperatures with the pulse sequence of Fig. 2.5a, with continuous or gated microwaves (fixed gating interval $\tau_{gate} = 500$ ms and τ_{SL} varied from 0 to 10 ms). With continuous microwaves, all $T_{1\rho}$ curves are alike, featuring a fast decay of the magnetization during spin locking. However, with gated microwaves, the magnetization can survive spin locking remarkably well, and especially at the lowest temperature $T = 1.2$ K where $\kappa = 0.00055$. On the other hand, the advantages of microwave gating diminish at higher temperatures as the thermal equilibrium electron spin polarization P_e^{TE} becomes significantly lower that unity.
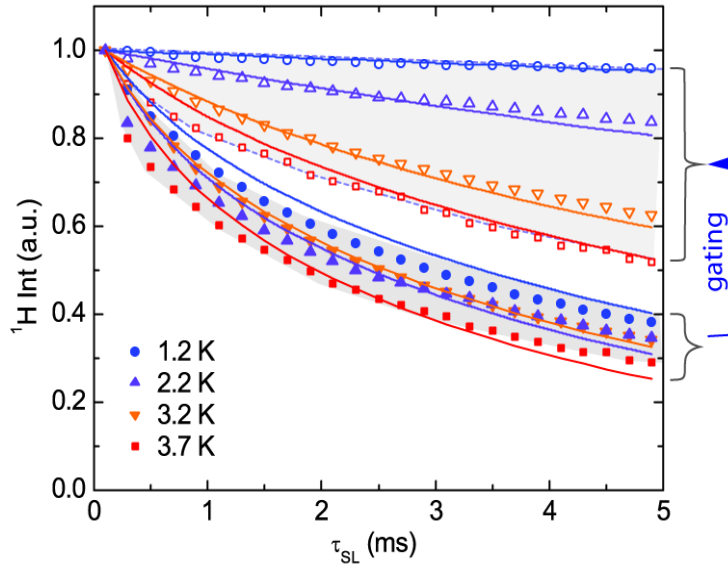
Figure 2.6. $T_{1\rho}(^1H)$ decay of the proton magnetization in 3 M [1-^{13}C]acetate in H$_2$O:D$_2$O:glycerol-d$_8$ (v:v:v = 1:4:5) doped with 40 mM TEMPOL with continuous or gated microwaves ($P_{\mu w} = 87.5$ mW, $f_{\mu w} = 188.3$ GHz, $\Delta f_{\mu w} = 50$ MHz, $f_{mod} = 10$ kHz) as a function of the sample temperature, i.e., as function of the electron Boltzmann polarization P_e^{TE}. The fast decays observed with continuous microwaves (lower curves) reflect varying degrees of saturation of the electron polarization, while the behavior with gated microwaves (upper curves) reflects the thermal electron spin polarization P_e^{TE} that depends on the sample temperature.

2.2.5 Microwave gating improves the efficiency of cross polarization

Jannin and coworkers have recently shown that D-DNP can be boosted by performing $^1H \rightarrow {}^{13}C$ cross-polarization (CP) in combination with DNP.[20] Here we show that the microwave gating strategy can greatly improve the CP efficiency by switching off the microwave prior to the CP. Fig. 2.7a shows the pulse sequence used for CP with gated microwaves, which is simply an extension of the sequence of Fig. 2.5a with spin locking also applied on ^{13}C to allow Hartmann-Hahn contact between ^1H and ^{13}C (pulse parameters for ^1H and ^{13}C are the same as in Fig. 2.2, except that a 50%→100% ramp with an average $\gamma B_1(^1H)/(2\pi) = 20$ kHz rather than a rectangular excitation is applied to ^{13}C during τ_{CP}). Fig. 2.7b shows the ^{13}C magnetization as a function of the CP contact time τ_{CP}, without and with microwave gating. With continuous microwaves, the optimum CP contact time lies around $\tau_{CP} = 1.5$ ms before the decay of the ^1H magnetization (see Fig. 2.7a) compromises the transfer of polarization to ^{13}C. With gated microwaves, CP contact times can be much longer (in this example with an optimum around $\tau_{CP} = 20$ ms) thanks to the extended relaxation time $T_{1\rho}(^1H)$ (see Fig. 2.6), leading to a significantly improved CP efficiency (more than 50% improvement in our sample). Note that this improvement is expected to be even more important for systems where the magnetization is transferred to ^{13}C from remote protons and necessitates extended CP contact times (for example for deuterated molecules immersed in a protonated solvent [21]).

a ^1H - ^{13}C Cross Polarization pulse sequence
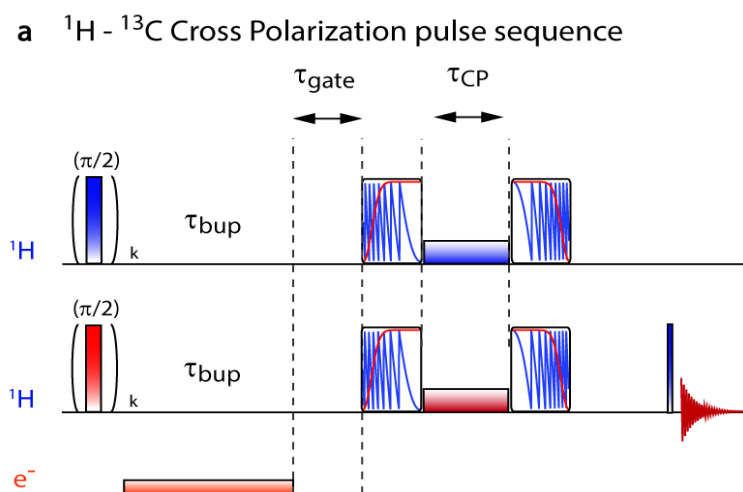
b CP efficiency varying τ_{CP}
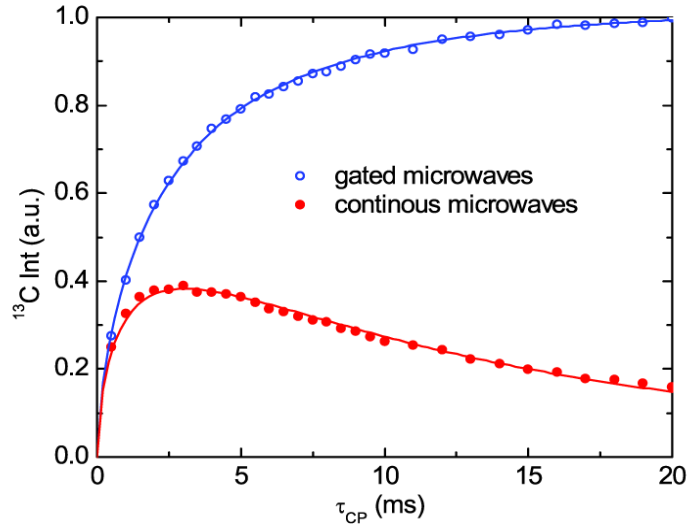with gated or continuous microwaves.

Figure 2.7. a) Pulse sequence for multiple-contact cross-polarization enhanced by DNP. The adiabatic half passage pulses sweep over 100 kHz in 175 μs. The rf amplitude for ^{13}C is ramped from 50% to 100% of the average rf amplitude which was $\gamma B_1(^1H)/(2\pi) =$ 20 kHz on both channels. The microwave irradiation is gated off during the intervals $\tau_{gate} = 500$ ms and τ_{CP}. **b**) Signal amplitude of ^{13}C after a single CP transfer from ^{1}H to ^{13}C as a function of the CP contact time τ_{CP}, with gated ($\bigcirc$) or continuous ($\bullet$) microwave irradiation ($P_{\mu w} = 87.5$ mW, $f_{\mu w} = 188.3$ GHz, $\Delta f_{\mu w} = 50$ MHz, $f_{mod} = 10$ kHz) in 3 M sodium [1-^{13}C]acetate with 40 mM TEMPOL at 1.2 K and 6.7 T. Details of the fits are given in the supplement of reference[15].

In a D-DNP experiment, one aims at building up the highest possible ^{13}C polarization prior to dissolution. We have shown that the ^{13}C polarization can be maximized by applying multiple CP contacts at intervals $\Delta_{CP} \sim \tau_{DNP}(^1H)$. The time interval Δ_{CP} allows for the proton polarization to be replenished by DNP before being drained again during the next CP contact. The use of microwave gating in this context has two favourable outcomes; (*i*) reducing losses of proton magnetization during spin locking (as shown in Figure 2.6) and (*ii*) improving the CP transfer efficiency (shown in Fig. 2.7b). Altogether, the efficiency of the multiple CP sequence is greatly improved by microwave gating, as shown in Fig. 2.8 where the evolution of both ^{1}H and ^{13}C polarizations is followed using small nutation angle pulses in the course of a multiple CP experiment. With a fixed

76

interval Δ_{CP} = 160 s, we applied optimal CP contact durations τ_{CP} = 16 ms and τ_{CP} = 1.5 ms respectively, which led to $P(^{13}C)$ = 64% with effective build-up time constants $\tau_{DNP}{}^{CP}(^{13}C)$ = 168 s with microwave gating. This compares favorably with and $P(^{13}C)$ = 38% with $\tau_{DNP}{}^{CP}(^{13}C)$ = 190 s with continuous microwaves. Using microwave gating thus enhances the build-up of the final ^{13}C polarization by a factor 1.7.

a ^{13}C CP build-ups (gated and cw-μw CP)   **b** ^{1}H build-ups (free, or during gated and cw-μw CP)
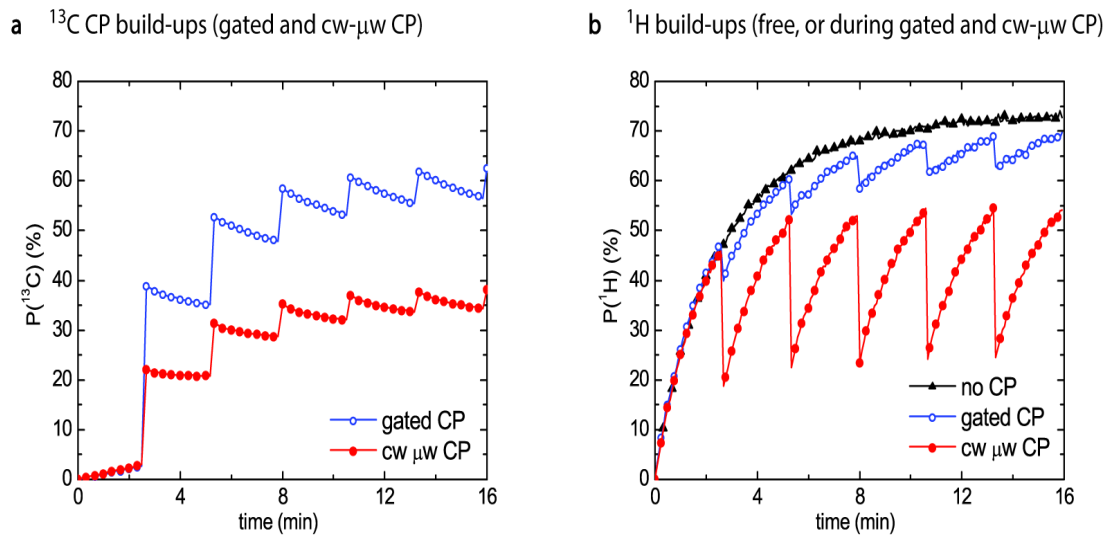
Figure 2.8. a) Build-up of polarization $P(^{13}C)$ during a multiple CP pulse sequence (see Fig. 5a) applied every 2.5 minutes with continuous (●) or gated (○) microwave irradiation ($P_{\mu w}$ = 87.5 mW, $f_{\mu w}$ = 188.3 GHz, $\Delta f_{\mu w}$ = 50 MHz, f_{mod} = 10 kHz) in 3 M sodium [1-^{13}C]acetate with 40 mM TEMPOL at 1.2 K and 6.7 T. b) DNP build-up of proton polarization $P(^1H)$ in the same sample and conditions without any CP (▲) or during multiple CP applied every 2.5 minutes with continuous microwave irradiation (●) or during multiple CP with gated microwave irradiation (○) (all lines are drawn to guide the eye)

2.2.6 Optimization of timing for several cross polarization steps

Next, experiments were performed to optimize the gap Δt_{CP} between consecutive CP contacts, using a multi-CP type of sequence. In Figure 2.9a, the maximal ^{13}C polarization reached is plotted as a function of Δt_{CP}. The apparent multi-CP build-

up time constant under the same conditions is also shown in Figure 2.9b. An optimal contact time of 5 ms was used when microwave gating is used, whereas it was reduced to a shorter value of 1.5 ms during microwave irradiation experiments, as less ^{1}H magnetization is lost during each CP contact, it is possible to accelerate the time under conditions when the microwaves are gated (optima of figure 2.7b).
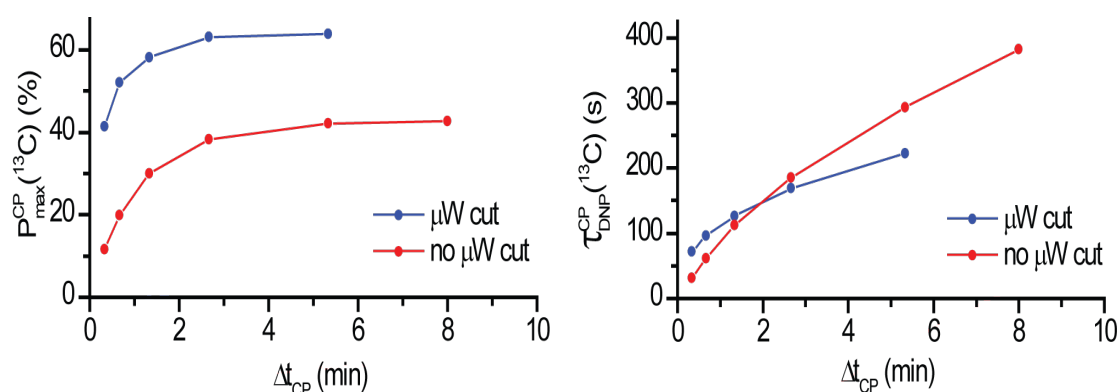

Figure 2.9. a) Maximal ^{13}C CP polarization as function of the inter-CP delay Δt_{CP} with continuous (●) or gated (○) microwave irradiation ($P_{\mu w} = 87.5$ mW, $f_{\mu w} = 188.3$ GHz, $\Delta f_{\mu w} = 50$ MHz, $f_{mod} = 10$ kHz) in 3 M sodium [1-^{13}C]acetate with 40 mM TEMPOL at 1.2 K and 6.7 T. b) CP build-up time constant as function of the inter-CP delay Δt_{CP} (all lines are drawn to guide the eye).

When the microwave irradiation is switched off prior to CP, an inter-CP delay Δt_{CP} = 160 s yields an optimal ^{13}C CP polarization. In this case, the ^{13}C CP buildup time constant is only τ_{DNP}^{CP} = 168 s. Without microwave gating, the optimal ^{13}C CP polarization is reached with Δt_{CP} = 320 s. The ^{13}C CP buildup time constant is then almost doubled to τ_{DNP}^{CP} = 292 s. Therefore, microwave gating allows one to build the polarization faster.

As the losses of $P(^1$H) during CP contacts are greatly reduced by microwave gating, the proton polarization in the course of a CP-DNP sequence with gated microwaves almost reaches the same value as when CP is not used. In samples containing methyl groups, such as sodium pyruvate or sodium acetate, the steady state is typically limited to $P(^1$H) = 70% because of relaxation induced by

the rotation of the CH$_3$ groups. Using non-methylated DNP samples, such as [^{13}C]urea dissolved in H$_2$O:D$_2$O:glycerol-d$_8$ (v:v:v = 1:4:5) with 40 mM TEMPOL, $P(^1$H) builds up to 90% under our DNP conditions at 1.2 K. Using CP with microwave gating, it was possible to reach a polarization of $P(^{13}$C) = 78% for this sample.

2.3 Conclusions

Low temperature DNP relies on the steady-state saturation of the electron spins of paramagnetic polarizing agents through microwave irradiation. We have shown here how this saturation leads to a significant deleterious shortening of the nuclear spin relaxation times in the rotating frame $T_{1\rho}$ (^{1}H). The shortening of $T_{1\rho}$ is obviously detrimental for cross-polarisation from ^{1}H to ^{13}C or other low-gamma nuclei. However, we demonstrate that this can be avoided by briefly gating off the microwave irradiation prior to cross-polarisation., For ^{1}H→^{13}C cross-polarization, the final ^{13}C polarization can be boosted by 70% (i.e., increased by a factor 1.7), resulting in $P(^{13}$C) = 64% in [1-^{13}C]acetate with a build-up time constant of 160 s, and $P(^{13}$C) = 78% in [^{13}C]urea with at time constant of 470 s. The characteristic time constant of the return of the electron spins to their thermal equilibrium can be determined by simulations and was found to be T_{1e} = 70 ms for the system under investigation at 1.2 K.

References for chapter 2

1.   Carver, T. R.; Slichter, C. P., Polarization of Nuclear Spins in Metals. *Physical Review* **1953,** *92* (1), 212-213.

2.   Overhauser, A. W., Polarization of Nuclei in Metals. *Physical Review* **1953,** *92* (2), 411-415.

3.   Jannin, S.; Comment, A.; Kurdzesau, F.; Konter, J. A.; Hautle, P.; van den Brandt, B.; van der Klink, J. J., A 140 GHz prepolarizer for dissolution dynamic nuclear polarization. *J Chem Phys* **2008,** *128* (24), 241102.

4.   Nelson, S. J.; Kurhanewicz, J.; Vigneron, D. B.; Larson, P. E. Z.; Harzstark, A. L.; Ferrone, M.; van Criekinge, M.; Chang, J. W.; Bok, R.; Park, I.; Reed, G.; Carvajal, L.; Small, E. J.; Munster, P.; Weinberg, V. K.; Ardenkjaer-Larsen, J. H.; Chen, A. P.; Hurd, R. E.;

Odegardstuen, L.-I.; Robb, F. J.; Tropp, J.; Murray, J. A., Metabolic Imaging of Patients with Prostate Cancer Using Hyperpolarized [1-(13)C]Pyruvate. *Science translational medicine* **2013,** *5* (198), 198ra108-198ra108.

5.   Sarkar, R.; Comment, A.; Vasos, P. R.; Jannin, S.; Gruetter, R.; Bodenhausen, G.; Hall, H.; Kirik, D.; Denisov, V. P., Proton NMR of (15)N-choline metabolites enhanced by dynamic nuclear polarization. *J Am Chem Soc* **2009,** *131* (44), 16014-5.

6.   Comment, A.; Jannin, S.; Hyacinthe, J. N.; Mieville, P.; Sarkar, R.; Ahuja, P.; Vasos, P. R.; Montet, X.; Lazeyras, F.; Vallee, J. P.; Hautle, P.; Konter, J. A.; van den Brandt, B.; Ansermet, J. P.; Gruetter, R.; Bodenhausen, G., Hyperpolarizing gases via dynamic nuclear polarization and sublimation. *Phys Rev Lett* **2010,** *105* (1), 018104.

7.   Ardenkjaer-Larsen, J. H.; Golman, K.; Gram, A.; Lerche, M. H.; Servin, R.; Thaning, M.; Wolber, J., Increase of signal-to-noise of more than 10,000 times in liquid state NMR. *Discov Med* **2003,** *3* (19), 37-9.

8.   Hartmann, S. R.; Hahn, E. L., Nuclear Double Resonance in the Rotating Frame. *Physical Review* **1962,** *128* (5), 2042-2053.

9.   Pines, A.; Gibby, M. G.; Waugh, J. S., Proton-Enhanced Nuclear Induction Spectroscopy. A Method for High Resolution NMR of Dilute Spins in Solids. *The Journal of Chemical Physics* **1972,** *56* (4), 1776-1777.

10.   Pines, A.; Gibby, M. G.; Waugh, J. S., Proton-enhanced NMR of dilute spins in solids. *The Journal of Chemical Physics* **1973,** *59* (2), 569-590.

11.   Rovnyak, D., Tutorial on analytic theory for cross-polarization in solid state NMR. *Concepts in Magnetic Resonance Part A* **2008,** *32A* (4), 254-276.

12.   Ernst, R. R.; Bodenhausen, G.; Wokaun, A., *Principles of Nuclear Magnetic Resonance in One and Two Dimensions*. Clarendon Press: 1987.

13.   Ardenkjaer-Larsen, J. H.; Leach, A. M.; Clarke, N.; Urbahn, J.; Anderson, D.; Skloss, T. W., Dynamic nuclear polarization polarizer for sterile use intent. *NMR in Biomedicine* **2011,** *24* (8), 927-932.

14.   Bornet, A.; Melzi, R.; Jannin, S.; Bodenhausen, G., Cross Polarization for Dissolution Dynamic Nuclear Polarization Experiments at Readily Accessible Temperatures 1.2 < T < 4.2 K. *Applied Magnetic Resonance* **2012,** *43* (1-2), 107-117.

15.   Bornet, A.; Pinon, A.; Jhajharia, A.; Baudin, M.; Ji, X.; Emsley, L.; Bodenhausen, G.; Ardenkjaer-Larsen, J. H.; Jannin, S., Microwave-gated dynamic nuclear polarization. *Phys Chem Chem Phys* **2016,** *18* (44), 30530-30535.

16.   Lowe, I. J.; Tse, D., Nuclear Spin-Lattice Relaxation via Paramagnetic Centers. *Physical Review* **1968,** *166* (2), 279-291.

17.   Tse, D.; Hartmann, S. R., Nuclear Spin-Lattice Relaxation Via Paramagnetic Centers Without Spin Diffusion. *Physical Review Letters* **1968,** *21* (8), 511-514.

18.   Wenckebach, W. T., *Essentials of Dynamic Nuclear Polarization*. Spindrift Publications: 2016.

19.   Bornet, A.; Milani, J.; Vuichoud, B.; Perez Linde, A. J.; Bodenhausen, G.; Jannin, S., Microwave frequency modulation to enhance Dissolution Dynamic Nuclear Polarization. *Chemical Physics Letters* **2014,** *602*, 63-67.

20.   Bornet, A.; Melzi, R.; Perez Linde, A. J.; Hautle, P.; van den Brandt, B.; Jannin, S.; Bodenhausen, G., Boosting Dissolution Dynamic Nuclear Polarization by Cross Polarization. *J Phys Chem Lett* **2013,** *4* (1), 111-4.

21.   Vuichoud, B.; Milani, J.; Bornet, A.; Melzi, R.; Jannin, S.; Bodenhausen, G., Hyperpolarization of deuterated metabolites via remote cross-polarization and dissolution dynamic nuclear polarization. *J Phys Chem B* **2014,** *118* (5), 1411-5.

3. Dissolution DNP of Deuterated Molecules

3.1 Introduction to DNP in Deuterated Systems

D-DNP is a method aiming at producing out-of-equilibrium polarization. Thus, processes that cause a return of nuclear polarization to its equilibrium value naturally counteract DNP effects. Such processes are summarized under the notion of relaxation. Hence, for efficient DNP we need either to find systems that relax intrinsically slow towards their equilibrium or we need to find methods that allow to overcome relaxation.

Spin ½ nuclei typically display slower relaxation, and most D-DNP applications were mostly focused on these. Apart from ^{1}H and ^{13}C, D-DNP also has been performed on ^{15}N,[1] ^{89}Y[2] and ^{107}Ag, ^{109}Ag complexes.[3] In contrast, spins with a quantum number >1/2 are influenced by an electric quadrupole moment, which constitutes an additional strong source of relaxation. In this thesis, I want to demonstrate how we can neutralize this additional source, at least partially. The approach is inspired by so-called long-lived states (LLS) that have been introduced by Levitt and co-workers approximately a decade ago.[4-5] LLS reduce the influence of dipolar contributions to relaxation by exploiting the Pauli principle, which leads to a separation of spin states that belong to different

symmetry manifolds. Likewise, a reduction of quadrupolar contributions by exploiting symmetry properties of a system will be introduced here.

At first sight, deuterium does not seem to be an attractive nucleus for D-DNP, since its polarization $P(D) = P(^2H)$ that is proportional to the longitudinal magnetization that we shall refer to as D_z usually decays rapidly with a characteristic longitudinal relaxation time $T_1(D_z)$ that is on the order of 1 s under our experimental conditions, i.e., for small molecules with correlation times in the low picosecond range at room temperature in high magnetic fields.[6] Since the transfer of hyperpolarized substances after dissolution to an NMR or MRI system typically requires 4-10 s (unless it is accelerated by high pressure[7]), most D_z magnetization will be lost by the time the sample arrives in the NMR or MRI apparatus because of rapid quadrupolar relaxation.

To circumvent the same problem, we have developed a means to hyperpolarize long-lived states involving pairs of deuterium nuclei that have scalar couplings to a ^{13}C nucleus. This approach is based on cross-polarization (CP) to polarize the nuclei of interest and on the subsequent exploitation of long-lived spin states.

Thus we have extended the LLS methodology by adding deuterium to the list of accessible nuclei, opening new avenues for D-DNP, such as the study of molecular dynamics of deuterated molecules and improved sensitivity of deuterium NMR. This work has now been published.[8]

In the following, I will discuss the most important relaxation mechanisms that we encounter at high magnetic fields used in modern NMR spectroscopy. Finally, a special focus will be on quadrupolar interactions, and we shall shed some light on the properties and principles of LLS.

3.2 General Considerations About Nuclear Relaxation

A process by which a perturbed spin system returns to thermal equilibrium is known as relaxation. This phenomenon is well known in all regimes of

spectroscopy. Relaxation in NMR is usually slower than in other spectroscopy methods. For example, an excited electronic spin state has a lifetime of a few microseconds, but vibrational and rotational energy levels have lifetimes of few nanoseconds, while in NMR, the magnetization returns back to its equilibrium in milliseconds, seconds or even a few minutes.

When the spin system is perturbed, its return back to its equilibrium state is achieved by two relaxation processes, longitudinal and transverse relaxation. When the bulk magnetization is rotated away from z-axis, the energy arrangement of the spin system is disturbed and spins will lose their energy. The process of the return of z-magnetization to its equilibrium value is denoted as longitudinal relaxation or spin-lattice relaxation. The longitudinal relaxation time constant T_1 is often determined by inversion recovery experiments. Simultaneously, transverse components of the magnetization vanish via transverse relaxation or spin-spin relaxation. The transverse relaxation time constant T_2 is often determined by spin echo experiments.

According to the Bloch equations[9] the relaxation process is an exponential process and the decay with the time describes the rate of energy exchange of the spins with the lattice (T_1) and with other spins (T_2). In the presence of cross-correlation, recovery of the longitudinal magnetization can also be observed to be non-exponential, as first predicted by Hubbard[10-11] and observed by Hilt and Hubbard[12], and by Anil Kumar.[13] In 1971, Buchner and Emmerich[14] observed differential relaxation rates of ^{13}C in the dynamic nuclear polarization of methyl groups of toluene and similar compounds. Cross correlations between spin rotation interactions can give non-exponential ^{13}C relaxation.[15] Thus we may conclude that longitudinal relaxation is an exponential process in the absence of strong cross correlations.

3.2.1 The Dipolar Interaction

For many spin-1/2 nuclei, the dipole-dipole interaction is the main dominating relaxation mechanism. In an ensemble of spins with non-zero spin quantum

number, every nucleus possesses a magnetic moment; these magnetic moments interact with each other through space via an interaction known as dipolar coupling. As a result, the dipolar interaction is the direct communication between two spins. In solution state NMR, the dipole-dipole interaction is averaged to its isotropic value due to fast molecular motion, and it is only active as a source of relaxation. In contrast, in solid state these interactions are not averaged.

The local dipolar field due to neighboring spins is inversely proportional to r^3, where r is the distance between the two spins. The local field is furthermore dependent on the molecular orientation of the two spins relative to the applied magnetic field. Taking additionally into account that the dipolar interaction is proportional to the gyromagnetic ratio of two nuclei we can write the static dipolar coupling Hamiltonian as:

$$\mathcal{H} = -d(3I_z S_z - \vec{I}.\vec{S}) \tag{3.1}$$

Where d is dipolar coupling constant, which is defined as:

$$d = \left(\frac{\mu_0}{4\pi}\right)\frac{\hbar\gamma_I\gamma_S}{r_{IS}^3}(3cos^2\theta - 1) \tag{3.2}$$

where γ_I and γ_S are the gyromagnetic ratios of spins I and S respectively and the angle θ between the axis connecting the two spins and the external magnetic field vector B_0.

In the laboratory frame, the dipolar interaction can be written as

$$H = -d\sum_{q=-2}^{2}F^q(\theta,\phi)A^q \tag{3.3}$$

where θ and Φ denote the polar angles. Values of the two tensors F^q and A^q are given in table 3.1 below.

A peculiar feature of the dipolar interaction is the fact that it can only couple spin states that belong to spin manifolds of similar symmetry. This will become important later in our discussion of so-called long-loved states (LLS).

In solution (or, more exotically, in gases) the dipolar interaction is averaged over all possible molecular orientations, so that the term $3cos^2\theta - 1$ becomes zero. However, intramolecular dipolar couplings between two spins can still cause relaxation.

Table 3.1. Tensor components of the Hamiltonian for the dipole-dipole interaction between the spins I and S.

q	F^q	A^q
0	$\sqrt{\dfrac{3}{2}}(3cos^2\theta - 1)$	$\dfrac{1}{\sqrt{6}}(3I_zS_z - I \cdot S)$
±1	$\mp(sin\theta cos\theta \exp{(\pm i\phi)})$	$\pm\dfrac{1}{2}(I_{\pm}S_z - I_z \cdot S_{\pm})$
±2	$\dfrac{3}{2}(sin^2\theta \exp{(\pm 2i\phi)})$	$\dfrac{1}{2}(I_{\pm}S_{\pm})$

Where signs of the tensors obey $F^q = (-1)^q F^{-q}$ and $A^q = (-1)^q A^{-q}$.

3.2.2 Long-Lived States for Dipolar Interactions

Usually, nuclear singlet states that are known as long-lived states (LLS) have much longer lifetimes compared to conventional longitudinal relaxation times (T_1). Their population relaxes back to equilibrium with a time constant often denoted as T_{LLS}, which should be much longer than T_1 in cases where intra-molecular dipolar couplings dominate nuclear relaxation. Frequently, NMR is limited by short lifetimes of nuclear Zeeman magnetization. Hence, this unique property of LLS (i.e., $T_{LLS} > T_1$), renders them a useful tool, among others, for *in-vivo* studies, drug-screening[16] and metabolomics. Levitt and co-workers introduced this concept of LLS in systems containing coupled pairs of spins-

1/2.[4-5] They observed smaller decay constants for singlet states compared to the conventional time constant T_1 for a sample of 2,3-dibromothiophene dissolved in degassed DMSO-d_6. Recently, in a R-CH=CH-R' group, for pair of protons, an enhancement in comparison to the lifetime of conventional Zeeman magnetization by a factor of 60 has been observed. For the case of two spin ½ nuclei, an LLS can be described as an imbalance between a triplet and a singlet state, which corresponds to a population imbalance between a symmetric spin manifold and an antisymmetric manifold.

In the case of two spin-1/2 nuclei, the intra-molecular dipole-dipole (DD) interaction is symmetric with respect to the exchange of two nuclei. This interaction cannot lead to any transitions between states of different symmetry. Hence singlet and triplet populations cannot mix. As a result, an imbalance between triplet and singlet state is immune to intra-molecular dipolar relaxation, which means that intra-molecular DD mechanism does not affect LLS.

For a spin-1/2 nucleus, in the presence of a magnetic field, nuclear spin states can be indicated by the kets |α> and |β>.

$$I_z|\alpha\rangle = \frac{1}{2}|\alpha\rangle,$$

$$I_z|\beta\rangle = -\frac{1}{2}|\beta\rangle \tag{3.4}$$

For a homonuclear pair of two degenerate spin-1/2 systems, the four Zeeman energy states (|αα>, |αβ>, |βα>, |ββ>) can be combined to define three triplet (|T_{+1}>, |T_0>, |T_{-1}>) and one singlet state (|S_0>).

$$|S_0\rangle = \frac{1}{\sqrt{2}}(|\alpha\beta\rangle - |\beta\alpha\rangle)$$

$$|T_{+1}\rangle = |\alpha\alpha\rangle$$

$$|T_0\rangle = \frac{1}{\sqrt{2}}(|\alpha\beta\rangle + |\beta\alpha\rangle)$$

$$|T_{-1}\rangle = |\beta\beta\rangle \tag{3.5}$$

The singlet state is anti-symmetric with respect to permutation of the spins while the three triplet states are symmetric with respect to permutation. The

singlet state ($|S_0>$) has a vanishing spin angular momentum whereas the three triplet states have a total spin angular momentum that is equal to 1.

The so-called long-lived triplet-singlet imbalance can be defined as;

$$\left|\overline{T}\rangle\langle\overline{T}\right| - |S_0\rangle\langle S_0| \tag{3.6}$$

$|S_0><S_0|$ denotes the population of the singlet state $|S_0>$ and $\left|\overline{T}\rangle\langle\overline{T}\right|$ is the mean population of the triplet manifold:

$$\left|\overline{T}\rangle\langle\overline{T}\right| = \frac{1}{3}\left[|T_{+1}\rangle\langle T_{+1}| + |T_0\rangle\langle T_0| + |T_{-1}\rangle\langle T_{-1}|\right] \tag{3.7}$$

Either enhancing or depleting the population of the singlet state with respect to the average population of the triplet manifold using D-DNP near cryogenic temperatures can generate such as imbalance. In general, the dipolar interaction is the main source of relaxation for spin-1/2 in liquid state NMR. LLS thus have longer lifetimes than states relaxing with T_1 because of the absence of the dominant relaxation mechanism, i.e., of the intramolecular dipole-dipole interaction. For LLS the most efficient mechanisms for relaxation are either intermolecular dipolar interactions, chemical shift anisotropy (CSA) or paramagnetic relaxation enhancement (PRE) due to unpaired electrons in the solution. Concluding, in absence of intramolecular DD relaxation, the magnetization can be stored for a long time in LLS and the resulting relaxation time constant will be longer than T_1.

3.2.3 CSA Relaxation

An important source of relaxation of LLS is the chemical shift anisotropy (CSA). In the presence of a strong applied magnetic field, electrons in a molecule give rise to a small induced field at the nuclei, which is opposed to the applied magnetic field. As a result, nuclear spins experience different magnetic fields depending on their environment. The Larmor frequency shifts according to the

size of the magnetic field. This effect is called the chemical shift. The magnetic field (B_j^{loc}) experienced by a nuclear spin j is given as:

$$B_j^{\text{loc}} = B_0 + B_j^{\text{induced}} \tag{3.8}$$

B_0 is the static external applied magnetic field and B_j^{induced} represents the magnetic field produced by the electron cloud at the site of spin j. The field B_j^{induced} is very small compared to the static magnetic field (approx. 10^6 times smaller). The magnitude of the induced field B_j^{induced} due to the electronic environment is directly proportional to the applied magnetic field B_0:

$$B_j^{\text{induced}} = \delta^j \cdot B_0 \tag{3.9}$$

where δ^j characterizes the chemical shift tensor of spin I_j, represented by a 3×3 matrix.

The chemical shift Hamiltonian of a nuclear spin can be written as:

$$\widehat{H}_{\text{CS}} = \gamma \sigma B_0 \hat{I} \tag{3.10}$$

where σ is the chemical shift tensor of the spin I and B_0 is the external magnetic field. In the principal axis frame, the Hamiltonian is:

$$H_{CS} = \gamma(\sigma_{\text{XX}} B_{0\text{X}} I_{\text{X}} + \sigma_{\text{YY}} B_{0\text{Y}} I_{\text{Y}} + \sigma_{\text{ZZ}} B_{0\text{Z}} I_{\text{Z}}) \tag{3.11}$$

This equation can be divided into isotropic and anisotropic terms.

The anisotropic part can be written as:

$$H_{\text{CSA}} = \gamma \frac{\sigma_{\parallel} - \sigma_{\perp}}{3} (B_0 \cdot I - 3B_{\text{Z}} I_{\text{Z}}) \tag{3.12}$$

where $\sigma_{\parallel} = \sigma_{\text{XX}}$ and $\sigma_{\perp} = \sigma_{\text{YY}} = \sigma_{\text{ZZ}}$.

The electronic environment around the nuclear spins is generally anisotropic and therefore the chemical shift is also anisotropic and depends on the orientation of the molecule with respect to the applied magnetic field.

3.2.5 Quadrupolar Interaction

Nuclei with a spin quantum number I = 1 or higher have a non-spherical electric charge distribution. They are called quadrupolar as they contain two positive and two negative poles. Consequently, they possess a non-zero quadrupolar moment, which interacts with the electric field gradient due to non-spherical forms of the electronic cloud that surrounds the nuclei. Frequently, one speaks of a quadrupolar interaction to denote the coupling of the quadrupolar momentum and the electric field gradient.
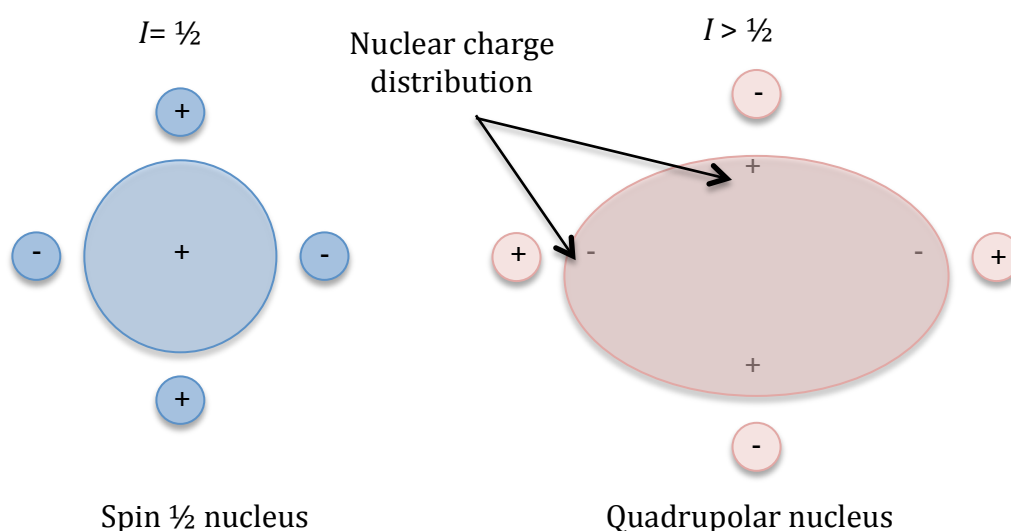
Figure. 3.1. Schematic representation of the charge distribution for nuclei with spin I = 1/2 (left) and spin I >½ (right). The charge distribution of nuclei with spin I = ½ is spherical and whereas for nuclei with spin I > ½, it is non-spherical and can be considered as resulting from two dipoles. A non-spherical nuclear charge distribution leads to an electric quadrupolar moment for spin I >1/2. The interaction is independent of the orientation of the electric field gradient (right). Positive and negative signs represent positive and negative poles.

The symmetry properties of quadrupolar interactions are similar to those of dipolar interactions. This will become important for our discussion of LLS later. It is therefore instructive to introduce this interaction in a similar way as the dipolar interaction.

A spin Hamiltonian of the interaction between a nuclear quadrupolar moment and an electric field gradient can be written as:

$$H_Q = \hat{I} \cdot \mathbf{Q} \cdot \hat{I}$$

(3.13)

Where I is nuclear spin vector and $\mathbf{Q}$ is the quadrupole moment of the nucleus and is expressed as:

$$\mathbf{Q} = \frac{eQ}{4I(2I-1)\hbar} \mathbf{V}$$

(3.14)

Where the symbol e is the elementary charge, Q is the nuclear quadrupole moment, I is the spin of the nucleus. $\mathbf{V}$ is the electric field gradient (EFG). A symmetric second rank tensor that depends on the molecular orientation can be described by:

$$\mathbf{V} = \begin{bmatrix} V_{11} & V_{12} & V_{13} \\ V_{21} & V_{22} & V_{23} \\ V_{31} & V_{32} & V_{33} \end{bmatrix}$$

(3.15)

which can be diagonalized in its principal axis system:

$$\mathbf{V}_{PAS} = \begin{bmatrix} V_{XX} & 0 & 0 \\ 0 & V_{YY} & 0 \\ 0 & 0 & V_{ZZ} \end{bmatrix}$$

(3.16)

where the principal components are ordered so that $|V_{ZZ}| > |V_{XX}| > |V_{YY}|$. The EFG tensor is traceless, so that $V_{XX} + V_{YY} + V_{ZZ} = 0$.

Combining equations 3.13 and 3.14 we can reformulate the Hamiltonian as:

$$H_L^Q = \frac{eQ}{4I(2I-1)\hbar} \hat{I} \cdot \mathbf{V} \cdot \hat{I} = \frac{eQ}{4I(2I-1)\hbar} (\hat{I}_X \; \hat{I}_Y \; \hat{I}_Z) \cdot \mathbf{V} \cdot \begin{pmatrix} \hat{I}_X \\ \hat{I}_Y \\ \hat{I}_Z \end{pmatrix}$$

(3.17)

The origin of this interaction is of electrostatic nature and it can be expressed via

the electrostatic potential V in terms of Cartesian components:

$$V_{ij} = \left[\frac{\partial E_i}{\partial x_j}\right]_{r=0} = \left[\frac{\partial^2 V}{\partial x_i x_j}\right]_{r=0} \tag{3.18}$$

E is the electric field vector and the electric field is the gradient of electrostatic potential, expressed as $E = -\nabla V$.

As the EFG is symmetric, V_{ij} should be equal to V_{ji} ($V_{ij} = V_{ji}$), where x_i, x_j denote Cartesian coordinates. If we diagonalize the electrostatic potential matrix in the principal axis frame, we retain only two parameters: the anisotropy and the asymmetry, which are respectively defined by following relations:

$$eq = V_{ZZ} - V_{iso} = V_{zz} \tag{3.19}$$

The lack of axial symmetry of the EFG tensor about the Z axis is measured by the dimensionless asymmetry parameter, η:

$$\eta = \frac{V_{XX} - V_{YY}}{V_{ZZ}} \tag{3.20}$$

Therefore, the quadrupolar Hamiltonian can be defined in the irreducible spherical form:

$$H_Q = \frac{eQ}{4I(2I-1)\hbar}\sum_{q=-2}^{2}(-1)^q V_{2,q}^{PAS}\hat{T}_{2,-q} \tag{3.21}$$

In the principal axis frame using the above parameters, the Hamiltonian can be compactly written:

$$H_Q = \frac{e^2qQ}{4I(2I-1)\hbar}\left[3\hat{I}_z^2 - I^2 + \frac{\eta}{2}\left(\hat{I}_X^2 - \hat{I}_Y^2\right)\right] \tag{3.22}$$

The spherical tensors are defined as

$$\hat{T}_{2,0} = \left[3\hat{I}_Z^2 - I(I+1)\hat{1}\right]$$

$$\hat{T}_{2,+2} + \hat{T}_{2,-2} = \sqrt{\frac{3}{2}}\hat{I}_+^2 + \sqrt{\frac{3}{2}}\hat{I}_-^2 = \sqrt{6}\,(\hat{I}_X^2 - \hat{I}_Y^2) \tag{3.23}$$

The function $V_{2,q}^{PAS}$ is defined as:

$$V_{2,0}^{PAS} = (6)^{1/2}eq$$

$$V_{2,\pm1}^{PAS} = 0 \tag{3.24}$$

$$V_{2,\pm2}^{PAS} = -\eta eq$$

The spin independent parameter $C_Q = e^2qQ/\hbar$ is called quadrupolar coupling constant. The quadrupolar coupling can be positive or negative, which depends on the relative signs of the nuclear quadrupole moment and the local electric field gradients. Determination of the absolute sign of the quadrupolar coupling is very difficult, at least by NMR methods. In general, typical values of $|C_Q|$ in solids are in the range of ∼ 100 kHz to ∼ 1 MHz.

A quadrupolar spin with $I \geq 1$ in a magnetic field splits into $2I+1$ Zeeman levels, which are characterized by a spin quantum number m. At high magnetic field, the Zeeman Hamiltonian dominates over the quadrupolar interaction. Due to the high Zeeman splitting, the spins are quantized in the laboratory frame. When the quadrupolar coupling does not dominate over the Zeeman interaction at high field, perturbation theoretical reasoning can be employed to describe its contribution to relaxation. A spin with quantum number I gives rise to $2I$ transitions in the NMR spectrum. In cases where the Zeeman interaction is dominating, the spin operators can be expressed in the laboratory frame. If the EFG tensor is axially symmetric and $V_{XX} = V_{YY}$ in the PAS of the EFG tensor, the asymmetry parameter η will be zero. Thus the dynamic quadrupolar Hamiltonian can be expressed as:

$$H_Q = \varepsilon_Q \sum_{q=-2}^{2} (-1)^q V_{2,q}^{PAS} \widehat{T}_{2,-q} \qquad (3.25)$$

The interaction strength is given by

$$\varepsilon_Q = \left(\frac{3\pi}{10}\right)^{1/2} \frac{eQ}{4I(2I-1)\hbar} \qquad (3.26)$$

In cases of non-axially symmetric EFG tensors, the relevant equation can become quite complicated, which would be beyond the scope of this introduction. Details can be found in the works of Werbelow.[17]

3.2.5 Combination of LLS with D-DNP

Dissolution DNP can be used to create imbalances between symmetric and antisymmetric manifolds by populating low-energy states. In systems with two magnetically inequivalent spins, D-DNP can readily be used to create long-lived states. Furthermore, D-DNP can also populate the imbalance in a spin system with two magnetically equivalent protons such as those of para-hydrogen and in three-spin systems of methyl groups, where A and E symmetry manifolds belong to irreducible representation of C_{3v} point group.[18-20] In the following, we will focus on CD_2 moities.

3.3 Dissolution DNP of Quadrupolar Nuclei

If present, the quadrupolar interaction is usually the dominant relaxation mechanism. Therefore, when considering relaxation due to quadrupolar interactions, other mechanisms can typically be neglected. Note that NMR signals of quadrupolar nuclei are generally broader than those of spin-1/2 nuclei due to rapid quadrupolar relaxation. For deuterium with spin $I = 1$, the longitudinal relaxation time T_1 is on the order of 1 s under typical experimental conditions (9.7-18.8 T, 298 K.) In our dissolution DNP apparatus, the usual transfer times from the polarizer to the detection NMR or MRI system is 1-10 s, so that most of

the deuterium polarization will be lost during this time because of the rapid quadrupolar relaxation, if we do not employ special techniques like LLS.

It is important to note that the transfer delay acts as a filter since only LLS deuterium terms can survive. All "conventional" deuterium polarization terms will have vanished at the time of detection, so that all non-equilibrium magnetization that we observe can be attributed to LLS involving several deuterium nuclei.

3.3.4 Theory

The sample that we investigated consisted of perdeuterated Ethanol-d_6, with ^{13}C in 1.1% natural abundance (the observed ^{13}C spin system is therefore highly dilute), H_2O to provide a reservoir of protons to allow 'remote' CP from the protons of the solvent to the ^{13}C nuclei in the deuterated molecules, glycerol as glass-forming agent, and TEMPOL as polarizing agent. Here, we focus on the spin dynamics of the $^{13}CD_2$ group of Ethanol-d_6. The $^{13}CH_2$ group of ethanol was discussed by Mammoli [21-22] and chapter 4 embraces a discussion of $^{13}CD_3$ groups.

Cross Polarization of Systems with Heteronuclear Couplings

The CP sequence in Fig. 3.2a uses adiabatic sweeps to convert part of the ^1H magnetization of the surrounding water molecules to the ^{13}C nuclei of Ethanol-d_6 through long-range intermolecular dipolar couplings by fulfilling the Hartmann-Hahn condition.[23] The objective of CP is to convert the transverse magnetization I_x into S_x in the rotating frame via a spin lock of duration τ_{SL} with rf amplitudes γB_1^I and γB_1^S. In the present case where $I = {}^1H$ and $S = {}^{13}C$ we use the notation $I_x = H_x$ and $S_x = C_x$. If the CP spin locking field is sandwiched between two $\pi/2$ pulses, one can transform H_z into C_z in the laboratory frame.[24] In practice, the conversion from H_x to C_x is not ideal because the rf field amplitudes are not strong enough to cover the full breadth of the spectra at 1.2 K. In CD_2 groups, scalar and dipole-dipole couplings between D and ^{13}C, denoted J_{CD} and $D_{CD'}$ affect the outcome of cross-polarization from ^1H to ^{13}C. The former are isotropic

and on the order of 20 Hz, while the latter depend on the orientation of the C-D bond with respect to the static field and are on the order of $-3.6 < D_{CD} < +1.8$ kHz. In the spirit of the pioneering work on dipolar oscillations by Müller et al.,[25] we shall describe the spin subsystem comprising three reasonably isolated spins – ^{13}C, D, and D' – in terms of a density operator that evolves coherently under the Hamiltonian, using products of angular momentum operators that are widely used to describe NMR in liquids, rather than spin thermodynamics. During CP, the couplings D_{CD} may lead to the appearance of antiphase and doubly antiphase coherences of the form $3^{-1/2}C_xD_z$, $3^{-1/2}C_xD'_z$ and $2^{-1/2}C_xD_zD'_z$ which after the final -$\pi/2$ 'flip-back' pulse lead to longitudinal two- and three-spin order terms $3^{-1/2}C_zD_z$, $3^{-1/2}C_zD'_z$ and $2^{-1/2}C_zD_zD'_z$.[26] Some of these terms project onto states with long lifetimes, as will be shown below. The norm of an operator A is defined as usual as the square root of its scalar product with itself, Tr$\{A^\dagger.A\}$. All product operators of the three isolated spins ^{13}C, D, and D' can be represented by 18x18 dimensional matrices.
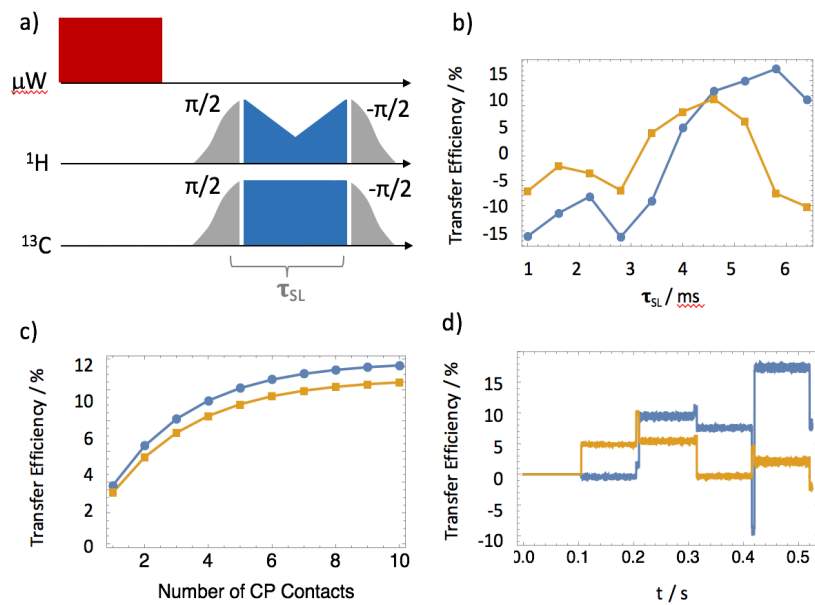
Fig. 3.2. (a) Cross polarization sequence designed to polarize ^{13}C nuclei starting from ^{1}H nuclei. If the rf field $\gamma B_1^C/(2\pi)$ is not strong enough to decouple the dipolar couplings D_{CD} between the ^{13}C nucleus and the two deuterons, cross-polarization leads to three terms $3^{-1/2}C_zD_z$, $3^{-1/2}C_zD'_z$ and $2^{-1/2}C_zD_zD'_z$ during the spin-locking interval τ_{SL}. The gray shapes indicate half-passage adiabatic 90° chirp pulses used to flip the ^{1}H and ^{13}C

magnetizations from the z to the x axes of the doubly rotating frame and back. The proton spin-lock amplitude $\gamma B_1(^1\text{H})$ is ramped (over 50% of its initial intensity) while the carbon spin-lock amplitude $\gamma B_1(^{13}\text{C})$ remains constant (indicated by the blue shapes). The frequency-modulated microwave irradiation (red rectangle) is interrupted ("gated") 1 s before the CP sequence to allow the electron polarization to return to its Boltzmann equilibrium (the time axis is not true to scale; for details see experimental section). (b) Build-up of the $3^{-1/2}C_zD_z$ (yellow) and $2^{-1/2}C_zD_zD'_z$ (blue) terms as a function of the duration τ_{SL} of the spin-locking interval for an rf amplitude $\gamma B_1(^{13}\text{C})/(2\pi) = 50$ kHz, obtained by numerical simulations using SpinDynamica with averaging over 200 orientations of Ethanol-d_6 molecules in the glassy state. The vertical scale corresponds to the fraction (%) of conversion of the longitudinal operators $2^{1/2}/3C_z$ into terms $3^{-1/2}C_zD_z$, $3^{-1/2}C_zD'_z$ and $2^{-1/2}C_zD_zD'_z$ during a single CP contact. c) Simulated consecutive build-up of the $3^{-1/2}C_zD_z$ (yellow) and $2^{-1/2}C_zD_zD'_z$ (blue) terms as a function of the number of CP contacts for $\tau_{SL} = 1$ ms and $\gamma B_1(^{13}\text{C})/(2\pi) = 50$ kHz. The vertical scale is relative to 100% ^{13}C polarization present before the first CP contact. d) Time evolution of $3^{-1/2}C_zD_z$ (yellow) and $2^{-1/2}C_zD_zD'_z$ (blue) terms for $\tau_{SL} = 5$ ms and $\gamma B_1(^{13}\text{C})/(2\pi) = 10$ kHz for a constant ^{13}C polarization (in the absence of cw-microwave irradiation) due to repetitions of the carbon pulses shown in (a).

The extent of the transformation of hyperpolarized H_z magnetization into the terms $3^{-1/2}C_zD_z$, $3^{-1/2}C_zD'_z$ and $2^{-1/2}C_zD_zD'_z$ varies with the duration τ_{SL} and the amplitudes $\gamma B_1(^1\text{H})$ and $\gamma B_1(^{13}\text{C})$ of the spin-locking fields. In the case at hand, $D_{CD} = -1.8 \times [3\cos^2\theta-1]$ kHz, $J_{CD} = 18.5$ Hz, $\gamma B_1^C/(2\pi) = \gamma B_1^H/(2\pi) = 10\text{-}50$ kHz, and $B_0 = 6.7$ T. The value of D_{CD} used in the simulations is based on the geometry of the spin system.

For the simulations of Fig. 3.2b it was assumed that some spin order terms $2^{1/2}/3C_z$, $3^{-1/2}/2D_z$ and $3^{-1/2}/2D_z'$ are present at the beginning of the cross-polarization period.[24] Subsequently, we computed the entire ^{13}C spin locking sequence, and incorporated off-resonance effects and all intramolecular dipolar and scalar interactions of a CD_2 system in an isotropic glass. The powder average over 200 orientations was computed to account for the angular dependence of the dipolar interaction. According to our simulations, approximately 15% of the initial carbon polarization is transformed after a single CP contact into $3^{-1/2}C_zD_z$,

$3^{-1/2}C_zD'_z$ and $2^{-1/2}C_zD_zD'_z$ terms. After a train of several CP contacts a significant fraction (about 50-60% as judged from our simulations, *vide infra*) of the total carbon polarization occurs in the form of such multi-spin terms (see Fig. 3.2c). In comparison to direct hyperpolarization of deuterium (using only microwave irradiation without CP)[27] the $3^{-1/2}C_zD_z$ and $2^{-1/2}C_zD_zD'_z$ terms are enhanced by an order of magnitude, without applying any radio-frequency field to the deuterium nuclei. In our experiments we applied a train of 15 CP contacts of duration τ_{SL} = 5 ms at intervals τ = 120 s with an rf amplitude $\gamma B_1^C/(2\pi)$ = 50 kHz. Under these conditions the spin order that can contribute to ^{13}C signals is, apart from $2^{1/2}/3C_z$, mostly found in the operator terms $3^{-1/2}C_zD_z$, $3^{-1/2}C_zD'_z$ and $2^{-1/2}C_zD_zD'_z$. According to our simulations about 30% of the initial carbon polarization can be transferred into $3^{-1/2}C_zD_z$, $3^{-1/2}C_zD'_z$ and $2^{-1/2}C_zD_zD'_z$ by a single CP contact (cf. Fig. 3.2b). A train of consecutive CPs can augment this share to 50-60% (Fig. 3.2c). However, it has to be taken into account that these simulations are built on an oversimplification of the spin system. Furthermore, once a steady ^{13}C polarization is reached the $3^{-1/2}C_zD_z$, $3^{-1/2}C_zD'_z$ and $2^{-1/2}C_zD_zD'_z$ terms will be further transformed by subsequent CP contacts (Fig 3.2d) in an unpredictable fashion as the dipolar couplings between carbon and deuterium spins leads to rapid oscillations between in-phase an anti-phase terms during the spin-locking interval. A coherent manipulation to populate the multi-spin terms is thus complicated in the absence of an rf field applied to the deuterium transitions. Experimentally, we found that 15 contacts yield a significant contribution of multi-spin terms to the overall polarization. To the best of our knowledge such side-effects of CP have never been described so far.

Observation of Long-Lived States after Dissolution

After the train of CP contacts, the hyperpolarized sample is dissolved with 5 ml D$_2$O heated to 180 °C at 10.5 bar. Subsequent transfer in 10 s to a conventional 400 MHz NMR spectrometer through a 0.9 T magnetic tunnel[28] is followed by ^{13}C detection of the hyperpolarized sample in solution at ambient temperatures.

During and after dissolution, several processes take place. The most important one for the interpretation of our observations is the projection of the term $2^{-1/2}C_z D_z D'_z$ onto states that feature much longer lifetimes than the longitudinal deuterium Zeeman magnetization terms $3^{-1/2}/2D_z$ and $3^{-1/2}/2D_z{}'$ which relax with $T_1(D_z)$ = 0.7 s in the CD_2 group of perdeuterated Ethanol-d6 under our experimental conditions.
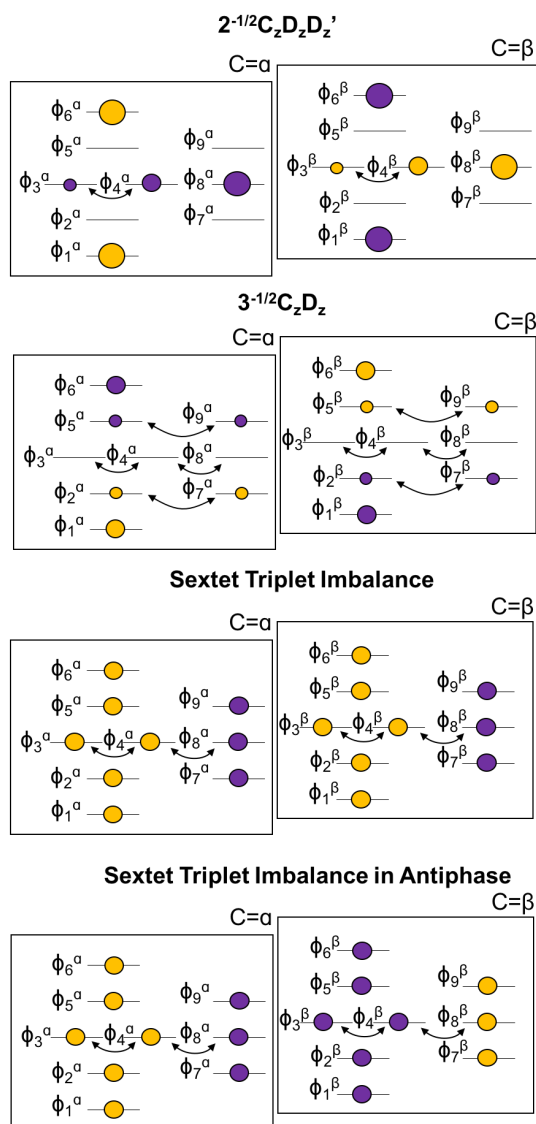

Figure 3.3. Energy-level diagrams of selected states of a $^{13}CD_2$ spin system. Black arrows represent zero-quantum coherences between almost degenerate pairs of spin states. These states are actually split by $^2J_{DD} \approx$ -0.28 Hz. The size of the spheres indicates the populations, with yellow for positive, and purple for negative deviations form a demagnetized state.

Additionally, the terms $3^{-1/2}C_zD_z$ and $3^{-1/2}C_zD'_z$ can also be transformed into longer-lived spin order through cross-relaxation. However, such processes are rather inefficient compared to the projection. A theoretical treatment of longitudinal and transverse relaxation processes in CD_n groups with $n = 2$ and 3 has been given by Kowalewski and co-workers.[26, 29-30] In conventional NMR without hyperpolarization, some effects are hard to detect. Through hyperpolarization by D-DNP, these become observable.

Certain relaxation pathways can be quite inefficient in CD_2 systems leading to longer lifetimes of certain states.

To label the spin states of the D_2 subsystem of the $^{13}CD_2$ group, the first and second numbers in the kets indicate the magnetic quantum numbers $m_z(D)$ and $m_z(D') = -1$, 0, or 1 of the two deuterons D and D':[26] There are six symmetrical states under permutation, which together constitute a sextet:

$\Phi_1 = |11>$

$\Phi_2 = (|10> + |01>) /\sqrt{2}$

$\Phi_3 = (|1-1> + |-11> + 2|00>)/\sqrt{6}$ (3.27)

$\Phi_4 = (|1-1> + |-11> -|00>)/\sqrt{3}$

$\Phi_5 = (|-10> + |0-1>)/\sqrt{2}$

$\Phi_6 = |-1-1>$

There are three states that are antisymmetrical under permutation, which together constitute a triplet:

$\Phi_7 = (|10> - |01>)/\sqrt{2}$

$\Phi_8 = (|1-1> - |-11>)/\sqrt{2}$ (3.28)

$\Phi_9 = (|0-1> - |-10>)/\sqrt{2}$,

These states are duplicated in the presence of a ^{13}C spin, which can adopt either the state α if $m_z(^{13}C) = + \frac{1}{2}$ or β if $m_z(^{13}C) = - \frac{1}{2}$, to yield 18 further states

(denoted $f_{1-9^{\alpha}}$ and $f_{1-9^{\beta}}$) for $m_z(C) = -\frac{1}{2}$. These 18 states constitute the energy levels shown in Fig. 3.3 with typical distributions of populations that can be achieved by hyperpolarization.

Diagonalizing the Liouvillian and analyzing its eigenvalues[31] reveals that long-lived spin order embracing a population imbalance between symmetric and antisymmetric states gives rise to long-lived states (in the case of anisotropic rotational diffusion). As these states involve population differences between the symmetric sextet and the antisymmetric triplet of the D_2 subsystem, we shall refer to such states as a sextet-triplet imbalances (STI) – not to be confused with a triplet-singlet imbalance or TSI[18] that can occur in systems with two equivalent $I = \frac{1}{2}$ spins. All six symmetric states have an equal excess population with respect to a demagnetized state, while all three antisymmetric states have an equal deficiency of populations, as shown in Fig. 3.3. This corresponds to an imbalance between the average populations of the symmetric and antisymmetric states of the spin system. The STI can be expressed as a linear combination of product operators:

$$Q_{STI}^{IP} = \tag{3.29}$$

$$\lambda_1 \, 2^{-1/2}/4 D_- D'_+ + \lambda_2 \, 2^{-1/2}/4 D_+ D'_- + \lambda_3 \, 2^{-1/2}/2 D_z D'_z$$

$$+ \lambda_4 \, 2^{-1/2}/4 \, (D_- D'_+)^2 + \lambda_5 \, 2^{-1/2}/4 \, (D_+ D'_-)^2$$

$$+ \lambda_6 \, 2^{-1/2}/4 \, [D_- D_z D'_+ D'_z + D_- D_z D'_z D'_+ + D_z D_- D'_+ D'_z + D_z D_- D'_z D'_+]$$

$$+ \lambda_7 \, 2^{-1/2}/4 [D_+ D_z D'_- D'_z + D_+ D_z D'_z D'_- + D_z D_+ D'_- D'_z + D_z D_+ D'_z D'_-]$$

$$+ \lambda_8 \, 2^{-1/2}/6 [-6 D_z^2 - 6 D_z'^2 + 9 (D_z D_z')^2 + 4E]$$

E is the identity operator, and $\lambda_1 = \lambda_2 = \lambda_3 = \lambda_4 = \lambda_5 = \lambda_6 = \lambda_7 = \lambda_8 = 8^{-1/2}$, which is the total norm of Q_{STI}^{IP}. Since Q_{STI}^{IP} is an eigenoperator of the Liouvillian, it cannot cross-relax into a state that contains a C_z operator.

Another set of operators Q_{STI} are in antiphase with respect to the ^{13}C nucleus.:

$$Q_{STI}^{AP} = Q_{STI}^{IP} \, C_z \tag{3.30}$$

Note that terms such as $2^{-1/2}C_zD_zD'_z$, which appear at the end of cross-polarization are included in Q_{STI}^{AP}, so that this eigenoperator is partly populated immediately after dissolution. Defining a projection operator $|Q_{STI}^{AP}><Q_{STI}^{AP}|$ we find that the projection of $2^{-1/2}C_zD_zD'_z$ onto Q_{STI}^{AP} gives a coefficient $2^{-1/2}/2$. (Note that this is also true for all other operators that constitute Q_{STI}^{IP} and Q_{STI}^{AP}. Yet, these are not as strongly populated as $3^{-1/2}C_zD_z$, $3^{-1/2}C_zD'_z$ and $2^{-1/2}C_zD_zD'_z$ according to our simulations.) Thus, CP of the ^{13}C nucleus of a CD_2 group leads to the occurrence of the Q_{STI}^{AP} term. Taking into account that approximately 15-20% of the $2^{-1/2}C_zD_zD'_z$ terms are populated during multiple contact CP, one may estimate that about 10% of the magnetization after CP are present in the form of Q_{STI}^{AP} due to the projection of $2^{-1/2}C_zD_zD'_z$. Other processes like cross relaxation of $3^{-1/2}C_zD_z$ and $3^{-1/2}C_zD'_z$ will further contribute.

Note that Q_{STI}^{AP} can cross-relax into detectable antiphase ^{13}C coherences, while Q_{STI}^{IP} cannot. If the unique axes of the two Q-tensors were parallel, the symmetric states (Φ_1- Φ_6) would be isolated from the antisymmetric states (Φ_7-Φ_9), since the matrix elements connecting these two sets of states would vanish. This case has been treated by Poupko et al.[32] A phenomenon similar to long-lived states known for spin ½ systems arises, which makes quadrupolar relaxation largely ineffective.

The relaxation properties of Q_{STI}^{IP} and Q_{STI}^{AP} are best understood by examining the relaxation matrix. In Fig. 3.4a this matrix is depicted for isotropic rotational diffusion. The Q-tensors are assumed to be cylindrical ($\eta = 0$) with their unique axes aligned along the C-D bond axes. Such a geometry leads to a mixing of the symmetric (Φ_1- Φ_6) and antisymmetric (Φ_7- Φ_9) states, as highlighted by red dashed boxes in Fig. 3.4a.

If rotational diffusion is anisotropic, these interconnecting matrix elements are attenuated, so that the symmetric and antisymmetric manifolds become largely isolated.[32] Assuming a symmetric top, we find that cross relaxation between symmetric and antisymmetric states is largely ineffective if $\tau_\parallel > \tau_\perp$, where the latter refers to motions around an axis perpendicular to the plane spanned by

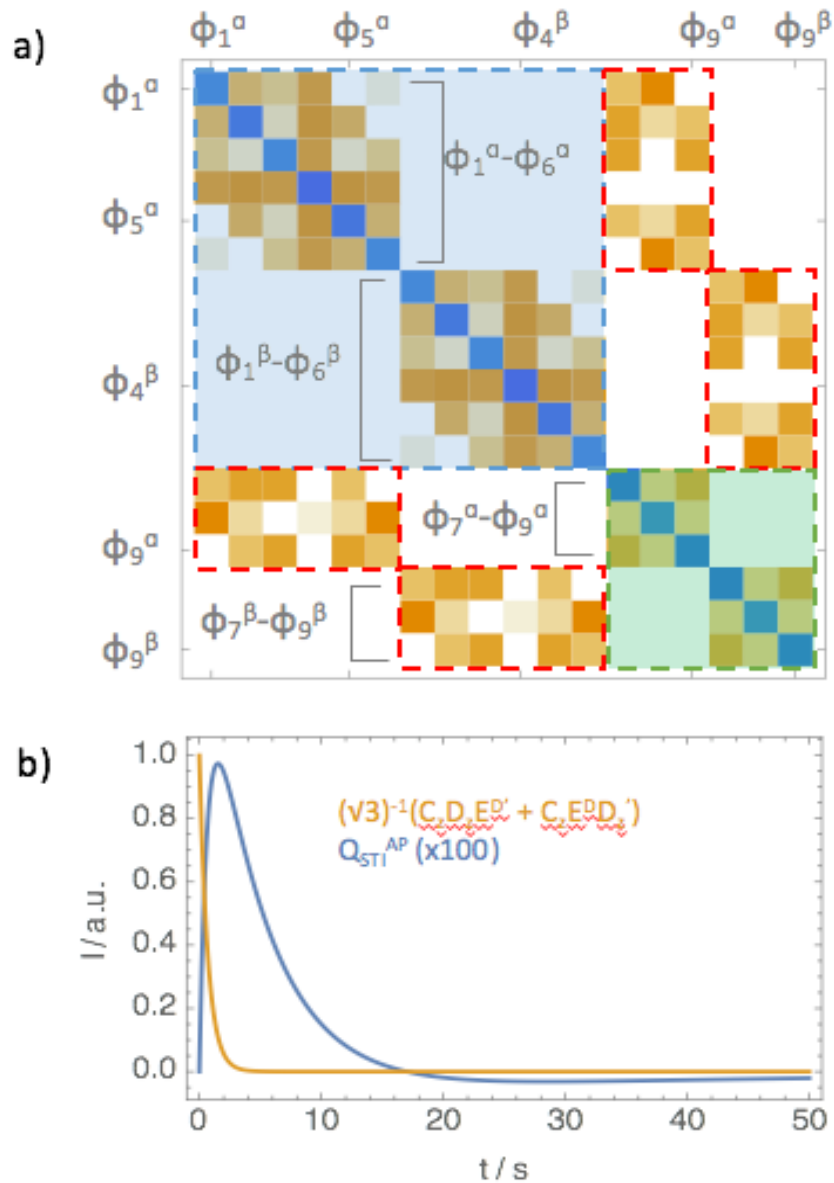the two C-D bonds, while the former denotes the rotation around an axis that bisects the D-C-D' angle.

Figure 3.4. (a) Typical Liouville relaxation matrix due to quadrupolar couplings in a CD_2 system for the case of isotropic rotational diffusion. Negative and positive elements are represented in blue and various shades of brown. The matrix elements connecting symmetric manifolds (blue areas) and antisymmetric manifolds (green areas) are highlighted by red dashed squares. For the sake of clarity, the relaxation matrix only shows populations, but in our simulations the entire Liouville space was taken into account, including all coherence orders. We did not assume that the two deuterons are magnetically equivalent. To treat the general case, we did not employ the simplifications proposed in reference[29]. (b) Relaxation of the expectation value of the operator $3^{-1/2}C_zD_z$

+ $3^{-1/2}C_zD'_z$ and the subsequent build-up of a sextet-triplet imbalance (Q_{STI}^{AP}) for anisotropic rotational diffusion $5\tau_\perp = \tau_\parallel$).

The rotational diffusion of Ethanol-d_6 defined by $\tau_\perp$ is fastest and therefore gives the weakest contribution to the relaxation rates. The Q-tensor elements parallel to this axis contribute predominantly to relaxation. These are symmetric with respect to spin exchange and hence do not cause any cross relaxation between symmetric and antisymmetric spin manifolds.[5] In other words, the projections of the two Q-tensors onto the main diffusion axis (which is perpendicular to the D-C-D' plane) are equal, so that symmetric and antisymmetric spin states are dynamically isolated. Additionally, an asymmetry of the Q-tensors ($\eta \neq 0$) will further diminish the influence of matrix elements connecting symmetric and antisymmetric spin states. As these matrix elements diminish, the population imbalance between the two manifolds will gain in lifetime. This is what gives rise to the long life-time of an STI.

Bernatowicz and Szymański[33-34] have discussed related effects on the ^{15}N line shape due to transverse relaxation in azide $[^{14}N^{15}N^{14}N]^-$ which is formally similar to our case of $D^{13}CD'$. In both cases, the energy levels Φ_3, Φ_4 and Φ_8 are coupled via zero quantum coherences ($|\Phi_3><\Phi_8|$, $|\Phi_4><\Phi_8|$, etc.), as indicated by black arrows in Fig. 2. Bernatowicz and Szymański[33-34] distinguish between magnetic equivalence and nuclear permutation symmetry of the two ^{14}N nuclei with a mutual coupling constant of $^2J(^{14}N, ^{14}N') = 11.54$ Hz. In our case, the two deuterons have a scalar coupling constant of $^2J(D, D') = {}^2J_{DD'} \approx -0.28$ Hz (cf. Fig. 3.3). However, the zero-quantum coherences between symmetric and antisymmetric states cannot cause a flow of populations, since such processes are symmetry forbidden under the assumption that the two Q-tensors are aligned, either in the linear $[^{14}N^{15}N^{14}N]^-$ ion or because of motional averaging in $D^{13}CD'$ in Ethanol-d_6. If the (quadrupolar) relaxation were very slow these coherences would oscillate with frequencies $\pm 3(^2J_{DD})$. However, the off-diagonal relaxation matrix elements involving the above-mentioned zero-quantum coherences might be of the order of the quadrupolar relaxation rate constants, so that the influence of such effects might be significant and could even reducing

the lifetimes of the STI. This effect can be readily investigated by simulations that take into account the complete set of spin states of the CDD' system. Simulations using several values of the quadrupolar constants and scalar coupling constants $^2J(D, D')$ did not reveal any significant effects on the relaxation matrix.

Note that the three-spin density operator term $2^{-1/2}C_zD_zD'_z$ that is present after CP-DNP is readily projected onto $Q_{STI,}{}^{IP}$ and $Q_{STI}{}^{AP}$, while the two-spin terms $3^{-1/2}C_zD_z + 3^{-1/2}C_zD'_z$ can be partly converted into long-lived spin order by cross-relaxation. Simulations of the build-up and decay are shown in Fig. 3.4b.

3.3.5 Results and Discussion

In ordinary ^{13}C spectra in solution at room temperature, the high temperature approximation is fulfilled, so that the $^{13}CD_2$ group of perdeuterated Ethanol-d_6 gives rise to a (non-binomial) 1:2:3:2:1 pentet that results from the convolution of a 1:1:1 triplet with another 1:1:1 triplet with the same splitting $^2J(D, {}^{13}C) = $ 18.5 Hz. In Fig. 3.5 the experimentally detected ^{13}C pentet of hyperpolarized perdeuterated Ethanol-d_6 is shown at different intervals after dissolution. Despite the slow transfer to the NMR spectrometer that required 10 s, the ^{13}C signal enhancement compared to thermal equilibrium signal was estimated to be e = 3900 immediately after injection.

The presence of hyperpolarized STI states involving deuterium spins is revealed by the relative amplitudes of the multiplet components depicted in Fig. 3.5. The intensities are denoted L_1 to L_5 from low to high field. In the hyperpolarized sample, one observes an asymmetry of the signal where the low-field transitions (L_1, L_2) are enhanced compared to the high temperature intensity ratios 1:2:3:2:1, while the high field-transitions (L_5, L_6) are attenuated. Additionally, L_3 is reduced with respect to the outer transitions, while $L_2/L_1 > 2$, and $L_4/L_5 > 2$. This asymmetry is reminiscent of similar observations for pairs of ^{13}C spins $I = S$ = ½, that have been analyzed recently by Vuichoud et al.[35] In a CD_2 system, the asymmetry can be traced back to $3^{-1/2}(C_zD_z + C_zD_z{}')$ and $2^{-1/2}C_zD_zD'_z$ terms as

explained in the Theory section. These lead to STIs which determine the intensities of the five transitions in the ^{13}C pentet after dissolution. As they relax slower than both $3^{-1/2}/2D_z$ and $3^{-1/2}/2D'_z$ terms, the effect of the STI is observable long after dissolution.[26, 29-30]

Simulations of the time evolution by the SpinDynamica software yields the signals shown in yellow in Fig. 3.5. These simulations assume that the initial density operator (immediately after dissolution) contains a mixture of $2^{1/2}/3C_z$, $3^{-1/2}C_zD_z$, $3^{-1/2}C_zD'_z$ and $2^{-1/2}C_zD_zD'_z$ terms. The simulations reproduce the experimental time evolution of the detected carbon signal remarkably well. Note that the ethanol sample under investigation is not enriched in ^{13}C, hence, 99% of the ethanol molecules in the sample do not contribute to the observed STI.

After a sufficient interval, all terms containing deuterium operators relax to their equilibrium values and only C_z magnetization remains (which is initially populated through CP) and the high-temperature intensity ratio of 1:2:3:2:1 is recovered. This can be observed in Fig. 3.5d.
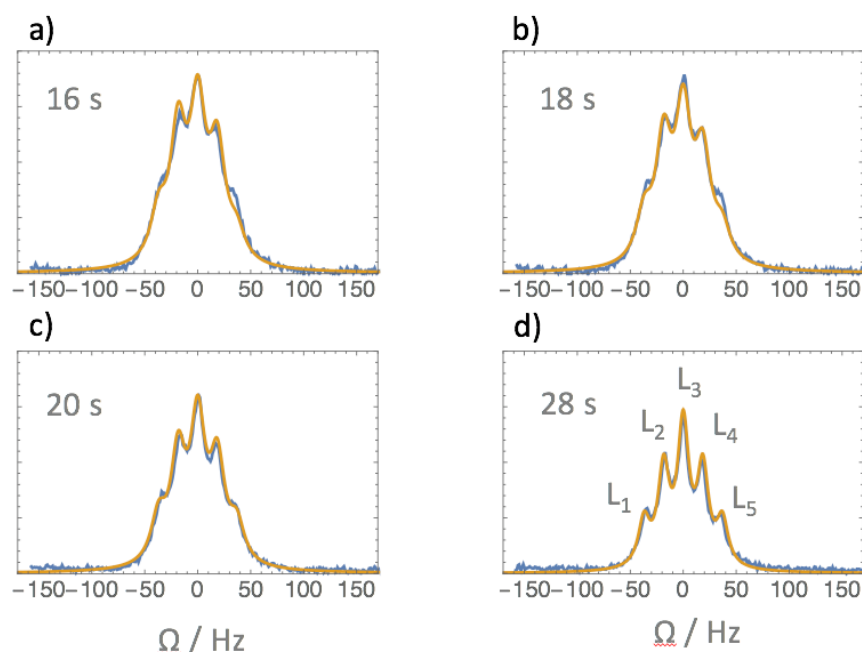

Figure 3.5. Blue: Experimental ^{13}C multiplets of the ^{13}CD$_2$ group of hyperpolarized Ethanol-d6, detected at intervals of 16, 18, 20 and 28 s after dissolution. Yellow: simulations by SpinDynamica. The individual transitions are labeled L$_1$ to L$_5$ from low to

high field (i.e., from high to low frequencies, see bottom right). In the high temperature approximation that prevails at room temperature, the CD_2 group gives rise to a symmetrical 1:2:3:2:1 pentet with a splitting $^1J(D, {}^{13}C) = 18.5$ Hz.

To assess the lifetime of the total deuterium polarization after dissolution, we fitted the individual lines L_1 to L_5 of the ^{13}C-pentet to five Lorentzians, using the so-called quasi-Newton Broyden-Fletcher-Goldfarb-Shanno algorithm,[36] as implemented in Scilab.[37] This method allows one to determine the intensities of the individual lines despite extensive overlap, as observed in our experiments (Fig. 3.5). The decays of the intensities of the five lines of the pentet are shown in Fig. 3.6a. The asymmetry due to the deuterium hyperpolarization can be expressed by the differences $(L_1 - L_5)$ and $(L_2 - L_4)$ as well as by the ratio between the central and the outer transitions (see labels in Fig. 3.5). By defining an overall asymmetry $A = (L_1 + L_2 - L_4 - L_5) / L_3$ we can indirectly characterize the deuterium polarization. This asymmetry decays mono-exponentially as shown in Fig. 3.6b. The characteristic relaxation time constant was fitted to be $T_{STI} = 15.9 \pm 5.4$ s. This decay time corresponds to an effective lifetime of long-lived spin order. As single-spin Zeeman magnetization $D_z = 3^{-1/2}/2D_z$ relaxes with a $T_1(D_z) = 0.7$ s under the same conditions[6] the extension of the lifetime is about $\kappa = T_{STI}/T_1(D_z) = 21.4$. Note that $T_1(C_z) = 23$ s. By calculating the ratio $R = (L_1+L_5/L_2+L_3+L_4)$, we can determine the fraction of the STI to be $\vartheta = 1 - R/3$ as the antisymmetric spin states contribute only to L_2 to L_4. We determined this fraction to be approximately $\vartheta = 15\%$ of the total carbon magnetization after the transfer delay. This is in agreement with the value estimated from our numerical simulations.

This phenomenon is based on the dynamic isolation of symmetric and anti-symmetric spin manifolds, which is a common principle behind many long-lived states (LLS).[4-5]
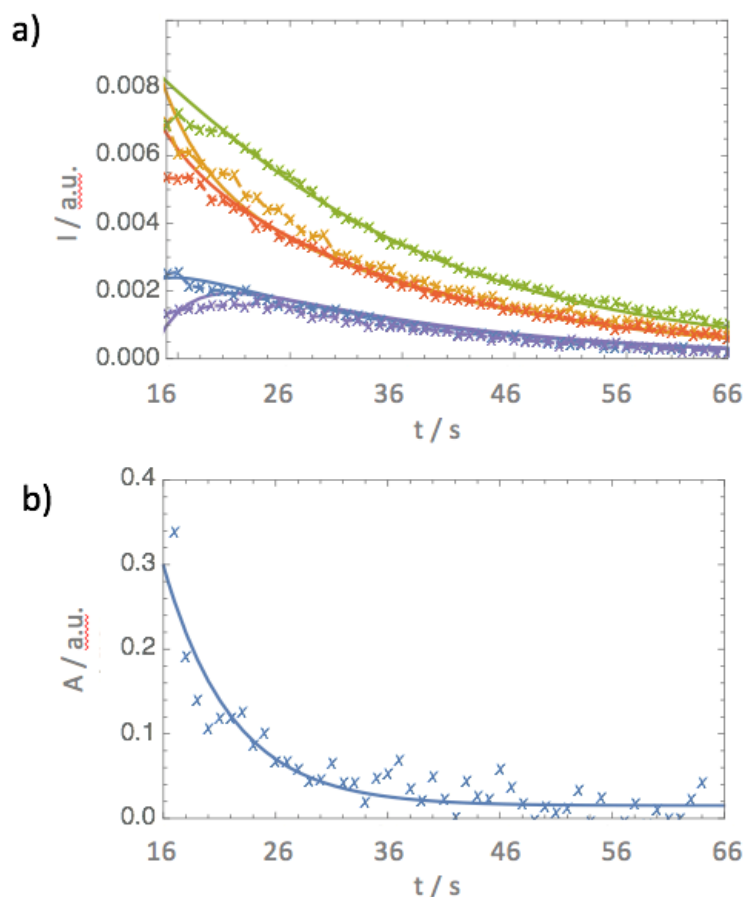
Figure 3.6. a) Decay of the individual lines L_1 to L_5 of the ^{13}C pentet of the CD_2 moiety of Ethanol-d6 after dissolution. b) Time-dependence of the asymmetry of the pentet defined as $A = (L_1 + L_2 - L_4 - L_5) / L_3$ (cf. Fig. 3.5).

In direct polarization experiments without CP, we did not observe any asymmetry since direct polarization of deuterium (including multi-spin terms), like direct polarization of ^{13}C, is rather inefficient compared to CP (see Fig. 3.7). Note that the multispin order terms C_zD_z, C_zD_z' and $C_zD_zD_z'$ that we discuss are not due to DNP, but are created during cross-polarization (CP) at low temperature, because the RF field strength applied to the ^{13}C channel is not sufficient to quench the dipolar couplings between ^{13}C and D. We intend to detect ^2H signals at 1.2 K to quantify the populations of various terms during CP. Further, we want to emphasize that the absence of any asymmetry in direct polarization experiments shows that cross-relaxation of $2^{1/2}/3C_z$ magnetization into $Q_{STI,}^{IP}$ and Q_{STI}^{AP} is quite inefficient. The observed asymmetry is not induced by the relaxation of the carbon nucleus.

3.3.6 Conclusions

The cross relaxation and projection of the initial of $2^{1/2}/3C_z$, $3^{-1/2}C_zD_z$, $3^{-1/2}C_zD'_z$ and $2^{-1/2}C_zD_zD'_z$ terms onto Q_{STI}^{IP} and Q_{STI}^{AP} leads to a population of STI terms on the order of a few percent of the initial C_z term directly after dissolution. (This explains the modest ^{13}C enhancement factor $\varepsilon = 3900$ as a large fraction of the multi-spin terms relaxes quite fast during the transfer after dissolution, which is typical for quadrupolar nuclei.) Only CP-based DNP can sufficiently boost the intensity to observe these long-lived states. The entire experiment described here can be summarized as follows: (i) Multi-spin terms are populated during CP at cryogenic temperatures, (ii) These terms project and cross-relax onto the STIs, (iii) The STIs are preserved upon dissolution, (iv) The STI is measurable indirectly via the asymmetry of ^{13}C spectrum of the CD_2 group.

In conclusion, we have shown how one can *indirectly* hyperpolarize deuterium nuclei coupled to a ^{13}C nucleus via CP from ^{1}H to ^{13}C using weak *rf* amplitudes. Furthermore, it has been shown that some constituents of the density operator of a CD_2 system can have lifetimes that, although shorter than $T_1(C_z) = 23$ s for the case at hand, are much longer than $T_1(D_z) = 0.7$ s of the Zeeman polarization of the individual deuterium nuclei in the same system. These observations expand the scope of DNP by adding another nucleus to the list of possible observables. Thus, deuterium-based NMR with improved sensitivity on longer time scales becomes possible.

3.3.7 Experimental Details

Hyperpolarization of the sample

DNP experiments were performed on a Bruker prototype operating at 6.7 T and 1.2 K. The ^{13}C hyperpolarization was obtained via cross polarization from ^{1}H to ^{13}C.[24] TEMPOL (4-hydroxy-2,2,6,6-tetramethylpiperidine-1-oxyl) was used as polarizing agent.

The optimal amplitude of the spin-locking rf field was found to be $\gamma B_1^C/(2\pi) = 50$ kHz for a duration of the Hartmann-Hahn contact of $\tau_{SL} = 5$ ms. The ^{13}C build-up curve for direct polarization and for CP are shown in Fig 3.7.
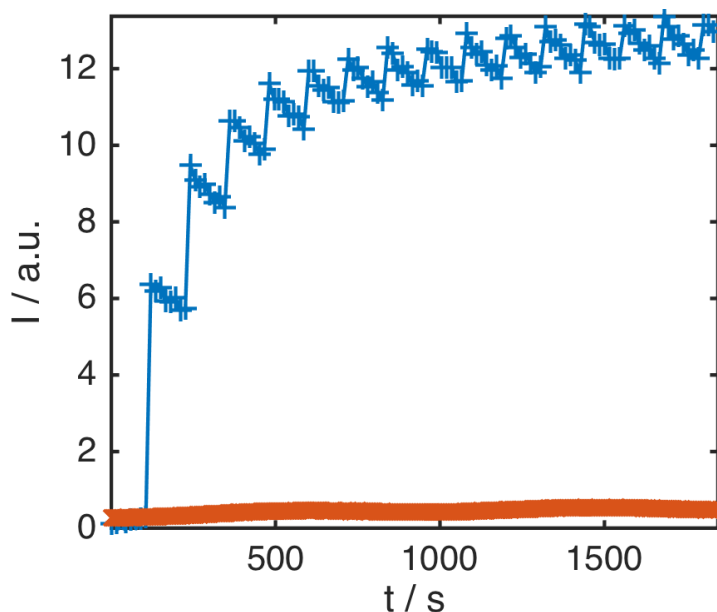

Figure 3.7. ^{13}C signal intensities of Ethanol-d_6 at 1.2 K for direct polarization (orange) and cross-polarization (CP) (blue).

A continuous µW field at 188 GHz with a power of 34 mW at the position of the sample, modulated with a saw-tooth function over a range of 100 MHz with a modulation frequency of 2 kHz, was used to saturate part of the EPR spectrum of the free radicals. The microwave field was switched off 1s before every CP step to allow the unpaired electrons to relax back to equilibrium.

Dissolution and transfer to the detection NMR spectrometer was performed with 5 mL D_2O at 10.5 bar heated to 180 ˚C, which was sprayed onto the frozen sample. The transfer of the dissolved hyperpolarized liquid to the NMR spectrometer took 10 s. The proton polarization that could be reached with our setup at 1.2 K was determined to be $P(^1H) = 81\%$ by comparison with a thermally equilibrated signal. The carbon polarization was determined to be $P(^{13}C) = 49\%$ after CP. However, due to a superposition of antiphase terms, positive and negative lines may partly cancel.

Sample preparation

A 50 mM solution of TEMPOL in a mixture of 60% Ethanol-d_6, 30% Glycerol-d_8 and 10% H_2O was shock-frozen in liquid nitrogen. The resulting glass was then transferred to the DNP polarizer. After dissolution with 5 mL D_2O, the final Ethanol-d_6 concentration was 1.04 mM.

Detection of the NMR signals

The signals were detected on a Bruker 400 MHz spectrometer using a 10 mm BBO broadband probe at room temperature. Pulses with 10° nutation angles were used at intervals of 1 s, with an acquisition time of 0.3 s. The spectra were processed with NMRPipe[38] using zero-filling but without apodization prior to analysis to avoid distorting the line shapes.

3.3.8 Appendix

Operator notation and normalization

We define the 18-dimensional operators as the following outer products:

$$3^{-1/2}/2D_z \equiv 3^{-1/2}/2 \; \underline{\underline{E^C}} \otimes \underline{\underline{D_z}} \otimes \underline{\underline{E^{D'}}}$$

$$3^{-1/2}/2D_z' \equiv 3^{-1/2}/2 \; \underline{\underline{E^C}} \otimes \underline{\underline{E^D}} \otimes \underline{\underline{D_z'}}$$

$$2^{1/2}/3C_z \equiv 2^{1/2}/3 \; \underline{\underline{C_z}} \otimes \underline{\underline{E^D}} \otimes \underline{\underline{E^{D'}}}$$

Where the doubly underlined operators represent the three-dimensional (in the case of D) or two-dimensional (in the case of C) matrix representations of the single spin operators. E denotes identity operators. Product operators in Liouville space involve simple matrix products:

$$3^{-1/2}C_zD_z = \; 3^{-1/2}(C_z \cdot D_z)$$

The norm $||A||$ of an operator A is defined as the square root of the scalar product $(A|A) = Tr\{A^\dagger . A\}$: $||A||^2 = (A|A)$

Relaxation Rates

The lifetimes of the $Q_{STI}{}^{IP}$ and $Q_{STI}{}^{AP}$ operators are almost the same (except if the ^{13}C nucleus has a large CSA relaxation rate at high field) and depend strongly on the anisotropy of the rotational diffusion of the molecule. For two axially symmetric Q-tensors the quadrupolar relaxation rate of the $Q_{STI}{}^{IP}$ and $Q_{STI}{}^{AP}$ terms is quite small but does not vanish:

$$R(Q_{STI}^{IP}) = R(Q_{STI}^{AP}) = \frac{3\tau_\perp \tau_\parallel}{4\tau_\parallel + \tau_\perp}\omega_Q^2$$

Where ω_Q denotes the quadupolar coupling constant in units of angular frequency. This rate decreases if $\tau_\parallel > \tau_\perp$. Longitudinal D_z Zeeman order decays with a rate:

$$R(D_z) = \left[\frac{3}{8}\frac{\tau_\parallel^3}{(\tau_\parallel + \tau_\perp/4)(\tau_\parallel + \tau_\perp)} + \frac{3}{4}\frac{\tau_\parallel^2 \tau_\perp}{(\tau_\parallel + \tau_\perp/4)(\tau_\parallel + \tau_\perp)} \right.$$
$$\left. + \frac{3}{8}\frac{\tau_\parallel \tau_\perp^2}{(\tau_\parallel + \tau_\perp/4)(\tau_\parallel + \tau_\perp)}\right]\omega_Q^2$$

The extension of the lifetime of the STI compared to the lifetime of Zeeman D_z order is therefore:

$$\kappa = \frac{R(D_z)}{R(Q_{STI}^{IP})}$$

If the rotational diffusion is very anisotropic with $\tau_\perp << \tau_\parallel$, one can expect $\kappa > 60$. For the case at hand of Ethanol-d6, we can simulate our observations with $\tau_\parallel \approx 4\tau_\perp$. The relaxation rates were found be evaluating the corresponding matrix elements $(Q_{STI}{}^{IP}\ |\Gamma_Q|\ Q_{STI}{}^{IP})$ and $(3^{-1/2}/2D_z\ \ |\Gamma_Q|\ 3^{-1/2}/2D_z)$. For any operator X, the Liouville bracket is denoted $(X|X)$. The relaxation rates underlying the matrix in Figure 3 were evaluated taking into account the entire Liouville space.

3.4 References for Chapter 3

1.   Sarkar, R.; Comment, A.; Vasos, P. R.; Jannin, S.; Gruetter, R.; Bodenhausen, G.; Hall, H.; Kirik, D.; Denisov, V. P., Proton NMR of (15)N-choline metabolites enhanced by dynamic nuclear polarization. *J. Am. Chem. Soc.* **2009,** *131* (44), 16014-5.

2.   Mieville, P.; Jannin, S.; Helm, L.; Bodenhausen, G., Kinetics of yttrium-ligand complexation monitored using hyperpolarized (89)Y as a model for gadolinium in contrast agents. *J. Am. Chem. Soc.* **2010,** *132* (14), 5006-7.

3.   Lumata, L.; Merritt, M. E.; Hashami, Z.; Ratnakar, S. J.; Kovacs, Z., Production and NMR characterization of hyperpolarized (107,109)Ag complexes. *Angew. Chem. Int. Ed. Engl.* **2012,** *51* (2), 525-7.

4.   Carravetta, M.; Johannessen, O. G.; Levitt, M. H., Beyond the T1 limit: singlet nuclear spin states in low magnetic fields. *Phys. Rev. Lett.* **2004,** *92* (15), 153003.

5.   Carravetta, M.; Levitt, M. H., Theory of long-lived nuclear spin states in solution nuclear magnetic resonance. I. Singlet states in low magnetic field. *J. Chem. Phys.* **2005,** *122* (21), 214505.

6.   Chen, T. k.; Beyerlein, A. L.; Savitsky, G. B., Rotational correlation times for ethanol by deuteron magnetic spin–lattice relaxation. *J. Chem. Phys.* **1975,** *63* (7), 3176-3177.

7.   Bowen, S.; Hilty, C., Rapid sample injection for hyperpolarized NMR spectroscopy. *Phys. Chem. Chem. Phys.* **2010,** *12* (22), 5766-5770.

8.   Kurzbach, D.; Weber, E. M.; Jhajharia, A.; Cousin, S. F.; Sadet, A.; Marhabaie, S.; Canet, E.; Birlirakis, N.; Milani, J.; Jannin, S.; Eshchenko, D.; Hassan, A.; Melzi, R.; Luetolf, S.; Sacher, M.; Rossire, M.; Kempf, J.; Lohman, J. A.; Weller, M.; Bodenhausen, G.; Abergel, D., Dissolution dynamic nuclear polarization of deuterated molecules enhanced by cross-polarization. *J. Chem. Phys.* **2016,** *145* (19), 194203.

9.   Bloch, F.; Hansen, W. W.; Packard, M., The Nuclear Induction Experiment. *Phys. Rev.* **1946,** *70* (7-8), 474-485.

10.   Hubbard, P. S., Nuclear Magnetic Relaxation of Three and Four Spin Molecules in a Liquid. *Phys. Rev.* **1958,** *109* (4), 1153-1158.

11.   Hubbard, P. S., Nonexponential Relaxation of Three-Spin Systems in Nonspherical Molecules. *J. Chem. Phys.* **1969,** *51* (4), 1647-1651.

12.   Hilt, R. L.; Hubbard, P. S., Nuclear Magnetic Relaxation of Three Spin Systems Undergoing Hindered Rotations. *Phys. Rev.* **1964,** *134* (2A), A392-A398.

13.   Kumar, A.; Jr., C. S. J., Proton spin-lattice relaxation studies of reorienting methyl groups in solids. *J. Chem. Phys.* **1974,** *60* (1), 137-146.

14.   Buchner, W.; Emmerich, B., A new type of multiplet effect in dynamic nuclear polarization of 13C-nuclei. *J. Magn. Reson. (1969)* **1971,** *4* (1), 90-98.

15.   Buchner, W., Some group theoretical considerations of nuclear magnetic relaxation in the methyl group. *J. Magn. Reson. (1969)* **1973,** *11* (1), 46-49.

16.   Salvi, N.; Buratto, R.; Bornet, A.; Ulzega, S.; Rentero Rebollo, I.; Angelini, A.; Heinis, C.; Bodenhausen, G., Boosting the Sensitivity of Ligand–Protein Screening by NMR of Long-Lived States. *J. Am. Chem. Soc.* **2012,** *134* (27), 11076-11079.

17.   Werbelow, L. G., NMR dynamic frequency shifts and the quadrupolar interaction. *J. Chem. Phys.* **1979,** *70* (12), 5381-5383.

18.   Tayler, M. C.; Marco-Rius, I.; Kettunen, M. I.; Brindle, K. M.; Levitt, M. H.; Pileio, G., Direct enhancement of nuclear singlet order by dynamic nuclear polarization. *J. Am. Chem. Soc.* **2012,** *134* (18), 7668-71.

19.   Ahuja, P.; Sarkar, R.; Jannin, S.; Vasos, P. R.; Bodenhausen, G., Proton hyperpolarisation preserved in long-lived states. *Chem. Commun. (Camb)* **2010,** *46* (43), 8192-4.

20.   Vasos, P. R.; Comment, A.; Sarkar, R.; Ahuja, P.; Jannin, S.; Ansermet, J. P.; Konter, J. A.; Hautle, P.; van den Brandt, B.; Bodenhausen, G., Long-lived states to sustain hyperpolarized magnetization. *Proc. Natl. Acad. Sci. U.S.A.* **2009,** *106* (44), 18469-73.

21.   Mammoli, D.; Vuichoud, B.; Bornet, A.; Milani, J.; Dumez, J. N.; Jannin, S.; Bodenhausen, G., Hyperpolarized para-ethanol. *J. Phys. Chem. B* **2015,** *119* (10), 4048-52.

22.   Zheng, Z. W.; Mayne, C. L.; Grant, D. M., Ethanol Molecular Dynamics Measured by Coupled Spin Relaxation Exhibiting Cross Correlation between Dipole-Dipole and Chemical-Shift Anisotropy. *J. Magn. Reson. A* **1993,** *103* (3), 268-281.

23.   Schmidt-Rohr, K.; Spiess, H. W., *Multidimensional Solid-state NMR and Polymers*. Academic Press: 1994.

24.   Jannin, S.; Bornet, A.; Colombo, S.; Bodenhausen, G., Low-temperature cross polarization in view of enhancing dissolution Dynamic Nuclear Polarization in NMR. *Chem. Phys. Lett.* **2011,** *517* (4), 234-236.

25.   Müller, L.; Kumar, A.; Baumann, T.; Ernst, R. R., Transient Oscillations in NMR Cross-Polarization Experiments in Solids. *Phys. Rev. Lett.* **1974,** *32* (25), 1402-1406.

26.   Bernatowicz, P.; Kruk, D.; Kowalewski, J.; Werbelow, L., 13C NMR lineshapes for the 13C2H2H' isotopomeric spin grouping. *Chemphyschem* **2002,** *3* (11), 933-8.

27.   Abragam, A.; Goldman, M., Principles of dynamic nuclear polarisation. *Rep. Prog. Phys.* **1978,** *41* (3), 395.

28.   Milani, J.; Vuichoud, B.; Bornet, A.; Mieville, P.; Mottier, R.; Jannin, S.; Bodenhausen, G., A magnetic tunnel to shelter hyperpolarized fluids. *Rev. Sci. Instrum.* **2015,** *86* (2), 024101.

29.   Werbelow, L. G.; Morris, G. A.; Kumar, P.; Kowalewski, J., Cross-correlated quadrupolar spin relaxation and carbon-13 lineshapes in the (13)CD(2) spin grouping. *J. Magn. Reson.* **1999,** *140* (1), 1-8.

30.   Kowalewski, J.; Mäler, L., *Nuclear spin relaxation in liquids : theory, experiments, and applications*. New York (N.Y.) : Taylor & Francis: 2006.

31.   Pileio, G.; Levitt, M. H., J-Stabilization of singlet states in the solution NMR of multiple-spin systems. *J. Magn. Reson.* **2007,** *187* (1), 141-5.

32.   Poupko, R.; Vold, R. L.; Vold, R. R., Density matrix calculations of the relaxation of two deuterons in an ordered medium. *J. Magn. Reson. (1969)* **1979,** *34* (1), 67-81.

33.   Bernatowicz, P.; Szymanski, S., NMR spectra of a spin-1/2 nucleus scalar coupled to two equivalent spin-1 nuclei in the limit of slow quadrupolar relaxation. *J. Magn. Reson.* **2001,** *148* (2), 455-8.

34.   Bernatowicz, P.; SzymaŃSki, S., Magnetic equivalence of terminal nuclei in the azide anion broken by nuclear spin relaxation. *Mol. Phys.* **2003,** *101* (3), 353-359.

35.   Vuichoud, B.; Milani, J.; Chappuis, Q.; Bornet, A.; Bodenhausen, G.; Jannin, S., Measuring absolute spin polarization in dissolution-DNP by Spin PolarimetrY Magnetic Resonance (SPY-MR). *J. Magn. Reson.* **2015,** *260*, 127-35.

36.   Nocedal, J.; Wright, S., *Numerical Optimization*. Springer New York: 2006.

37.   Scilab, E. S. Le logiciel open source gratuit de calcul numérique.

38.   Delaglio, F.; Grzesiek, S.; Vuister, G. W.; Zhu, G.; Pfeifer, J.; Bax, A., NMRPipe: a multidimensional spectral processing system based on UNIX pipes. *J. Biomol. NMR* **1995,** *6* (3), 277-93.

4. Long-Lived Deuterium Spin State Imbalance in Methyl Groups

Methyl groups are omnipresent starting from small organic molecules up to large biomolecular species. Various ^{1}H NMR relaxation methods allow studying their dynamics. Several models have been designed to study dipolar relaxation of protons and carbon-13 nuclei in methyl groups.[1-2] Methyl group rotation can be a fruitful source of information, e.g., in polymer dynamics, especially with a focus on deuterated systems.[3-7] Furthermore, deuterium labelling of methyl groups has triggered biophysical studies of proteins,[8-9] since deuterium spin with several well-defined relaxation pathways can provide a valuable source of information. In this chapter I will discuss some observations of deuterated methyl groups, which can be useful as they prolong the experimentally accessible time window. The results reported here have been published recently.[10]

4.1 Study of Deuterated Methyl Groups by Dissolution-DNP

Long-lived spin states have been created using many spin ½ nuclei and combined with dissolution DNP. Dissolution DNP enables an exciting range of previously inaccessible applications.[11-13] In chapter 3, we have discussed the investigation of a new area by creating long-lived states involving quadrupolar nuclei in $^{13}CD_2$ groups that are reminiscent of the triplet-singlet imbalance (TSI) that has been observed in $^{13}CH_2$ groups,[14] where an imbalance can be created between symmetric triplet and antisymmetric singlet states by depleting or over populating one with respect to the other. Multiplet asymmetries can be exploited for spin polarimetry (SPY),[15] and an imbalance between symmetric and non-

symmetric spin states (A/E imbalance or AEI) in $^{13}CH_3$ groups has been discussed by Levitt, Dumez and co-workers.[16-17] They observed long-lived states in the methyl group of ^{13}C-γ-picoline (4-[^{13}C-methyl] pyridine) due to the fast methyl group rotation. A similar phenomenon will here be reported here for CD_3 groups.

4.1.1 Symmetry-Adapted Basis Set

To label the spin states of the D_3 subsystem of a $^{13}CD_3$ group, we indicate the base-kets of the symmetry adapted basis (C_{3v}) by the magnetic quantum numbers $m_z(D)$, $m_z(D')$ and $m_z(D'') = -1$, 0, or 1 of the three deuterons D, D' and D'' as described in reference.[18] This yields the following 27 states:

$\Phi_1 = |111>$

$\Phi_2 = (|100> + |101> + |011>) /\sqrt{3}$

$\Phi_3 = (|11-1> + |1-11> + |-111> + 2|100> + 2|010> + 2|001>)/\sqrt{15}$

$\Phi_4 = (|10-1> + |01-1> + |0-11> + |-101> + |1-10> + |-110> + 2|-000>)/\sqrt{10}$

$\Phi_5 = (|-1-11> + |-11-1> + |1-1-1> + 2|-100> + 2|0-10> + 2|00-1>)/\sqrt{15}$

$\Phi_6 = (|-100> + |-10-1> + |0-1-1>) /\sqrt{3}$

$\Phi_7 = |-1-1-1>$

$\Phi_8 = (2|100> - |101> - |011>) /\sqrt{6}$

$\Phi_9 = (2|11-1> - |1-11> - |-111> - 2|001> + 2|010> + 2|100>)/\sqrt{12}$

$\Phi_{10} = (|10-1> + |01-1> - |0-11> - |-101>)/2$

$\Phi_{11} = (2|00-1> - |0-10> - |-100> - 2| -|1-11> + |-11-1> + |1-1-1>)/\sqrt{12}$

$\Phi_{12} = (-2|-1-10> + |0-1-1> + |-10-1>) /\sqrt{6}$

$\Phi_{13} = (|101> - |011>)/\sqrt{2}$

$\Phi_{14} = (|1-11> - |-111> + |100> - |010>)/2$

$\Phi_{15} = (2|1-10> - 2|-110> + |10-1> + |0-11> - |01-1> - |-101>)/\sqrt{12}$

$\Phi_{16} = (|0-10> - |100> + |1-1-1> - |-11-1>)/2$

$\Phi_{17} = (|0-1-1> - |-10-1>)/\sqrt{2}$

$\Phi_{18} = (2|11-1> -2 |1-11> -2 |-111> + |100> + |010> + |001>)/\sqrt{15}$

$\Phi_{19} = (|10-1> + |01-1> + |0-11> + |-101> + |1-10> + |-110>-3|-000>)/\sqrt{15}$

$\Phi_{20} = (-2|-1\text{-}11\rangle\ \text{-}2\ |\text{-}11\text{-}1\rangle\ \text{-}2\ |1\text{-}1\text{-}1\rangle + |\text{-}100\rangle + |0\text{-}10\rangle + |01\text{-}1\rangle)/\sqrt{15}$

$\Phi_{21} = (2|11\text{-}1\rangle - |1\text{-}11\rangle - |\text{-}111\rangle + 2|001\rangle - |010\rangle - |100\rangle)/\sqrt{12}$

$\Phi_{22} = (-2|1\text{-}10\rangle\ \text{-}2\ |\text{-}110\rangle + |10\text{-}1\rangle + |01\text{-}1\rangle - |0\text{-}11\rangle - |\text{-}101\rangle)/\sqrt{12}$

$\Phi_{23} = (2|00\text{-}1\rangle - |0\text{-}10\rangle - |\text{-}100\rangle + 2|-1\text{-}11\rangle - |\text{-}11\text{-}1\rangle - |1\text{-}1\text{-}1\rangle)/\sqrt{12}$

$\Phi_{24} = (|1\text{-}11\rangle - |\text{-}111\rangle + |010\rangle - |100\rangle)/2$

$\Phi_{25} = (|01\text{-}1\rangle + |0\text{-}10\rangle - |10\text{-}1\rangle - |10\text{-}1\rangle)/2$

$\Phi_{26} = (|0\text{-}10\rangle - |\text{-}100\rangle + |\text{-}11\text{-}1\rangle - |1\text{-}1\text{-}1\rangle)/2$

$\Phi_{27} = (|10\text{-}1\rangle - |0\text{-}11\rangle + |\text{-}110\rangle - |01\text{-}1\rangle - |\text{-}101\rangle - |1\text{-}10\rangle)/\sqrt{6}$

Each of these eigenstates belongs to one of the four spin manifolds (A, E_1, E_2, B).

These states are duplicated in the presence of a ^{13}C spin, which can adopt either the state α if $m_z(^{13}C) = + \frac{1}{2}$, or β if $m_z(^{13}C) = - \frac{1}{2}$, to yield 54 states.

4.1.2 Results and Discussion

In this chapter we focus, as in the preceding chapter, on a curious and potentially valuable side-effect of hyperpolarisation by D-DNP: the creation of non-equilibrium population distributions in symmetrical deuterated spin systems. The utility of this finding lies in the long-lived nature of these population imbalances, which exhibit lifetimes that can be 20 times longer than the spin-lattice relaxation time $T_1(D_z)$ of the Zeeman polarization D_z of deuterium nuclei (see chapter 3) that often relaxes too quickly (typically $0.5 < T_1(D_z) < 2$ s) considering the time required to transfer a hyperpolarized solution to an NMR spectrometer or to an MRI system for spectroscopy or imaging.

Here we report the observation of a spin-state imbalance (SSI) in deuterated CD_3 methyl groups. The lifetime $T_{SSI}(D_3)$ provides a new way to access the activation energy of the rotation of methyl groups.

A $^{13}CD_3$ group contains an SI_3 system with nuclear spins $S = \frac{1}{2}$ and $I = 1$. To understand relaxation in $^{13}CD_3$ groups, it is important to consider the C_{3v} point group symmetry of the time-averaged Hamiltonian (in the absence of relaxation) by using the symmetry-adapted eigenbasis described by Bernatowicz et al.[18] Each of the 27 symmetrized eigenstates of the D_3 subsystem belongs to one of

the four manifolds (irreducible representations) A, E1, E2 and B of the C_{3v} point group (Fig. 4.1). Various relaxation pathways between these eigenstates can be identified.
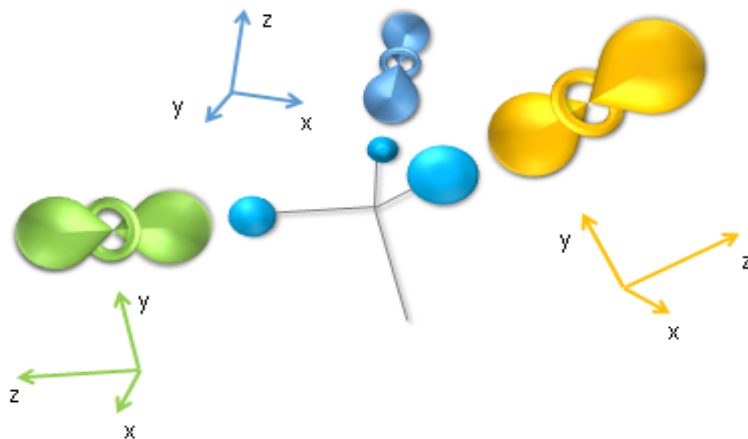

Figure 4.1. Sketch of a CD_3 group with its three quadrupolar tensors. The deuterons are represented by blue spheres. In the static limit, the principal components of the Q-tensors (assumed to have axial symmetry) are represented by green, blue and yellow spherical tensors (analogous to d_{z2} orbitals) that are aligned along the three C-D bond axes. The spherical tensors represent the spatially dependent part of the nuclear quadrupole Hamiltonians through the tensor components ($V_{+/-2}$, $V_{+/-1}$, V_0) of the electric field gradient at the nucleus.

The principal components of the quadrupolar tensors of the three deuterons are aligned along the C-D bonds as shown in Fig 4.1. The tensors are assumed to have cylindrical symmetry ($\eta = 0$). Fast 120° jumps of the CD_3 group around the C_{3v} symmetry axis lead to averaging of the quadrupolar tensors so that the three deuterons are no longer distinguishable with respect to quadrupolar relaxation.

Under these conditions a peculiar phenomenon arises: any imbalance generated between populations that belong to different irreducible representations (A, E1, E2 or B) will persist and the return to thermal Boltzmann equilibrium will be inhibited. This is because the flow of populations between these eigenstates is forbidden to first order.

Quantum states that feature an imbalance between populations belonging to different symmetry manifolds[14, 19] vanish in thermal equilibrium and are difficult

to observe. Here, using both hyperpolarization and a hitherto unexplored type of coherence transfer under radiofrequency pulses, we generated such imbalances in the CD_3 groups of DMSO-d_6 and acetone-d_6. Evidence of their existence was then observed in liquid-state ^{13}C NMR spectra after dissolution. In thermal equilibrium, the ^{13}C multiplets feature a symmetric 1:3:6:7:6:3:1 septet pattern due to the scalar couplings $^1J(D, ^{13}C)$ = 18 Hz to the three equivalent neighboring deuterons with I = 1. However, in our experiments, an imbalance between the different symmetry manifolds is produced, which results in an *asymmetric septet* instead of the normally symmetric septet. The lifetime T_{SSI} of the non-equilibrium deuterium spin state imbalance was obtained by monitoring the decay of this asymmetry.[20-23]
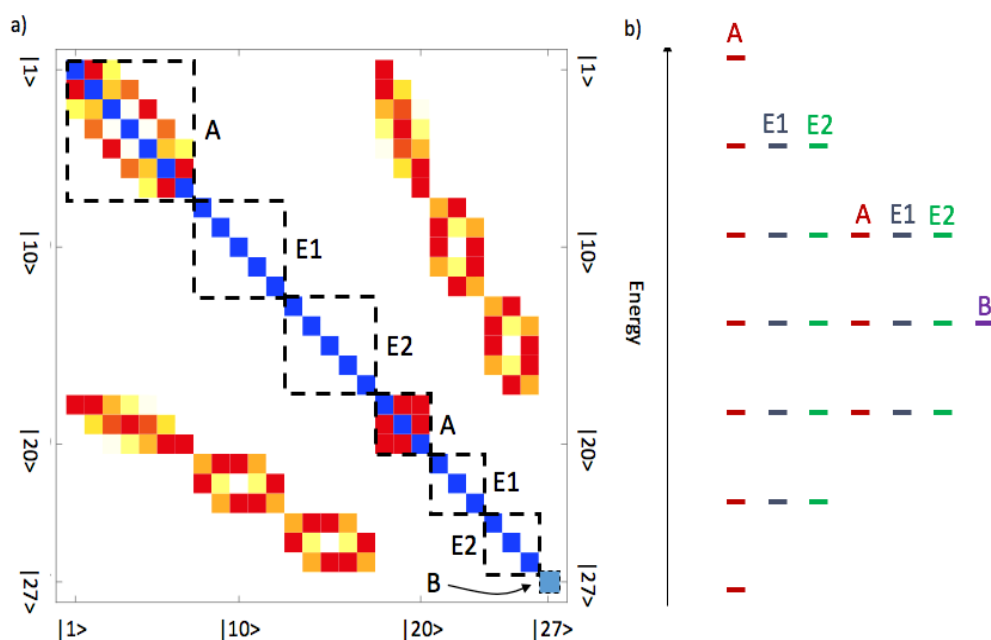

Figure 4.2. a) Pictorial representation of the symmetry-adapted eigenstates and the relaxation matrix of the 27 states of the D_3 subsystem of a $^{13}CD_3$ group after dissolution, appropriate for the extreme narrowing regime ($\omega_L \tau_c$ << 1). Positive relaxation matrix elements are represented by yellow and red boxes, and negative elements by blue boxes. Each of the 27 symmetry-adapted states belongs to one of the four symmetry manifolds A, E1, E2 and B. There are no matrix elements that connect different irreducible representations. Therefore, if one considers only quadrupolar relaxation, the populations cannot flow freely between states belonging to different irreducible representations. b) Energy level diagram associated with the D_3 spin system.

In recent work[24] we described how the hyperpolarization of ^{13}C nuclei in a ^{13}CD$_2$ group can be transferred to the attached deuterium nuclei via multispin order terms like C$_z$D$_z$, etc., through side-effects of non-ideal cross-polarization (CP) from protons to ^{13}C. Similar principles apply to ^{13}CD$_3$ groups. During the CP-driven buildup of ^{13}C polarization from the DNP-polarized protons of the frozen solvent, the relatively weak CP irradiation of ^{13}C is insufficient to decouple its dipolar interactions with nearby deuterons. Consequently, ^{1}H-^{13}C CP leads to multispin carbon-deuterium coherences of the form 1/3C$_z$D$_z$, 1/√6C$_z$D$_z$D$_z$' and 1/2C$_z$D$_z$D$_z$'D$_z$'' and permutations thereof. After dissolution, these operators project onto long-lived spin state imbalances that are in antiphase with respect to ^{13}C.[24]

These forms of antiphase spin state imbalances feature much longer relaxation times than one would expect, considering the large quadrupolar interactions involved. A pictorial representation of the relaxation matrix, Γ$_Q$, that describes the flow of populations between states of the D$_3$ subsystem under the influence of quadrupolar couplings is shown in Fig. 4.2. Each of the 27 symmetry-adapted eigenstates |1> to |27> belongs to one of the four symmetry manifolds, A, E1, E2 and B. States belonging to different irreducible representations are not connected by any off-diagonal matrix elements if the methyl group rotation is infinitely fast. This implies that the return to thermal equilibrium of a spin state imbalance between different symmetry manifolds cannot occur via quadrupolar relaxation. The relaxation time of the SSI can be found by evaluating the corresponding matrix elements (Q$_{SSI}$ |Γ$_Q$| Q$_{SSI}$), where Q$_{SSI}$ denotes the product operator description of the SSI. The Liouville bracket is denoted (X|X). The relaxation rates underlying the matrix in Figure 4.2 were evaluated taking into account the entire Liouville space. This leads to the following expression for the lifetime of the spin state imbalance in deuterated methyl groups:

$$T_{SSI}(D_3) = \left(\frac{\tau_R}{\tau_R+\tau_C} \omega_Q^2 + \frac{2\tau_R}{\tau_R+4\tau_C} \omega_Q^2 \right)^{-1} \qquad (4.1)$$

Here τ_R denotes the correlation time for rotation around the C$_{3v}$ main symmetry axis, while τ_C refers to the overall tumbling. The lifetime T_{SSI}(D$_3$) would thus be

infinite for infinitely fast methyl group rotation, since τ_R would be zero. $T_{SSI}(D_3)$ thus provides a measure of the frequency of methyl group rotation, and will be short if the activation energy for jumps around the C_{3v} axis is high. However, for infinitely fast rotation around the C_{3v} axis, chemical shift anisotropy (CSA) relaxation of the SSI can still occur in a manner that is analogous to the case described by Dumez et al. for protonated methyl groups.[12]

The multiplets of the ^{13}C spins of the ^{13}CD$_3$ groups in DMSO-d$_6$ after dissolution and transfer to a conventional 400 MHz spectrometer are depicted in Fig. 4. They consist of seven lines numbered L_1-L_7. Deuterium populations that are not stored in the form of an imbalance have relaxed to thermal equilibrium. In the first acquired spectrum (at time $t = 0$) the ^{13}C multiplet of the hyperpolarized sample displays a significant asymmetry due to the presence of non-equilibrium deuterium populations that gradually disappears as the multiplet returns to its equilibrium distribution. The central line L_4 is attenuated, whilst the outer lines L_1 and L_7 are enhanced. In addition, antiphase terms of the form $n_1 C_x D_z$, $n_2 C_x D_z D_z'$ and $n_3 C_x D_z D_z' D_z''$ (with norms $n_1 = 3^{-1}$, $n_2 = 6^{-1/2}$ and $n_3 = 2^{-1}$) give rise to the observed deviations from the 1:3:6:7:6:3:1 multiplet in Fig. 4.3. Simulations with SpinDynamica confirm that the spectra can be reproduced by a superposition of antiphase terms, spin state imbalances and C_x magnetization.
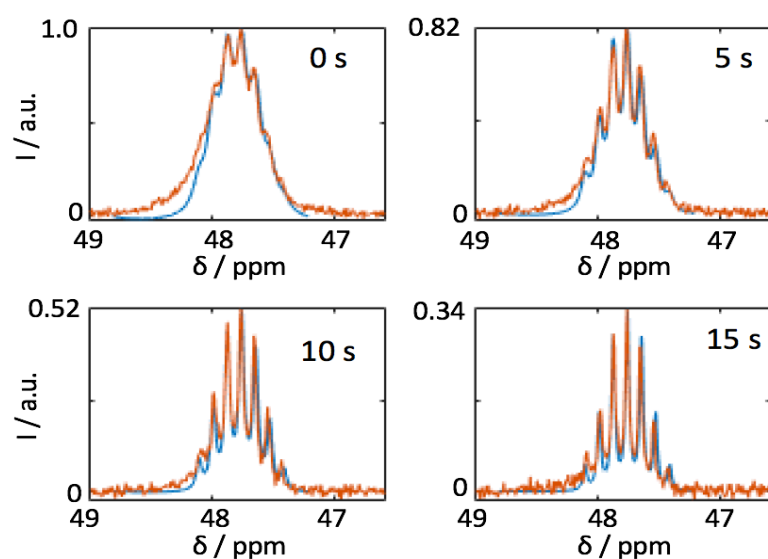

123

Figure 4.3. Experimentally observed signals (orange) due to the hyperpolarization of the $^{13}CD_3$ groups in DMSO-d_6 after DNP, dissolution and transfer to a conventional NMR spectrometer operating at 9.4 T, and simulations (blue) obtained with the SpinDynamica software package. Immediately after dissolution (t = 0) the septet shows a strong asymmetry. After 15 s the thermal equilibrium distribution is recovered with amplitudes 1:3:6:7:6:3:1. Note that the overall signal intensity decreases as the carbon hyperpolarization decays towards thermal equilibrium with $T_1(^{13}C)$ = 19.6 s (the vertical scale is reduced stepwise from 100 to 82, 52 and 34%.)

The observed deviation of the multiplet from equilibrium provides a direct measure of the magnitude of the spin state imbalance between different symmetry manifolds. The asymmetry A can be quantified via the intensities of the individual multiplet components:

$$A = (L_1 + L_2 + L_3 - L_5 - L_6 - L_7) / L_4. \qquad (4.2)$$

Note that only fast rotation about the C_{3v} axis can average the three quadrupolar tensors in the CD_3 group. Thus, the faster the rotation of the CD_3 group, the better the separation of the four symmetry manifolds. Hence, a long lifetime $T_{SSI}(D_3)$ of the asymmetry constitutes an indirect measure of fast rotation of deuterated methyl groups. A similar behaviour has been shown by Levitt and co-workers for CH_3 groups.[17, 25] Werbelow *et al.* have given a theoretical treatment of the effects of methyl group rotation on ^{13}C NMR spectra.[26]

Importantly, no asymmetry of the ^{13}C multiplet was observed in direct polarization experiments (without CP), which confirms that that the antiphase terms in the solid state that project on spin state imbalances only arise when employing CP.

Fig. 4.4 shows the experimental asymmetry A defined in Eq. 4.1 in DMSO-d_6 and acetone-d_6. The characteristic lifetimes of the multiplet asymmetry, denoted $T_{SSI}(D_3)$, were found to be 6.8 s in DMSO-d_6, and 12.8 s in acetone-d_6. The S–O bond in DMSO tends to adopt a zwitterionic character (S$^+$O$^-$), in contrast to the neutral double bond (C=O) in acetone. Because the polarity of the CO moiety is lower than that of the SO moiety, the methyl group rotation in acetone is expected to be faster than in DMSO. The oxygen atom of the carbonyl group

therefore constitutes a greater hindrance for the rotation of the deuterons in DMSO than in acetone, thus explaining the differences in $T_{SSI}(D_3)$.[27]

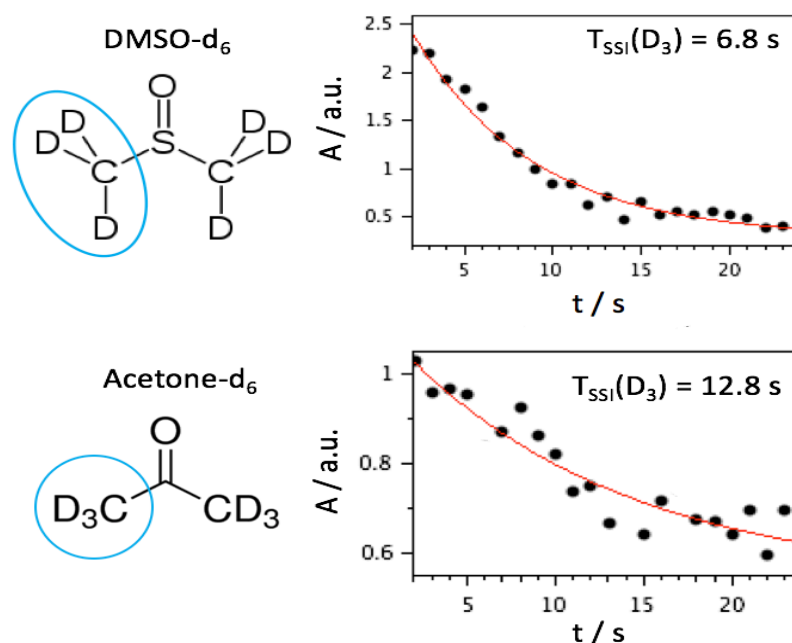**Figure 4.4.** Decay of the experimentally observed asymmetry A defined in eq. (2) of the amplitudes of the septet in the $^{13}CD_3$ groups of DMSO-d_6 (top) and Acetone-d_6 (bottom). The characteristic life times $T_{SSI}(D_3)$ are about 20 times longer than $T_1(D_3)$.

It is obvious from eq. 4.1 that lower energy barriers for methyl group rotation result in shorter τ_R, therefore leading to increased lifetimes and longer $T_{SSI}(D_3)$. An increased negative charge on the neighboring oxygen, resulting in stronger interactions with the deuterons of the CD_3 moiety and a larger rotational energy barrier, will thus lead to reduced lifetimes $T_{SSI}(D_3)$. These lifetimes therefore provide an indirect measure of the activation energy of rotational jumps in deuterated methyl groups.

As longitudinal relaxation times of deuterons are typically on the order of a few seconds, the long lifetime of the here reported spin-state imbalance enlarges the experimental time window significantly, thus extending the scope of quadrupolar NMR.

4.1.3 Experimental Methods

The ^{13}C spectra of DMSO-d$_6$ in 1.1% natural isotopic abundance were observed in a mixture of Ethanol:DMSO-d$_6$:Glycerol-d$_8$ (v:v:v = 1:2:1). The Acetone-d$_6$ containing samples were prepared in analogy to the DMSO samples. The Ethanol-d$_6$ samples were prepared as described in chapter 3.[24] Dissolution DNP and NMR experiments are explained in detail in Chapter 3 (see section 3.3.7).

DNP experiments were performed on a Bruker prototype operating at 6.7 T and 1.2 K. The ^{13}C hyperpolarization was obtained via cross polarization from ^{1}H to ^{13}C.[28] TEMPOL (4-hydroxy-2,2,6,6-tetramethylpiperidine-1-oxyl) was used as polarizing agent for all samples.

A spin-locking rf field amplitude $\gamma B_1^C/(2\pi)$ = 50 kHz was used for a duration of the Hartmann-Hahn contact of τ_{SL} = 5 ms. A continuous μW field with a power of 34 mW at 188 GHz at the position of the sample, modulated with a saw-tooth function over a range of 100 MHz with a modulation frequency of 2 kHz, was used to saturate part of the EPR spectrum of the free radicals. The microwave irradiation was switched of 1s before every CP step to allow the unpaired electrons to relax back to equilibrium.

Dissolution and transfer to the detection NMR spectrometer was performed with 5 mL D$_2$O at 10.5 bar heated to 180 ℃, which was sprayed onto the frozen sample, using the same parameters for other experiments. The transfer of the hyperpolarized liquid to the NMR spectrometer required around 10 s.

4.2 References for Chapter 4

1.   Hilt, R. L.; Hubbard, P. S., Nuclear Magnetic Relaxation of Three Spin Systems Undergoing Hindered Rotations. *Phys. Rev.* **1964,** *134* (2A), A392-A398.

2.   Runnels, L. K., Nuclear Spin-Lattice Relaxation in Three-Spin Molecules. *Phys. Rev.* **1964,** *134* (1A), A28-A36.

3.   Huntress, W. T., Nuclear magnetic resonance study of anisotropic molecular rotation in liquid chloroform and in chloroform-benzene solution. *J. Phys. Chem.* **1969,** *73* (1), 103-111.

4.   Wallach, D.; Jr., W. T. H., Anisotropic Molecular Rotation in Liquid N,N-Dimethylformamide by Nuclear Magnetic Resonance. *J. Chem. Phys.* **1969,** *50* (3), 1219-1227.

5.   Huntress, W., The study of anisotropic rotation of molecules in liquids by NMR quadrupolar relaxation. *Adv. Magn. Reson* **1970,** *4* (1).

6.   Ericsson, A.; Kowalewski, J., Internal motion in 1-methylnaphthalene. A variable temperature NMR study using 13C and 2H spin—lattice relaxation time measurements. *Chem. Phys.* **1981,** *60* (3), 387-391.

7.   Bopp, T. T., Magnetic Resonance Studies of Anisotropic Molecular Rotation in Liquid Acetonitrile-d3. *J. Chem. Phys.* **1967,** *47* (9), 3621-3626.

8.   Millet, O.; Muhandiram, D. R.; Skrynnikov, N. R.; Kay, L. E., Deuterium Spin Probes of Side-Chain Dynamics in Proteins. 1. Measurement of Five Relaxation Rates per Deuteron in ^{13}C-Labeled and Fractionally 2H-Enriched Proteins in Solution. *J. Am. Chem. Soc.* **2002,** *124* (22), 6439-6448.

9.   Skrynnikov, N. R.; Millet, O.; Kay, L. E., Deuterium Spin Probes of Side-Chain Dynamics in Proteins. 2. Spectral Density Mapping and Identification of Nanosecond Time-Scale Side-Chain Motions. *J. Am. Chem. Soc.* **2002,** *124* (22), 6449-6460.

10.   Jhajharia, A.; Weber, E. M.; Kempf, J. G.; Abergel, D.; Bodenhausen, G.; Kurzbach, D., Communication: Dissolution DNP reveals a long-lived deuterium spin state imbalance in methyl groups. *J. Chem. Phys.* **2017,** *146* (4), 041101.

11.   Ardenkjaer-Larsen, J. H.; Fridlund, B.; Gram, A.; Hansson, G.; Hansson, L.; Lerche, M. H.; Servin, R.; Thaning, M.; Golman, K., Increase in signal-to-noise ratio of > 10,000 times in liquid-state NMR. *Proc. Natl. Acad. Sci. USA* **2003,** *100* (18), 10158-63.

12.   Dumez, J. N.; Milani, J.; Vuichoud, B.; Bornet, A.; Lalande-Martin, J.; Tea, I.; Yon, M.; Maucourt, M.; Deborde, C.; Moing, A.; Frydman, L.; Bodenhausen, G.; Jannin, S.; Giraudeau, P., Hyperpolarized NMR of plant and cancer cell extracts at natural abundance. *Analyst* **2015,** *140* (17), 5860-3.

13. Vasos, P. R.; Comment, A.; Sarkar, R.; Ahuja, P.; Jannin, S.; Ansermet, J. P.; Konter, J. A.; Hautle, P.; van den Brandt, B.; Bodenhausen, G., Long-lived states to sustain hyperpolarized magnetization. *P. Natl. Acad. Sci. USA* **2009,** *106* (44), 18469-18473.

14. Mammoli, D.; Vuichoud, B.; Bornet, A.; Milani, J.; Dumez, J. N.; Jannin, S.; Bodenhausen, G., Hyperpolarized para-Ethanol. *J. Phys. Chem. B* **2015,** *119* (10), 4048-4052.

15. Vuichoud, B.; Milani, J.; Chappuis, Q.; Bornet, A.; Bodenhausen, G.; Jannin, S., Measuring absolute spin polarization in dissolution-DNP by Spin PolarimetrY Magnetic Resonance (SPY-MR). *J. Magn. Reson.* **2015,** *260*, 127-135.

16. Tayler, M. C.; Marco-Rius, I.; Kettunen, M. I.; Brindle, K. M.; Levitt, M. H.; Pileio, G., Direct enhancement of nuclear singlet order by dynamic nuclear polarization. *J. Am. Chem. Soc.* **2012,** *134* (18), 7668-71.

17. Dumez, J. N.; Hakansson, P.; Mamone, S.; Meier, B.; Stevanato, G.; Hill-Cousins, J. T.; Roy, S. S.; Brown, R. C.; Pileio, G.; Levitt, M. H., Theory of long-lived nuclear spin states in methyl groups and quantum-rotor induced polarisation. *J. Chem. Phys.* **2015,** *142* (4), 044506.

18. Bernatowicz, P.; Kowalewski, J.; Kruk, D.; Werbelow, L. G., C-13 NMR line shapes in the study of dynamics of perdeuterated methyl groups. *J. Phys. Chem. A* **2004,** *108* (42), 9018-9025.

19. Carravetta, M.; Levitt, M. H., Theory of long-lived nuclear spin states in solution nuclear magnetic resonance. I. Singlet states in low magnetic field. *J. Chem. Phys.* **2005,** *122* (21), 214505.

20. Feng, Y.; Davis, R. M.; Warren, W. S., Accessing long-lived nuclear singlet states between chemically equivalent spins without breaking symmetry. *Nat. Phys.* **2012,** *8* (11), 831-837.

21. Pileio, G.; Carravetta, M.; Levitt, M. H., Storage of nuclear magnetization as long-lived singlet order in low magnetic field. *Proc. Natl. Acad. Sci. USA* **2010,** *107* (40), 17135-9.

22. Pileio, G.; Levitt, M. H., Theory of long-lived nuclear spin states in solution nuclear magnetic resonance. II. Singlet spin locking. *J. Chem. Phys.* **2009,** *130* (21), 214501.

23. Kiryutin, A. S.; Zimmermann, H.; Yurkovskaya, A. V.; Vieth, H. M.; Ivanov, K. L., Long-lived spin states as a source of contrast in magnetic resonance spectroscopy and imaging. *J. Magn. Reson.* **2015,** *261*, 64-72.

24.   Kurzbach, D.; Weber, E. M. M.; Jhajharia, A.; Cousin, S. F.; Sadet, A.; Marhabaie, S.; Canet, E.; Birlirakis, N.; Milani, J.; Jannin, S.; Eshchenko, D.; Hassan, A.; Melzi, R.; Luetolf, S.; Sacher, M.; Rossire, M.; Kempf, J.; Lohman, J. A. B.; Weller, M.; Bodenhausen, G.; Abergel, D., Dissolution Dynamic Nuclear Polarization of Deuterated Molecules Enhanced by Cross-Polarization *J. Chem. Phys.* **2016,** *accepted.*

25.   Meier, B.; Dumez, J. N.; Stevanato, G.; Hill-Cousins, J. T.; Roy, S. S.; Hakansson, P.; Mamone, S.; Brown, R. C.; Pileio, G.; Levitt, M. H., Long-lived nuclear spin states in methyl groups and quantum-rotor-induced polarization. *J. Am. Chem. Soc.* **2013,** *135* (50), 18746-9.

26.   Werbelow, L. G.; Grant, D. M., Determination of Motional Asymmetry of Methyl Rotators from C-13 Spin Dynamics. *Can. J. Chem.* **1977,** *55* (9), 1558-1563.

27.   McLain, S. E.; Soper, A. K.; Luzar, A., Orientational correlations in liquid acetone and dimethyl sulfoxide: a comparative study. *J. Chem. Phys.* **2006,** *124* (7), 74502.

28.   Jannin, S.; Bornet, A.; Colombo, S.; Bodenhausen, G., Low-temperature cross polarization in view of enhancing dissolution Dynamic Nuclear Polarization in NMR. *Chem. Phys. Lett.* **2011,** *517* (4), 234-236.

5. Conclusions

While discussing the results obtained on deuterated molecules in this thesis we hope that DNP can open new avenues for the study of such deuterated molecules.

As shown in chapter 2, we can improve the ^{13}C polarization with cross polarization at low temperatures, which depends on the saturation of the unpaired electron spins via microwave irradiation. The saturation of the electron spins shortens the nuclear spin relaxation times $T_{1\rho}(^1\text{H})$ in the rotating frame. Shortening of the relaxation time in the rotating frame affects the cross-polarization efficiency from ^{1}H to ^{13}C or other low-gamma nuclei. We have shown that the efficiency of cross-polarization from ^{1}H to ^{13}C can be boosted by 70% at 1.2 K by gating the microwave irradiation off prior to the cross polarization. Our experimental results prove that switching off the microwave irradiation allows the electrons to relax back to a highly-polarized state, resulting in an extension of $T_{1\rho}(^1\text{H})$. Finally, a 64% polarization of ^{13}C was achieved for [1-^{13}C] acetate with a build-up time constant of 160 s. Similarly, a huge ^{13}C polarization of 78% was achieved for ^{13}C urea with a time constant of 470 s.

In chapter 3, a new kind of long-lived states was introduced. This can accur in deuterated molecules depending on the symmetry point group of the molecules. After the ^{1}H-^{13}C cross polarization with DNP at a temperature near 1.2 K, we observed that cross polarization plays a key role by creating an asymmetry in the ^{13}C pentet in the NMR spectrum at ambient temperature just after dissolution. This results from the population imbalances between spin manifolds belonging to different symmetry manifolds. This imbalance could be observed indirectly through the ^{13}C NMR spectrum of the $^{13}\text{CD}_2$ group.

In CD_2 groups, these long-lived states result from an imbalance between symmetric and antisymmetric manifolds of the C_{2v} group. This imbalance is

described as a sextet-triplet imbalance (STI), which is similar to a triplet-singlet imbalance (TSI) as defined by Levitt in the case of the two equivalent spin-1/2 nuclei. These imbalances are pronounced if the polarization is transferred from ^1H to ^{13}C through CP at 1.2 K due to imperfect Hartmann-Hahn conditions. In cases of direct polarization this phenomenon is less pronounced, yet still observable. Only CP based DNP can sufficiently boost the intensity to observe this unique behavior of ^{13}C NMR signals. During CP at cryogenic temperatures, multi-spin terms can be populated, which transform into longer-lived spin terms through cross relaxation through ^2D to ^{13}C. These terms can have much longer lifetimes than the Zeeman magnetization of a deuterium spin.

Chapter 4 focuses on deuterated methyl moieties. Similar effects were observed just after dissolution, giving rise to an asymmetry in the septet in the ^{13}C NMR spectrum, which differs from the usual thermal equilibrium signal at ambient temperature. Again CP imperfections played a pivotal role in this observation. These spin state imbalances between the four distinct irreducible representations of the C_{3v} point group can be measured by the asymmetry of the septet in the ^{13}C NMR spectrum. Such imbalances were created in the CD_3 groups of DMSO-d_6 and actone-d_6, and were called spin state imbalances (SSI). The lifetime of the SSI can be obtained by tracking the decay of the asymmetry of the ^{13}C septet. The lifetime of the SSI can exceed the spin lattice relaxation time (T_1) of deuterium by a factor up to 20. In addition, rotation of the methyl group can affect the lifetime of SSI: the faster the rotation, the better the separation of the spin manifolds belongs to different groups. This results in a longer lifetime of SSI. This lifetime can thus provide an indirect measurement of the rotation frequency of deuterated methyl groups.

In conclusion, we have shown how deuterium nuclei coupled to a ^{13}C nuclear spin can be hyperpolarized indirectly via CP through weak RF amplitudes in both CD_2 and CD_3 groups. These observations can expend the scope of DNP by adding another nucleus to the list of possible observables.

The here reported findings shed light on some puzzling aspects of the combination of CP-based DNP and the dissolution approach. Multiplet asymmetries and line distortions are frequently observed phenomena throughout the dissolution-DNP community. These are often not well-understood and therefore not welcome. This thesis may help to overcome this problem by explaining in detail the origin and quantum mechanics of such phenomena.

Curriculum Vitae

Aditya Jhajharia

Date of Birth: 31.08.1992   Email: aditya.jhajharia@ens.fr,

Nationality: Indian   adityaiiserm@gmail.com

Mobile: +33 751310930

Education

PhD student, École Normale Supérieure Paris   November 2014-Present

Department of Chemistry, Laboratary of Biomolecules (UMR 7203)
Thesis advisor: Prof. Geoffrey Bodenhausen

Master of Science and Bachelor of Science in *Chemistry*   2009-2014
(Dual degree BS-MS)
Indian Institute of Science Education and Research (IISER), Mohali.

Fellowships and Achievements

Awarded *Visiting Summer Research Programme* (VSRP) fellowship at Tata Institute of Fundamental Research (TIFR), Mumbai.   May 2013-July 2013

Awarded *Innovation in Science Pursuit for Inspired Research* (*INSPIRE*) Scholar for a period of five years.   2009 - 2014

Master's Dissertation

NMR Relaxation Studies of Fluorinated Drugs   Aug 2013 -Apr 2014

Research Publications

Sadet A.; Weber E. M. M.; **Jhajharia A.**; Kurzbach D.; Bodenhausen G.; Miclet E.; and Abergel D. Kinetic rates of chemical metabolic processes deter- mined by NMR boosted by dissolution dynamic nuclear polarization. *Manuscript under revision.*

Jhajharia, A.; Weber, E. M. M.; Kempf, J. G.; Abergel, D.; Bodenhausen, G.; and Kurzbach, D. Dissolution DNP Reveals a Long-Lived Deuterium Spin State Imbalance in Methyl Groups. *J. Chem. Phys.* 2017, *146*, 041101.

Kurzbach D.; Canet E.; Flamm A. G.; **Jhajharia A.**; Weber E. M. M.; Konrat R.; and Bodenhausen G. Investigation of Intrinsically Disordered Proteins through

Exchange with Hyperpolarized Water. *Angew. Chem., Int. Ed. Engl.* 2016, 56(1), 389–392.

Kurzbach D.; Weber E. M. M.; **Jhajharia A.**; Cousin S. F.; Sadet A.; Marhabaie S.; Canet E.; Birlirakis N.; Milani J.; Jannin S.; Eshchenko D.; Hassan A.; Melzi R.; Luetolf S.; Sacher M.; Rossire M.; Kempf J.; Lohman J. A. B.; Weller M.; Bodenhausen G.; Abergel D. Dissolution Dynamic Nuclear Polarization of Deuterated Molecules Enhanced by Cross-Polarization. *J. Chem. Phys.* 2016, *145*, 194203.

Bornet A.; Pinon A.; **Jhajharia A.**; Baudin M.; Ji X.; Emsley L.; Bodenhausen G.; Ardenkjaer-Larsen J. H.; Jannin S. Microwave-gated dynamic nuclear polarization. *Phys. Chem. Chem. Phys.* **2016**,18, 30530–30535.

Oral/Poster presentations

Aditya Jhajharia, Emmanuelle M. M. Weber, James G. Kempf, Daniel Abergel, Geoffrey Bodenhausen, and Dennis Kurzbach. Observation of Long-Lived ^{2}H Spin State Imbalance in Methyl Groups by Dissolution DNP. EUROMAR (**2017**) Warsaw, Poland (*Poster presentation*).

Aditya Jhajharia, Emmanuelle M. M. Weber, James G. Kempf, Daniel Abergel, Geoffrey Bodenhausen, and Dennis Kurzbach. Observation of Long-Lived Deuterium Spin State Imbalance in Deuterated Methylene and Methyl Groups by Dissolution DNP. *58th* Experimental Nuclear Magnetic Resonance Conference (**2017**) Pacific Grove, California (*Poster presentation*).

A. Jhajharia, D. Kurzbach, E. Weber, S. Cousin, A. Sadet, S. Marhabaie, E. Canet, N. Birlirakis, J. Milani, S. Jannin, D. Eshchenko, A. Hassan, R. Melzi, S. Luetolf, M. Sacher, M. Rossire, J. Kempf, J. Lohman, M. Weller, G. Bodenhausen, D. Abergel. Dissolution Dynamic Nuclear Polarization of Deuterated Molecules. Journée des Facultés de Biologie de Chimie, (**2016**) UPMC Paris (*Poster presentation*).

Aditya Jhajharia, Nicolas Birlirakis, Daniele Mammoli, Geoffrey Bodenhausen. Long-lived magnetization of *para* states, Journées Jeunes Chercheurs (**2015**) ENS Paris (*Oral presentation*).

Aditya Jhajharia, Kavita Dorai. NMR studies of fluorinated drugs using PFG spin-echo experiments and cross-correlated spin relaxation, National Magnetic Resonance Society Symposium (**2014**) Tezpur, India (*Poster presentation*).

Résumé

La résonance magnétique nucléaire (RMN) est désormais devenue une technique spectroscopique incontournable à de nombreux domaines de la science et de la médecine. Cependant, elle est limitée par une faible sensibilité en raison d'une polarisation nucléaire insuffisante, définie par la différence des populations entre les niveaux d'énergie impliqués, ce qui résulte à des temps expérimentaux assez longs. Cet inconvénient peut être compensé en transférant l'énorme polarisation des électrons non appariés aux spins nucléaires à l'aide d'une irradiation par micro-ondes à basse température - une méthode connue sous le nom de polarisation nucléaire dynamique (DNP).

Sami Jannin et ses collègues ont récemment combiné la méthode de polarisation croisée (CP) avec la DNP, à des températures très basses, afin de polariser plus rapidement les noyaux de faible γ en transférant la polarisation des électrons aux protons et ensuite aux noyaux de faible γ, comme le carbone-13. Cette thèse démontre que l'efficacité de cette méthode peut être améliorée en arrêtant l'irradiation par micro-ondes pendant quelques centaines de millisecondes avant la CP. En effectuant ces expériences, la polarisation du carbone-13 de l'acétate de sodium [1-^{13}C] peut monter jusqu'à 64% avec une constante de temps d'accumulation de polarisation très courte de 160 s.

L'échantillon hyperpolarisé peut ensuite être rapidement dissous pour obtenir un signal RMN amplifié à l'état liquide et à la température ambiente. Cette méthode a été développée par Ardenkjaer-Larsen et ses collègues en 2003 et est connue sous le nom de polarisation nucléaire dynamique par dissolution (D-DNP). Elle peut fournir une amplification du signal d'un facteur jusqu'à quatre ordres de grandeur.

La combinaison de la D-DNP avec les techniques de CP peut être utilisée pour créer des états de longue durée de vie (LLS) dans des molécules deutériées comme l'éthanol-d6 et le DMSO-d6. Ces états peuvent avoir des durées de vie beaucoup plus longues que l'aimantation conventionnelle de Zeeman. Ces états peuvent être détectés indirectement via des multiplets asymétriques dans les spectres RMN du carbone-13 en solution, à température ambiante après dissolution, via les couplages scalaires entre le carbone-13 et les noyaux du deutérium. Ces LLS résultent du déséquilibre des populations entre les représentations irréductibles des groupes de symétrie des molécules deutériées étudiées. Dans cette thèse, nous avons étudié les LLS dans les groupes CD$_2$ et CD$_3$. Les durées de vie de ces LLS peuvent dépasser les temps de relaxation T$_1$(^{2}H) des noyaux de deutérium par un facteur jusqu'à 20 (dépendant de la dynamique moléculaire) et peuvent être observées par la décroissance de l'asymétrie du multiplet du carbone-13. Ces observations peuvent élargir les applications de la DNP en ajoutant le noyau de ^{2}H à la liste des observables possibles.

Mots Clés

Résonance Magnétique Nucléaire (RMN), Polarisation Nucléaire Dynamique (DNP), Polarisation Croisée (CP), Polarisation Nucléaire Dynamique par Dissolution (D-DNP), Longue Durée de Vie (LLS)

Abstract

Nowadays, Nuclear Magnetic Resonance (NMR) has become an inevitable spectroscopic technique that can be applied in many fields of science and medicine. However it is limited by low sensitivity due to the low nuclear polarization, defined by the difference of populations between the energy levels involved, thus leading to long experimental times. This drawback can be overcome by using the huge polarization of unpaired electrons compared to nuclear spins and its transfer to nuclear spins at low temperatures (using microwave irradiation) to achieve a large nuclear magnetization - a method know as dynamic nuclear polarization (DNP).

Sami Jannin and co-workers have recently combined the cross-polarization (CP) method with DNP at very low temperatures to polarize low γ nuclei faster by transferring the electron polarization to protons and then to low γ nuclei like ^{13}C. This thesis demonstrates that the efficiency of the CP method can be improved by switching the microwave irradiation off for a few hundred milliseconds prior to CP. By performing these microwave gating experiments, ^{13}C polarizations for sodium [1-^{13}C]acetate as high as 64% could be achieved with a polarization build-up time constant as short as 160 s.

The hyperpolarized sample can subsequently be rapidly dissolved to achieve NMR signal enhancement in the liquid state at ambient temperature. This method has been developed by Ardenkjaer-Larsen and co-workers in 2003 and became known as dissolution-dynamic nuclear polarization (D-DNP). It can provide signal enhancements by a factor of up to four orders of magnitude in liquid state at room temperature.

Combining D-DNP with CP techniques from ^{1}H to ^{13}C can be used to create to create long-lived states (LLS) in deuterated molecules like ethanol-d$_6$ and DMSO-d$_6$, which can have much longer life times than conventional Zeeman magnetization. These LLS can be detected indirectly via the asymmetric multiplets in ^{13}C NMR spectra in solution state at room temperature after dissolution due to scalar couplings between ^{13}C and ^{2}H. These LLS result from population imbalances between spin manifolds of distinct irreducible representations of the relevant symmetry groups of the investigated deuterated moities. In this thesis we have investigated LLS in CD$_2$ and CD$_3$ groups. Lifetimes of these LLS can exceed the spin-lattice relaxation times T_1(^{2}H) of deuterium nuclei by a factor up to 20 (depending on the underlying molecular dynamics) and can be obtained by monitoring the decay of the asymmetry of the ^{13}C multiplet. These observations can expend the scope of DNP by adding ^{2}H nucleus to the list of possible observables.

Keywords

Nuclear Magnetic Resonance (NMR), Dynamic Nuclear Polarization (DNP), Cross-Polarization (CP), Dissolution-Dynamic Nuclear Polarization (D-DNP), Long-Lived States (LLS)